

# Evc2 regulates Hedgehog Signaling at Primary Cilia

Inaugural-Dissertation

Zur Erlangung des Doktorgrades  
der Mathematisch-Naturwissenschaftlichen Fakultät  
der Heinrich-Heine-Universität Düsseldorf

vorgelegt von

Karolin Viktoria Dorn  
aus Rottweil

Düsseldorf, September 2012

Aus dem Institut für Entwicklungs- und Molekularbiologie der Tiere der Heinrich-Heine-Universität Düsseldorf

Gedruckt mit der Genehmigung der Mathematisch-Naturwissenschaftlichen Fakultät der Heinrich-Heine-Universität Düsseldorf

Referent: Prof. Dr. U. Rüter

Ko-Referent: Prof. Dr. T. Klein

Tag der mündlichen Prüfung: 7. Dezember 2012

Parts of the presented thesis are published in:

Humke, E.W., **Dorn, K.V.**, Milenkovic, L., Scott, M.P., and Rohatgi, R. (2010). The output of Hedgehog signaling is controlled by the dynamic association between Suppressor of Fused and the Gli proteins. *Genes Dev.* 24, 670–682.

**Dorn KV**, Hughes CE, Rohatgi R (2012). A Smoothened-Evc2 complex transduces the Hedgehog signal at primary cilia. *Dev Cell.* 23 (4), 823-835.

## TABLE OF CONTENTS

<b>1. INTRODUCTION</b>	<b>1</b>
1.1 HOW CELLS COMMUNICATE – MOLECULAR SIGNALING PATHWAYS	1
1.2 THE PRIMARY CILIUM	2
1.2.1 <i>The formation of primary cilia</i>	3
1.2.2 <i>The structure of primary cilia</i>	5
1.2.3 <i>Intraflagellar transport (IFT)</i>	7
1.3 MECHANISMS OF HEDGEHOG SIGNAL TRANSDUCTION	10
1.3.1 <i>The Hedgehog ligands</i>	10
1.3.2 <i>Secretion and reception of the Hh signal</i>	12
1.3.3 <i>Intracellular Hh signal transduction</i>	13
1.4 CILIOPATHIES	16
1.4.1 <i>Cilia defects and Hedgehog Signaling</i>	17
1.4.2 <i>Ellis van Creveld Syndrome and Weyers Acrofacial Dysostosis</i>	19
1.5 HEDGEHOG SIGNALING AND HUMAN CANCER	20
1.6 AIM OF THE PRESENT THESIS	22
<b>2. MATERIALS AND METHODS</b>	<b>24</b>
2.1 MATERIALS	24
2.1.1 <i>Chemicals and Biochemicals</i>	24
2.1.2 <i>Solutions and Buffers</i>	25
2.1.3 <i>Constructs</i>	25
2.1.4 <i>Cell lines</i>	26
2.1.5 <i>Antibodies</i>	26
2.1.6 <i>Kits</i>	27
2.1.7 <i>Consumables</i>	28
2.1.8 <i>Instruments</i>	28
2.1.9 <i>Software</i>	29
2.2 METHODS	29
2.2.1 <i>SDS polyacrylamide gel electrophoresis (SDS-PAGE)</i>	29
2.2.2 <i>Immunoblotting and detection</i>	30
2.2.3 <i>Antibody generation</i>	31
2.2.3.1 <i>Antigen production</i>	31
2.2.3.2 <i>Antiserum generation and antibody purification</i>	32

2.2.4	<i>Cell culture</i> .....	33
2.2.5	<i>DNA transfection in mammalian cells</i> .....	34
2.2.6	<i>siRNA and esiRNA transfection</i> .....	34
2.2.7	<i>Stable cell line production</i> .....	35
2.2.8	<i>Assays for Hedgehog pathway activation</i> .....	36
2.2.8.1	Luciferase-based Hh-reporter assay.....	36
2.2.8.2	Gli1 protein expression.....	37
2.2.8.3	Alkaline phosphatase expression assay .....	37
2.2.9	<i>Immunofluorescence and Microscopy</i> .....	38
2.2.9.1	Immunofluorescence of fixed cells .....	38
2.2.9.2	Mouse tissue preparation and cryo-sectioning.....	38
2.2.9.3	Immunofluorescence of mouse tissue sections.....	39
2.2.9.4	Microscopy .....	39
2.2.10	<i>Analysis of protein glycosylation</i> .....	39
2.2.11	<i>Subcellular fractionation</i> .....	40
2.2.12	<i>Purification of protein complexes</i> .....	41
2.2.12.1	Immunoprecipitation .....	41
2.2.12.2	Tandem-affinity purification (TAP) .....	45
2.2.12.3	Affinity Purification.....	46
2.2.13	<i>Mass spectrometry</i> .....	49
2.2.14	<i>DSP crosslink of cultured cells</i> .....	49
2.2.15	<i>In situ proximity ligation assay</i> .....	50
2.2.16	<i>Data analysis</i> .....	51
2.2.16.1	Microscopy.....	51
2.2.16.2	Western blots.....	51
<b>3.</b>	<b>RESULTS</b> .....	<b>52</b>
3.1	<b>EVC2 IS REQUIRED FOR HEDGEHOG SIGNALING AT A STEP BETWEEN SMOOTHENED AND PKA/SUFU</b> 52	
3.1.1	<i>The function of Evc2 in fibroblasts</i> .....	52
3.1.2	<i>Evc2 is not required for cilia formation in fibroblasts</i> .....	55
3.1.3	<i>Evc2 localizes to a novel compartment in the primary cilium</i> .....	57
3.1.4	<i>Identification of the step in Hedgehog signaling that requires Evc2</i> .....	59
3.1.5	<i>The role of Evc2 in trafficking Hh pathway proteins to primary cilia</i> .....	62
3.2	<b>THE LOCALIZATION OF EVC2 TO THE PRIMARY CILIUM IS CRITICAL FOR ITS FUNCTION</b> .....	65
3.2.1	<i>The ciliary localization of Evc2<math>\Delta</math>W</i> .....	65
3.2.2	<i>A localization signal for the EvC Zone</i> .....	67

3.2.3	<i>The localization of Evc2 mutants predicts their phenotype in Hh signaling</i>	69
3.3	THE FORMATION OF A HEDGEHOG SIGNALING COMPLEX AT THE EVC ZONE	71
3.3.1	<i>Evc2 associates with Smo in response to Hh signaling</i>	71
3.3.2	<i>The dominant negative effect of Evc2<math>\Delta</math>W</i>	73
3.3.3	<i>Spatial restriction of the Smo-Evc2 interaction to primary cilia</i>	75
3.3.4	<i>Smo signaling in the Evc Zone</i>	79
3.4	IDENTIFICATION OF EVC2 BINDING PARTNERS	81
3.4.1	<i>Purification of Evc2 complexes</i>	81
3.4.2	<i>Evcbp1 and Evcbp2 interact with Evc and Evc2</i>	83
3.4.3	<i>Evidence for a role of Evcbp1 and Evcbp2 in Hedgehog Signaling</i>	86
<b>4.</b>	<b>DISCUSSION AND FUTURE PERSPECTIVES</b>	<b>88</b>
4.1	MODELS FOR THE FUNCTION OF EVC2 IN HEDGEHOG SIGNALING	88
4.1.1	<i>Discussion</i>	88
4.1.2	<i>Future Perspectives</i>	90
4.2	EVC2-BINDING PROTEINS AND THEIR ROLE IN HEDGEHOG SIGNALING	91
4.2.1	<i>Discussion and future perspectives</i>	91
4.3	THE EVC ZONE IS A NEW COMPARTMENT WITHIN THE PRIMARY CILIUM	94
4.3.1	<i>Discussion</i>	94
4.3.2	<i>Future Perspectives</i>	96
4.4	THE BIOCHEMICAL BASIS FOR ELLIS VAN CREVELD AND WEYERS SYNDROMES	97
4.4.1	<i>Discussion</i>	97
4.4.2	<i>Future Perspectives</i>	99
4.5	THE TISSUE-SPECIFIC ROLE OF EVC2 IN HEDGEHOG SIGNALING	100
4.5.1	<i>Discussion and future perspectives</i>	100
4.6	EVC2 AS A POTENTIAL DRUG TARGET IN HEDGEHOG-RELATED CANCERS	101
4.6.1	<i>Discussion</i>	101
4.6.2	<i>Future Perspectives</i>	101
<b>5.</b>	<b>SUMMARY</b>	<b>103</b>
<b>6.</b>	<b>ZUSAMMENFASSUNG</b>	<b>104</b>
<b>7.</b>	<b>ABBREVIATIONS</b>	<b>106</b>
<b>8.</b>	<b>REFERENCES</b>	<b>109</b>

<b>9. APPENDIX.....</b>	<b>126</b>
<b>9.1 THE OUTPUT OF HEDGEHOG SIGNALING IS CONTROLLED BY THE DYNAMIC ASSOCIATION BETWEEN SUPPRESSOR OF FUSED AND THE GLI PROTEINS .....</b>	<b>126</b>
<b>9.1.1 Summary.....</b>	<b>126</b>
<b>9.1.2 Contribution.....</b>	<b>126</b>
<b>9.2 SEQUENCES OF OLIGONUCLEOTIDES USED IN THIS STUDY.....</b>	<b>128</b>
<b>10. ACKNOWLEDGEMENTS .....</b>	<b>130</b>
<b>11. CURRICULUM VITAE .....</b>	<b>132</b>
<b>12. DECLARATION .....</b>	<b>135</b>

# 1. INTRODUCTION

## 1.1 How cells communicate – molecular signaling pathways

Language is the medium of communication. Without communication there is chaos. This is particularly true for the development of multicellular organisms. Cell-cell communication is critical for the complexity and functionality of single cells, tissues, and whole organisms. Despite the seemingly infinite number of different cell types and patterns found in the animal kingdom surprisingly few signaling cascades account for them. Seven major cell-cell signaling pathways including Hedgehog (Hh), Wingless related (Wnt), transforming growth factor beta (TGF $\beta$ ), Notch, Receptor tyrosine kinase (RTK), Janus kinase (JAK)/ Signal transducer and activator of transcription (STAT), and nuclear hormone pathways are responsible for most animal development (Pires-daSilva and Sommer, 2003). The observation that the same seven pathways are used many times during development indicates that signaling systems are highly flexible. The specificity of the signal response is achieved by “cross-talk” between different signaling modules, the strength of the initiating signal, and the context of the signal event eventually leading to the signal-dependent regulation of transcription factors that lead to the activation of specific target genes. Of these signaling modules the Hh signaling pathway plays an important role not only in embryogenesis but also in the adult organism as its mis-regulation has been implicated in the formation of various human cancers (Barakat et al., 2010; Goetz and Anderson, 2010). However, despite its importance for both development and cancer the molecular mechanisms of Hh signal transduction remain poorly understood.

Our knowledge of mammalian Hh signaling is largely based on work performed in the fruit fly *Drosophila melanogaster*. In 1980, Christiane Nüsslein-Volhard and Eric Wieschaus who studied pattern formation of fly larva first described *hedgehog* and other members of the Hh signal transduction cascade as important players in larva segment formation (Nüsslein-Volhard and Wieschaus, 1980). Today we know that the requirement for proper Hh signal transduction is not limited to the segment patterning

of the fly embryo, but is critical for various aspects of animal development. In vertebrates, Hh signaling has been implicated in a variety of processes in the developing embryo from patterning the limb and neural tube to regulating cardiac and lung morphogenesis (Goetz and Anderson, 2010). Thus, it is not surprising that malfunction of the Hh pathway leads to various human disorders including birth defects and cancer. Although various components of the *Drosophila* Hh cascade are conserved in the mammalian pathway the molecular mechanisms have diverged considerably. The probably most striking difference is the dependence of the mammalian pathway on the primary cilium, a micron-scale cell protrusion found on almost every cell in the human body (Wong and Reiter, 2008). The next paragraph focuses on cilia biology followed by a detailed description of the mammalian Hh signaling pathway and its implications in developmental disorders and cancer.

## 1.2 The primary cilium

Cilia are microtubule-based organelles that project from the surface of nearly every cell in the human body. There are three categories of cilia – nodal, motile, and primary – that are structurally related but have developed different functions. Nodal cilia are localized to the node in gastrulation-stage embryos and have been implicated in specifying the left-right body axis (Sulik et al., 1994; Nonaka et al., 1998). Motile cilia of multicellular animals are found concentrated in large numbers on epithelial cells in various tissues such as for example cells of the trachea or cells lining the oviducts and the epididymis of reproductive tracts. Their coordinated rhythmic beating activity driven by ATP hydrolysis creates a fluid flow. One example is the beating of motile cilia on cells of the trachea, a process important for pulmonary clearance (Stannard and O'Callaghan, 2006; Roy, 2009). In contrast to motile cilia, primary cilia are non-motile solitary organelles (Singla and Reiter, 2006). They have long been considered a curiosity of vertebrate cells and it was thought that primary cilia are largely non-functional (reviewed in Davenport and Yoder, 2005). However, genetic experiments revealed that primary cilia are essential sensory organelles functioning

as antennas of cells and are critical for patterning of the mouse embryo (Huangfu et al., 2003; Goetz and Anderson, 2010). Mutations that disrupt the function of primary cilia have been implicated in a plethora of developmental disorders such as cystic kidneys, cardiac and skeletal malformations (Novarino et al., 2011; Waters and Beales, 2011).

### **1.2.1 The formation of primary cilia**

The assembly and disassembly of primary cilia is tightly coupled to the cell cycle consisting of mitosis, G1-, S-, and G2-phase. Cilia are typically formed during the quiescent state (G0) and are disassembled around the time of mitosis. This was first described in experiments performed in 3T3 fibroblast cells in culture as high cell-density and/or growth in low-serum medium induced quiescence resulting in many ciliated cells (Tucker et al., 1979). The formation of cilia is directly linked to centrioles, microtubule-based barrel-shaped structures (Nigg and Raff, 2009). A pair of centrioles, embedded in pericentriolar material (PCM) is the core of a centrosome. The centrosome is the major microtubule organizing center (MTOC) in cells and is important for spindle pole organization during mitosis and cell division (Klotz et al., 1990). Centrioles duplicate exactly once during the cell cycle resulting in a mother and a daughter centriole, which can be distinguished by distinct appendages between the two. It is only the mother centriole that can give rise to a primary cilium, thus resulting in a single primary cilium per cell (Ishikawa and Marshall, 2011) (Figure 1A). Much of what we know about cilia formation is derived from electron microscopy studies performed in fibroblasts and smooth muscle cells in organ cultures (Sorokin, 1962).

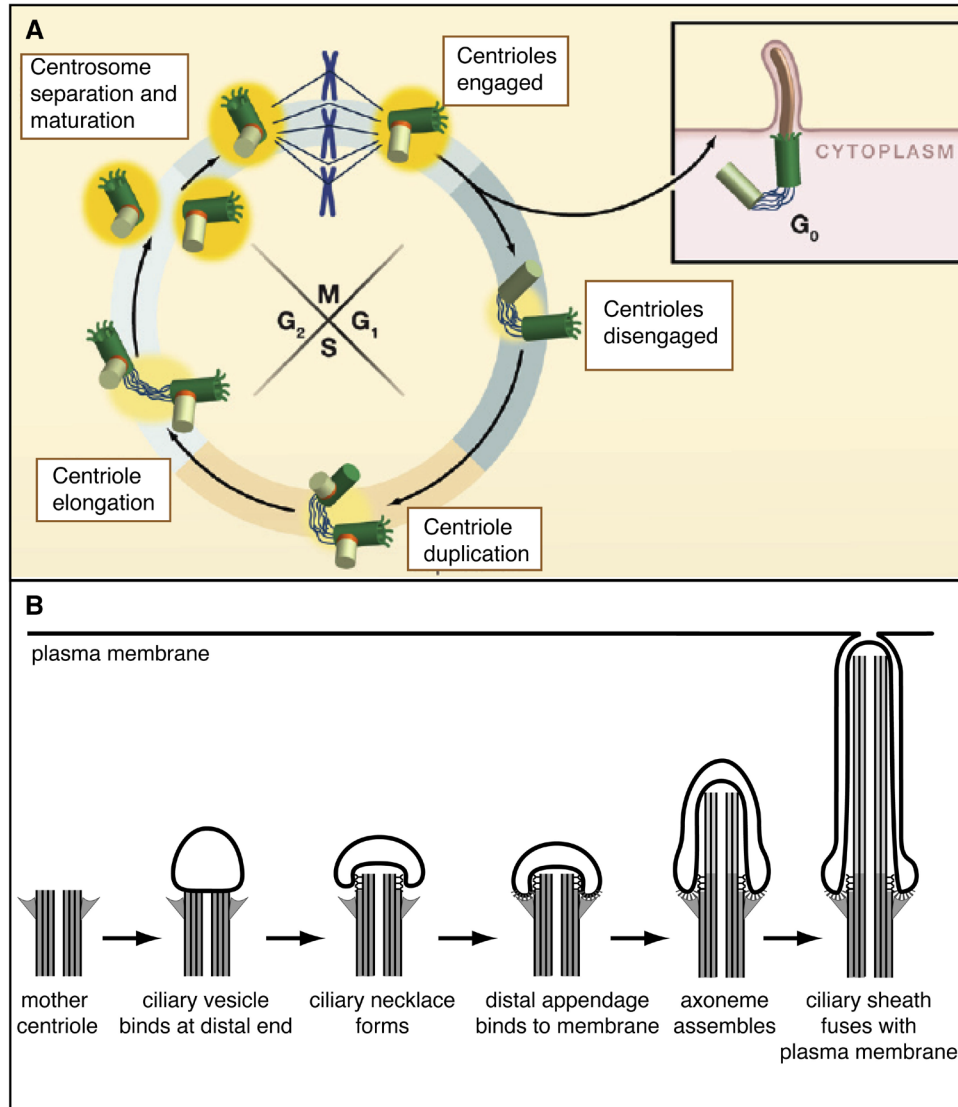


### Figure 1: The formation of a primary cilium

(A) Schematic of the centriole duplication events during cell cycle. New centrioles form during S-phase and continue to elongate in G<sub>2</sub>-phase. During G<sub>2</sub>/M transition they accumulate pericentriolar material (PCM, in yellow) and start to separate eventually forming the mitotic spindle. In late mitosis the two centrioles separate (disengage), which is required for centriole duplication. In G<sub>0</sub>, the mother centriole becomes a basal body and forms a primary cilium. Modified after Nigg and Raff, 2009. (B) A model for the formation of a primary cilium derived from Sorokin, 1962 and modified after Rohatgi and Snell, 2010. See main text for a detailed description.

The molecular pathways involved in the assembly of primary cilia remain largely obscure, but the steps in ciliogenesis are proposed as follows (Pedersen et al., 2008; Rohatgi and Snell, 2010) (Figure 1B): First, the mother centriole is converted into a basal body that nucleates the primary cilium by association of Golgi-derived centriolar vesicles with the distal end of the mother centriole (“capping”). The conversion to basal bodies also includes the addition of accessory structures such as ciliary rootlets, basal feet, and transition fibers providing structural support to the cilium and orienting it relative to other organelles. Newly assembled doublet microtubules emerge from the basal body, followed by the formation of the ciliary necklace, the region of tight contact between the membrane of the centriolar vesicles and the microtubule doublets. In a second step, more vesicles fuse with the new membrane to create a double membrane sheath around the elongating axonemal shaft. In the third stage, the sheath membrane reaches the cell surface and fuses with the plasma membrane, allowing the cilium to emerge into the extracellular space (Figure 1B). Given that basal bodies/primary cilia are assembled from centrioles makes the presence of a primary cilium incompatible with cell division and thus cilia formation only occurs in quiescent cells. Tight controls are necessary to prevent inappropriate assembly of basal bodies/primary cilia in cycling cells. The detailed mechanisms of cilia formation are only beginning to emerge, but it has been shown that ciliogenesis is positively influenced by appendage proteins such as CEP164 and is suppressed by centriolar proteins such as CP110 and CEP97 and the actin-related protein ACTR3 (Graser et al., 2007; Spektor et al., 2007; Kim et al., 2010a).

### **1.2.2 The structure of primary cilia**

The primary cilium is composed of a microtubule-based core-structure called the axoneme surrounded by a ciliary membrane (Figure 2). The ciliary axoneme is only ~0.25  $\mu\text{m}$  in diameter, but it can reach up to 20  $\mu\text{m}$  in length depending on the cell type. The ciliary membrane, although continuous with the plasma membrane, exhibits a distinct lipid and protein composition (Rohatgi and Snell, 2010). The axoneme of primary cilia is constructed of nine outer microtubule doublets, termed 9+0 pattern, and lacks the central pair of microtubules, radial spokes and dynein arms typical for

motile cilia (9+2 pattern) (Figure 2). The outer doublets consist of a complete microtubule (A microtubule) connected to an incomplete microtubule (B microtubule), but in contrast to the triplet microtubule pattern of the basal body lack the third microtubule (C microtubule) (Gerdes et al., 2009). The tubulin of the axoneme is subject to various post-translational modifications such as acetylation (Piperno et al., 1987), detyrosination (Gundersen and Bulinski, 1986), or glutamylation (Lee et al., 2012), which are thought to be important for primary cilia formation and function (Konno et al., 2012).

Between the basal body and the axoneme of the primary cilia sits yet another substructural zone, named the transition zone (TZ) (Czarnecki and Shah, 2012). By definition the TZ is the region within the cilium where the shift from triplet microtubules of the basal body to doublet microtubules of the axoneme occurs. At the distal end of the basal body the TZ includes a propeller-like arrangement of so-called transitional fibers (“alar sheets”) (Anderson, 1977), which emerge from the B microtubule of the

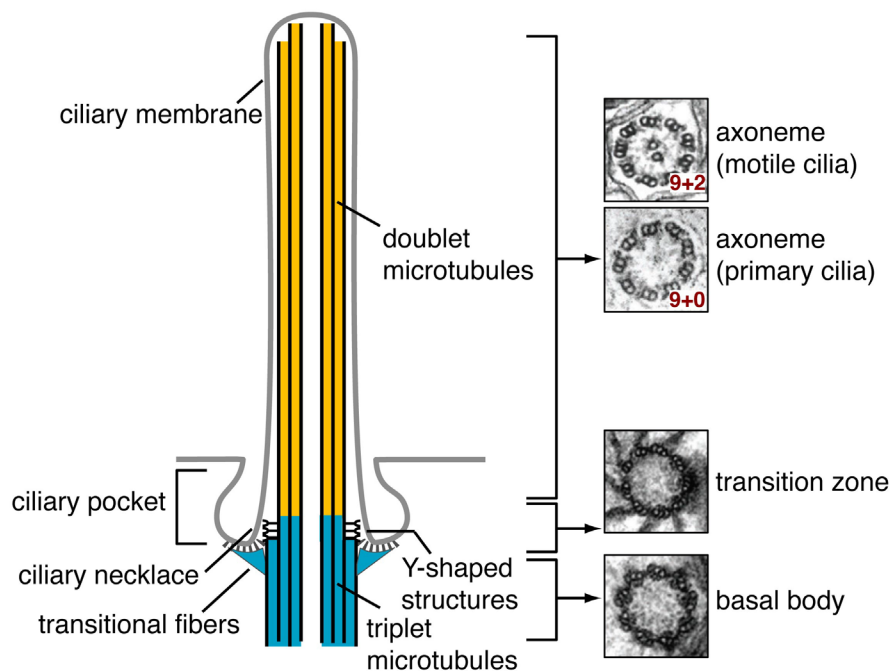


**Figure 2: Cilia structure:** Cilia consist of a basal body (in blue), a transition zone, a microtubule-based axoneme (in yellow), and a cilia membrane (in grey). Additional structures such as the ciliary pocket, the ciliary necklace, transitional fibers, and Y-shaped structures have been identified by electron microscopy. The main difference between motile and primary cilia is the 9+2 versus 9+0 microtubule pattern, respectively. Modified after Rohatgi and Snell, 2010 and Gerdes et al., 2009.

basal body and insert in the periciliary plasma membrane defining the border between plasma membrane and ciliary membrane (Figure 2). Further, the TZ contains multiple rows of Y-shaped structures connecting the outer microtubule doublets of the axoneme with the ciliary membrane. Characteristic of this interaction is the presence of intramembranous particles as seen by freeze-fracture electron microscopy, also referred to as the ciliary necklace (Gilula and Satir, 1972). Another feature of the ciliary membrane is the so-called ciliary pocket, a deep cleft that forms a double membrane sheath encircling the base of the cilium. The base of the ciliary pocket is connected with the basal body through the transitional fibers (Rohatgi and Snell, 2010). The presence of clathrin-coated pits in the ciliary pocket suggests a vesicle-trafficking activity of this membrane compartment (Molla-Herman et al., 2010). In addition, the ciliary pocket together with structures of the TZ including the ciliary necklace, the Y-shaped structures, and the transitional fibers are thought to be involved in forming a physical barrier that prevents free mixing of membrane proteins between the plasma membrane and the ciliary membrane (Czarnecki and Shah, 2012).

### **1.2.3 Intraflagellar transport (IFT)**

The assembly, maintenance, and function of primary cilia critically depend on a process called intraflagellar transport (IFT) (Pedersen and Rosenbaum, 2008). IFT is the bidirectional movement of multiprotein complexes along the outer microtubules of the ciliary axoneme that was first described through differential interference contrast (DIC) microscopy as a bidirectional movement of large granule-like particles, named IFT particles, along the flagella of the green algae *Chlamydomonas reinhardtii* (Kozminski et al., 1993). IFT particles are transported from the base of the cilium to its distal tip (anterograde transport) by plus-end-directed motor proteins of the Kinesin-2 family. They return back to the cell body (retrograde transport) by the minus-end-directed cytoplasmic Dynein-2 (Figure 3). IFT particles were first purified from *Chlamydomonas* flagella by sucrose density centrifugation (Piperno and Mead, 1997) and were found to consist of two distinct complexes named IFT complex A (IFT-A) and IFT complex B (IFT-B). The polypeptides of IFT particles range in apparent

molecular weights from 20 to 172 kDa and were thus named IFT20 through IFT172 (Cole, 2003). Many IFT proteins are conserved in mammals and contain protein-protein interaction motifs such as N-terminal WD repeats and C-terminal TPR motifs likely used for cargo specification (Jékely and Arendt, 2006; Pedersen and Rosenbaum, 2008). Structural and sequence homology to components of coat protein I (COPI) and clathrin-coated vesicles suggest that the non-vesicular, membrane-bound IFT evolved as a specialized form of coated vesicle transport from a so called “protocoatamer complex” (Jékely and Arendt, 2006). IFT-B is associated with Kinesin-2 and is thought to be involved in anterograde transport as originally shown by experiments performed in *Caenorhabditis elegans* (Orozco et al., 1999). In contrast, IFT-A contributes mainly to retrograde transport, for example for the recycling of IFT components (Scholey, 2008). However, recent studies in mouse models suggest that this simple distinction between IFT-A and IFT-B function is probably an oversimplification.

Two types of Kinesin-2 motors have been implicated in IFT, a canonical heterotrimeric complex and a homodimeric complex (Scholey, 2008). In mice, the heterotrimeric motor consists of two kinesin-2 family members, Kif3a and Kif3b, and the non-motor component Kap (KIF-associated protein) and has been shown to be essential for the assembly of primary cilia (Verhey et al., 2011). For example, the removal of *Kif3a* specifically in the mouse kidney by Cre-loxP mutagenesis resulted in a failure of cilia assembly and development of polycystic kidney disease (Lin et al., 2003). The homodimeric Kinesin complex was first described in *C. elegans* as OSM-3 (Shakir et al., 1993; Signor et al., 1999) as an accessory anterograde motor in a subset of sensory cilia. The mammalian OSM-3 homolog, Kif17 is involved the transport of cyclic nucleotide-gated (CNG) channels to the olfactory cilia and has also been shown to be required for photoreceptor development and maintenance in the zebrafish *Danio rerio* (Jenkins et al., 2006; Insinna et al., 2008). The motor that powers retrograde transport is the multiprotein complex cytoplasmic dynein 2, best studied in *Chlamydomonas* (Pazour et al., 1998). Knockdown or mutation of cytoplasmic dynein components such as the heavy chain Dync2h1 produced short, bulbous cilia with accumulated IFT particles in various organisms suggestive for a

role of cytoplasmic dynein 2 in retrograde transport (May et al., 2005; Ocbina et al., 2011).

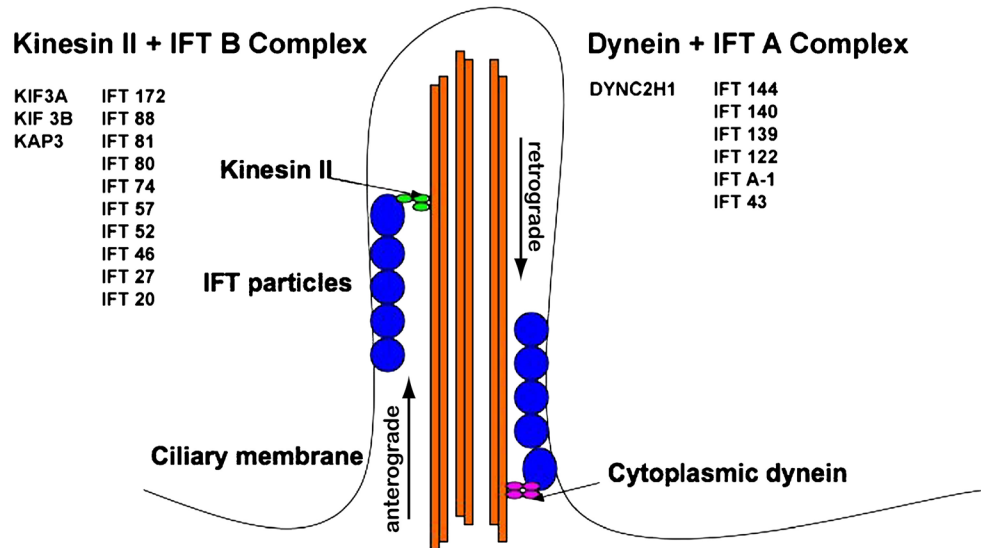


**Figure 3: Intraflagellar transport:** Intraflagellar transport (IFT) is required for transport processes along the axoneme of cilia. The canonical anterograde IFT motor, heterotrimeric Kinesin-2, transports IFT particles and various cargo proteins to the tip of the cilium. Retrograde transport is mediated by cytoplasmic dynein 2, which moves retrograde IFT particles back to the cell body. Modified after Water and Beales, 2010.

An interesting question is how IFT connects to other transport systems in the cell in order to facilitate the transport of cargo, including axonemal components, ciliary membrane proteins, and signal transduction proteins from the site of protein synthesis in the cytoplasm to the primary cilium. One model for ciliary trafficking of membrane proteins suggests a vesicle-mediated trafficking pathway from the Golgi to the base of the cilium (Satir et al., 2010). Some players involved in this process have been identified and include, cytoplasmic Dynein 1, Ift20 (the only IFT protein localized to the Golgi apparatus), the small GTPase Rab8, and the coat-like BBSome consisting of various Bardet-Biedl Syndrome (BBS) proteins (Follit et al., 2006; Nachury et al., 2007; 2010; Ishikawa and Marshall, 2011). The protein content of primary cilia is different from the rest of the cell suggesting a mechanism for the selection of ciliary proteins or the exclusion of non-ciliary proteins. The tight connection between the

ciliary membrane and the axoneme in the transition zone (TZ) (see paragraph 1.2.2) is considered a “fence” hindering the free entry of soluble proteins. There is also evidence that a diffusion barrier at the base of the cilium prevents uncontrolled entry of non-ciliary membrane proteins. It has been shown that the centrosomal protein CEP290 is involved in this ciliary barrier as well as Septin 2, a member of a class of proteins called Septins, that are known to form diffusion barriers during cell division (Craigie et al., 2010; Hu et al., 2010). In addition to this diffusion barrier there must be mechanisms that allow for the correct proteins to selectively pass through this “gate” at the ciliary base. It has been suggested that this transport process involves proteins and mechanisms similar to the transport between the cytoplasm and the nucleus through the nuclear pore (Kee et al., 2012; Obado and Rout, 2012). In fact, some ciliary proteins contain a ciliary targeting signal analogous to the nuclear localization sequence (NLS) (Geng et al., 2006; Mazelova et al., 2009; Follit et al., 2010). However, until today there is no evidence for a consensus sequence that is predictive of ciliary localization and no machinery detecting these targeting sequences has been identified yet.

## **1.3 Mechanisms of Hedgehog signal transduction**

### **1.3.1 The Hedgehog ligands**

After the pioneering work by Nüsslein-Volhard and Wieschaus in 1980 on the Hh gene and its role in establishing the *Drosophila* larval body plan (Nüsslein-Volhard and Wieschaus, 1980), the first vertebrate Hh genes were reported in 1993 (Echelard et al., 1993; Krauss et al., 1993; Riddle et al., 1993). Unlike the fly, which has a single *hedgehog* gene, mice and humans possess three genes encoding for the Hh ligands Desert hedgehog (Dhh), Indian hedgehog (Ihh), and Sonic hedgehog (Shh). The Hh proteins can trigger different responses depending on the context in which these signals operate (Ryan and Chiang, 2012). Dhh plays a role in the regulation of spermatogenesis (Bitgood et al., 1996) and the formation of peripheral nerve sheaths

(Parmantier et al., 1999). *Ihh* functions primarily in bone development where it regulates the rate of chondrocyte proliferation and differentiation (Vortkamp et al., 1996). Among the three Hh ligands, *Shh* features the most widespread functions and much of what we know about vertebrate Hh signaling comes from work on *Shh*. *Shh* is important for morphogenesis of various tissues such as eye, skin, lung, muscles, and pancreas. It acts both as a mitogen by influencing cell proliferation and as a morphogen, inducing distinct molecular responses at discrete concentration thresholds (McMahon et al., 2003). The best understood roles of *Shh* are as a morphogen in the patterning of the neural tube and limb bud. During normal mouse development the expression of *Shh* in the notochord of the developing neural tube results in a gradient of *Shh* (highest at the notochord and the floor plate) determining the different ventral neuron fates in a concentration- and time-dependent manner (Figure 4A) (Wong and Reiter, 2008; Ribes and Briscoe, 2009).

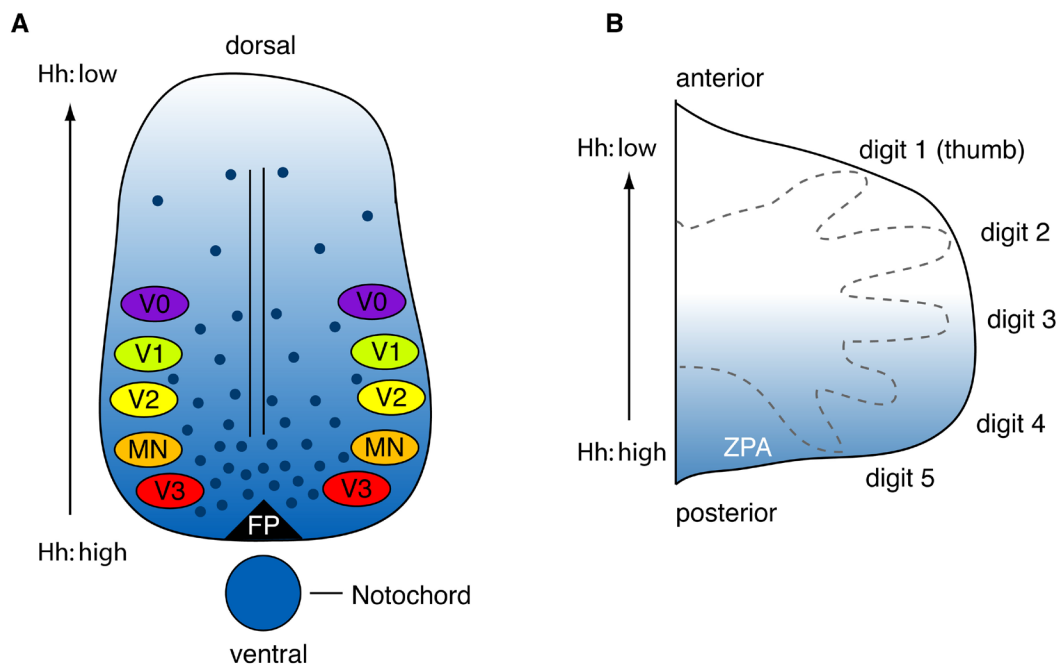


**Figure 4: Hedgehog gradients in the neural tube (A) and the limb bud (B).** (A) In the developing neural tube *Shh* is secreted from the floor plate and the notochord to form a ventral [V] to dorsal [D] concentration gradient leading to a spatially restricted expression profile of various transcription factors. The expression of a unique combination of transcription factors directs the formation of neural progenitor cells along the D/V axis, which generate V0-V3 interneurons and motorneurons (MN). (B) In the vertebrate limb bud the production of *Shh* in the zone of polarizing activity (ZPA) establishes a posterior to anterior concentration gradient specifying digit identity and number. In both limb and neural tube development not only the spatial, but also temporal aspect of the Hh gradient is important.

As a consequence dorsal neural subtypes are largely expanded into the ventral neural tube in *Shh* deficient mutants (Chiang et al., 1996). Another prominent example of *Shh* activity is its involvement in the patterning of the limb bud, where its expression in the zone of polarizing activity (ZPA) leads to an anterior-posterior gradient specifying digit number and identity (Figure 4B). Cells localized around the ZPA are exposed to high concentrations of *Shh* for the longest period of time and are specified to form digit #5 (little finger). In contrast, cells at the anterior side are exposed to very little *Shh* and are specified to form digit #1 (thumb). *Shh*<sup>-/-</sup> mutants form only a single digit (Chiang et al., 2001).

### 1.3.2 Secretion and reception of the Hh signal

The Hh proteins are synthesized as 45 kDa precursor proteins. Following translation the Hh precursor peptide undergoes a cholesterol-dependent autocatalytic cleavage in the endoplasmic reticulum (ER) resulting in a cholesterol-modified N-terminal peptide (Hh-N) and a C-terminal fragment, which undergoes ER-associated degradation. The cleavage is critical for ligand function and mutations disrupting the cleavage process have been implicated in developmental disorders such as holoprosencephaly (Maity et al., 2005). After the attachment of a palmitate to the N-terminal end of Hh-N the Hh ligand has two covalently attached lipid moieties: cholesterol at the C-terminus and palmitate at the N-terminus (Ryan and Chiang, 2012). The release of this lipid-modified Hh molecule and its long-range signaling capability require the proteins Dispatched (Disp) and Scube (Caspary et al., 2002; Creanga et al., 2012; Johnson et al., 2012; Tukachinsky et al., 2012). On the receiving cell Hh is received by the receptor Patched 1 (Ptc1), a 12-pass transmembrane (TM) protein. Additional Hh-binding proteins including the Cdo/Boc family of immunoglobulin/fibronectin-repeat containing proteins, the member of the low density lipoprotein (LDL) receptor family Lrp2, and GPI-anchored membrane bound protein Gas1 positively modulate the Hh signal reception on the receiving cell suggesting that they may function as co-receptors (Izzi et al., 2011; Christ et al., 2012). In addition to its function as Hh receptor Ptc1 is also a potent negative regulator of the pathway. In the absence of ligand the receptor Ptc1 is found in the

cilium and around the base of the cilium where it inhibits the function of the downstream Hh component Smoothed (Smo), a membrane protein with 7-pass TM regions (Rohatgi et al., 2007). When Shh is received, Ptc1 leaves the cilium, allowing the accumulation of Smo to high levels in cilia (Corbit et al., 2005; Rohatgi et al., 2007). The mode of signal transduction by Ptc1 remains largely unknown, but its homology to the RND family of prokaryotic proton-driven transporters suggests that Ptc1 transports an endogenous small molecule that inactivates or activates the downstream Hh component Smo (Taipale et al., 2002). Oxysterols, hydroxylated forms of cholesterol, have been identified as positive regulators in the pathway downstream of Ptc1 that directly bind to Smo (Corcoran and Scott, 2006; Dwyer et al., 2007; Nachtergaele et al., 2012). However, it remains to be determined whether oxysterols are the endogenous molecules regulating Smo function.

### **1.3.3 Intracellular Hh signal transduction**

The high accumulation of Smo in the primary cilium triggers downstream events in the pathway that lead to the activation of the Gli transcription factors that ultimately shape the transcriptional output of Hh signaling (Wong and Reiter, 2008) (Figure 5). The details of this step connecting Smo signaling to Gli activation remain mysterious, but might involve the coupling of Smo to heterotrimeric G-proteins (DeCamp et al., 2000; Riobo et al., 2006; Low et al., 2008). It is an intriguing idea that Smo activation is directly linked to downstream effectors by altering intracellular or intraciliary cAMP levels. Although Smo is structurally related to G-protein coupled receptors (van den Heuvel and Ingham, 1996) the involvement of G-proteins in canonical Hh signaling remains controversial (Low et al., 2008). Although the precise signaling steps remain obscure it is clear that activated Smo has to somehow overcome the two negative regulators of the Gli proteins: Suppressor of Fused (SuFu) and Protein Kinase A (PKA). PKA is a powerful suppressor of Hh signaling and blocking PKA activity is sufficient to fully activate Hh target gene transcription even in the absence of Shh (Lepage et al., 1995; Hammerschmidt et al., 1996; Tuson et al., 2011). Genetic inactivation of SuFu leads to constitutive activation of Hh signaling in mice and cultured cells (Cooper et al., 2005; Svärd et al., 2006).



proteasome resulting in a N-terminal repressor fragment (GliR) containing the Zinc-finger DNA binding domain (Tempé et al., 2006; Wang and Li, 2006). The conversion of GliFL to GliR depends on SuFu, the kinesin-4 family member Kif7, and the primary cilium. SuFu retains GliFL in the cytoplasm preventing its nuclear localization and activation. In the presence of Hh ligands, Smo mediates the dissociation of SuFu from GliFL, which enters the nucleus and gets converted in a transcriptional activator (GliA) that is quickly degraded, a process mediated by the Cullin3-based E3 ubiquitin ligase SPOP (Zhang et al., 2006; Chen et al., 2009; Kim et al., 2009; Humke et al., 2010; Tukachinsky et al., 2010). Kif7 seems to be required for Gli processing as Kif7 deficient mice show high levels of GliFL and low levels of GliR (Cheung et al., 2009). Genetic experiments revealed that the primary cilium is necessary for Gli regulation as the disruption of various IFT proteins affected Hh signaling *in vivo* (Huangfu et al., 2003; Ko et al., 2009). Further details of the connection between defects in primary cilia and Hh signaling are described in paragraph 1.4.1.

Of the three Gli proteins only Gli2 and Gli3 have a dual role of transcriptional activators and repressors and are the primary mediators of Hh signaling essential for embryogenesis (Hui and Angers, 2011). In mouse embryos lacking both Gli2 and Gli3 the response to Hh stimulation is lost (Buttitta et al., 2003). The processing of Gli3 is significantly more efficient than that of Gli2 (Pan et al., 2006). Thus, Gli3 mainly functions as transcriptional repressor (Gli3R) and Gli2 as transcriptional activator (Gli2A) in Hh signaling (Buttitta et al., 2003; Lei et al., 2004). Gli1 is an early Hh-target gene and appears to be part of a positive feedback loop as it functions exclusively as transcriptional activator of the pathway (Park et al., 2000; Bai et al., 2002).

## 1.4 Ciliopathies

The term “ciliopathy” describes a set of rare human diseases associated with mutations encoding defective ciliary (including basal body) proteins, which result in either abnormal formation or function of cilia (Waters and Beales, 2011). Today, more than a dozen disorders are considered to be within the ciliopathy spectrum. Some are listed here and include Joubert syndrome (JBTS), Alström syndrome (ALMS), Nephronophthisis (NPHP), Senior-Loken syndrome (SLNS), Ellis van Creveld syndrome (EVC), Orofaciodigital syndrome (OFD), Jeune asphyxiating thoracic dystrophy syndrome (JATD), autosomal dominant and recessive polycystic kidney disease (ADPKD and ARPKD), Leber congenital amaurosis (LCA), Meckel-Gruber syndrome (MKS), Bardet-Biedl syndrome (BBS), Usher syndrome (US), and some forms of retinal dystrophy. Because cilia are found on almost every cell in the human body ciliopathies can affect many organ systems including kidney, brain, limb, retina, liver, and bone. There is considerable clinical overlap between the different syndromes and the main clinical features are summarized in Figure 6 (Quinlan et al., 2008; Novarino et al., 2011; Waters and Beales, 2011). For example most patients show cystic kidneys and liver disease, some have laterality defects and retinal degeneration and polydactyly. Ciliopathies can be further divided into those with skeletal involvement including include short rib polydactyly disorders (SRP) (Huber and Cormier-Daire, 2012) and those without (BBS, NPHP, MKS, JBTS, ALMS). BBS was the first disorder described as a ciliopathic disorder caused by mutations in *BBS8* (Ansley et al., 2003). Today, more than 40 genes implicated in ciliopathies have been identified facilitated by the powerful resource of a ciliary proteome database (Gherman et al., 2006; Waters and Beales, 2011). Some of the ciliopathy genes are associated with only one disorder; e.g. mutations in *ARL13B* are restricted to patients with JBTS. However, mutations in other ciliopathy genes can result in phenotypes along the entire ciliopathy clinical spectrum. For example, *RPGRIP1L* mutations can cause MKS and JBTS and mutations in *CEP290* can cause MKS, NPHP, BBS, LCA or JBTS (Delous et al., 2007; Coppieters et al., 2010), which is likely due to distinct mutations within the same affected gene (multiple allelism). In addition, it became

clear that also epistatic interactions and mutational load influence the penetrance of a ciliopathy (Novarino et al., 2011).

Only recently, the picture emerges that many proteins encoded by ciliopathy genes localize to a common ciliary structure, the transition zone (TZ). Based on genetic analyses, proteomic interaction patterns and correlation of localization data, the current model suggests a TZ protein network consisting of four ciliopathy communicating multiprotein complexes including NPHP1/4/8, MKS/B9, NPHP5/6 and the Inv (Inversin) compartment (Novarino et al., 2011; Czarnecki and Shah, 2012). However, it remains largely obscure how these modules influence TZ assembly and the assembly of signaling pathways in the TZ under both normal and disease conditions.

Feature	BBS	MKS	JBTS	NPHP	SLSN	JATD	OFD1	EVC	ALMS	PKD
Renal cysts	✓	✓	✓	✓	✓	✓	✓		✓	✓
Hepatobiliary disease	✓	✓	✓	✓	✓	✓	✓		✓	✓
Laterality defects	✓	✓		✓		✓				
Polydactyly	✓	✓	✓			✓	✓	✓		
Agenesis of corpus callosum	✓	✓	✓			✓	✓		✓	
Cognitive impairment	✓	✓	✓			✓	✓	✓		
Retinal degeneration	✓	✓	✓		✓	✓			✓	
Posterior fossa defects/ encephalocoele	✓	✓	✓			✓		✓		
Skeletal bone defects						✓	✓	✓		
Obesity	✓								✓	

**Figure 6: Ciliopathy syndromes:** Common clinical features between the ciliopathies BBS (Bardet-Biedl syndrome), MKS (Meckel-Gruber syndrome), JBTS (Joubert syndrome), NPHP (Nephronophthisis), SLSN (Senior Loken syndrome), JATD (Jeune asphyxiating thoracic dystrophy syndrome), OFD1 (Orofacioidigital syndrome type 1), EVC (Ellis van Creveld syndrome), ALMS (Alström syndrome), and PKD (polycystic kidney disease). From Quinlan et al. 2008.

#### 1.4.1 Cilia defects and Hedgehog Signaling

Many clinical features seen in patients affected by ciliopathies can be attributed to defective Hh signaling. For example, polydactyly may be explained by a loss of Gli3 repressor formation in the developing limb and a mouse model for MKS revealed that altered Hh signaling underlies some of the defects, including craniofacial abnormalities, caused by loss of Mks1 (Weatherbee et al., 2009; Goetz and Anderson, 2010). However, for some of the most common abnormalities associated with ciliopathies such as renal cyst formation the underlying mechanisms remain obscure.

As described above many components of the Hh pathway localize to the primary cilia and as such, proper Hh signal transduction critically depends on this organelle. The link between Hh signaling and cilia was first described in 2003. In a phenotype-based screen for altered Hh-dependent patterning of the mouse embryo mutants in the IFT genes *Ift88* and *Ift172*, and in the Kinesin-2 motor *Kif3a* showed patterning defects indicative of a loss of pathway activity (Huangfu et al., 2003). Mutations in IFT-B components, such as the ones in *Ift88* and *Ift172*, prevent ciliogenesis due to their role in anterograde trafficking and influence Hh signaling by affecting both GliA and GliR function (Huangfu et al., 2003; Huangfu and Anderson, 2005; Liu, 2005; May et al., 2005). The effect of mutations in genes involved in retrograde transport including IFT-A components is more complex and differ depending of the component mutated, the mutant alleles, and the tissue studied (Ko et al., 2009). For example loss-of-function mutations in *Thm1* (IFT139 homolog) and *Ift122* cause increased Hh signaling, but disruption of the retrograde motor *Dync2h1* function leads to a reduced Hh response (Tran et al., 2008; Ocbina et al., 2011; Qin et al., 2011). Surprisingly, both heterozygosity for *Ift172*, a gene involved in anterograde transport, and a reduction of *Ift122*, a gene involved in retrograde transport, can suppress the *Dync2h1* phenotype (Ocbina et al., 2011). Studies in *Ift144* mutants (also an IFT-A component) have shown that a partial-loss of function *Ift144* allele leads to ectopic Hh activation (similar to *Ift122* and *Thm1* mutants), but homozygous mutation in a strong allele leads to a reduction of Hh signaling (Liem et al., 2012). It became clear that both IFT-A and IFT-B can regulate Hh signaling by influencing both GliA and GliR function. However, their role in cilia formation, their involvement in either retrograde or anterograde trafficking (or both), their role in trafficking of signaling molecules and thus their role in shaping the Hh output are more complex and we are just beginning to understand the underlying mechanisms.

#### 1.4.2 Ellis van Creveld Syndrome and Weyers Acrofacial Dysostosis

Despite the genetic and cell-biological evidence linking the Hh pathway to primary cilia, surprisingly few protein interactions have been described between ciliopathy proteins and core components of the Hh pathway. An obstacle to dissecting Hh biochemistry at cilia is presented by the fact that many defects seen in ciliopathies compromise the structural integrity of cilia, making it difficult to disentangle direct from indirect effects. Amongst ciliopathies that lead to defects in Hh signaling (Goetz and Anderson, 2010), Ellis van Creveld syndrome (EvC; OMIM 225500) is uniquely characterized by ultra-structurally normal cilia and is considered a ciliopathic disorder based on the finding that the proteins implicated in the disease, localize to the basal body of primary cilia (Ruiz-Perez et al., 2000; Galdzicka et al., 2002; Takeda et al., 2002; Ruiz-Perez et al., 2003; Blair et al., 2011). EvC was first described by the pediatricians Richard Ellis and Simon van Creveld in 1940 as a “Syndrome characterized by ectodermal dysplasia, polydactyly, chondro-dysplasia and congenital morbus cordis” (Ellis and van Creveld, 1940). EvC is a rare disease with estimated less than 200 cases reported since its first description in 1940. An unprecedentedly high frequency of affected individuals occurs in the Amish community in Lancaster county, Pennsylvania and the beneficial relation between this community and geneticists revealed a lot of what we know about this disease today (McKusick, 2000). The EvC phenotype is variable, but most commonly includes bone abnormalities including short stature, narrow chest, shorter limbs, and polydactyly in hand and feet as well as oral features such as cleft palate and lip and teeth abnormalities (Baujat and Le Merrer, 2007). Congenital heart defects occur in 50-60% of the cases comprising mainly single atrium and atrioventricular canal defects (Digilio et al., 1999). The inheritance of EvC is autosomal recessive and numerous mutations in two genes, *EVC* and *EVC2*, have been mapped in patients diagnosed with this disease. EvC patients with mutations in either *EVC* or *EVC2* or both are phenotypically indistinguishable (Temtamy et al., 2008). Interestingly, mutations in *LIMBIN*, the bovine orthologue of *EVC2*, can cause chondrodysplastic dwarfism in Japanese cattle (Takeda et al., 2002). Both *EVC* and *EVC2* are localized to the distal short arm of chromosome 4 in a head to head orientation, separated by only 1643

base pairs (bp). There is no sequence homology between the two genes at either DNA or protein level (Blair et al., 2011). The proteins encoded by the *EVC* or *EVC2* genes are single-pass transmembrane (TM) proteins and have been shown to form a complex (Blair et al., 2011). Mutations in the *EVC2* gene can cause both EvC and a related disease named Weyers Acrofacial Dysostosis (Weyers; OMIM 193530), which is in contrast to EvC an autosomal dominant disorder (Ruiz-Perez et al., 2000). *Evc2* mutations have been shown to impair Hh signaling in cardiac, skeletal and orofacial tissues during development (Ruiz-Perez and Goodship, 2009; Blair et al., 2011). However, the mechanism of *Evc2* function in Hh signaling, including the critical question of whether its effect is direct or indirect, has remained unknown.

## 1.5 Hedgehog signaling and human cancer

Hh signaling is critical for the development of the normal embryo, but is subsequently silenced in most adult tissues. However, after injury the pathway can be reactivated promoting tissue repair and regeneration (Watkins et al., 2003; Karhadkar et al., 2004). Furthermore, abnormal Hh pathway activation has been detected in various human cancers affecting skin, brain, lung, breast, prostate, and many more (Barakat et al., 2010; McMillan and Matsui, 2012). A link between aberrant Hh signaling and cancer was initially provided by studies in Gorlin Syndrome, an autosomal dominant condition causing skeletal and craniofacial abnormalities as well as an increased risk for the development of advanced basal cell carcinoma (BCC) and medulloblastoma. Loss-of-function mutations affecting *PTC1* were identified as cause of Gorlins Syndrome leading to hyperactivation of the pathway (Hahn et al., 1996; Johnson et al., 1996). This observation has lead to the discovery of *PTC1* and *SMO* mutations also in the more common sporadic forms of BCC and medulloblastoma (Unden et al., 1997). One hallmark of these cancers is the activation of Hh signaling independent of the Hh-ligand (Figure 7A). Ligand-dependent cancers are caused by either autocrine (signal originates and is received by tumor cells) or paracrine (ligand secretion and Hh activation occurs in different types of cells of either stroma or tumor) activation of

the pathway (Rubin and de Sauvage, 2006; Barakat et al., 2010) (Figure 7B and C). The autocrine mechanism has been called into question recently, but might be relevant in cancers such as lung and prostate (Singh et al., 2011; Tzelepi et al., 2011) whereas paracrine signaling occurs in cancers affecting pancreas, prostate, and metastatic colon cancer (Barakat et al., 2010). Targeting cancers caused by mis-activated or mis-regulated Hh signaling focuses mainly on Smo as a drug target with more than 40 clinical trials across a wide range of tumor types (Lin and Matsui, 2012). In January 2012, the small-molecule Smo-inhibitor Vismodegib got approved by the FDA (US Food and Drug Administration) for the treatment of BCC and represents an important milestone (Robarge et al., 2009; Dlugosz et al., 2012; Keating, 2012). However, many challenges in treating Hh-related cancer remain with drug resistance being an important concern.

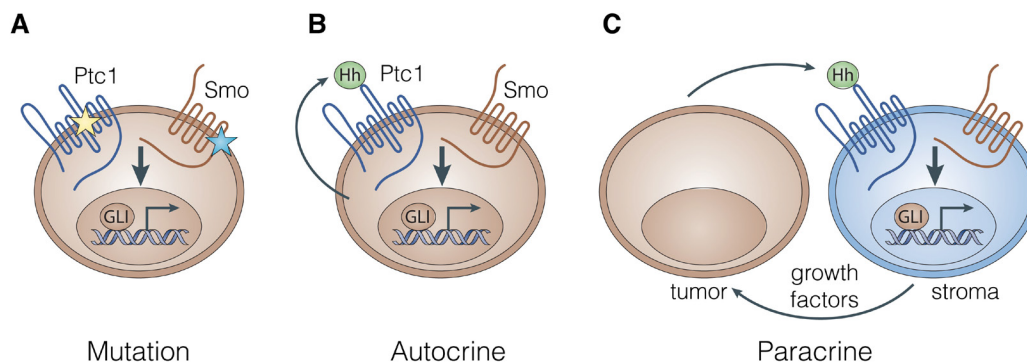


**Figure 7: Models of Hh pathway activation in cancer.** (A) Loss-of-function mutations in inhibitory proteins such as Ptc1 (yellow star) or gain-of-function mutations in positive regulators such as Smo (blue star) lead to constitutive active Hh signaling. (B) Autocrine model in which tumor cells both overexpress and respond to the Hh ligand. (C) Paracrine model in which tumor cells produce Hh ligand and adjacent stromal cells respond by producing growth factors to support tumor growth or survival. Modified after Rubin and de Sauvage, 2006.

## 1.6 Aim of the present thesis

The present study sits at the intersection between Hh signaling and primary cilia. As described in the previous paragraphs damage to Hh signaling or primary cilia can lead to birth defects. EvC and Weyers syndrome are two skeletal dysplasia syndromes recently identified as ciliopathies despite the fact that cilia are ultra-structurally normal in these syndromes (see paragraph 1.4.2). Both disorders are characterized by chondrodysplasias, polydactyly, craniofacial abnormalities, and heart defects and in accordance with these Hh-related phenotypes *EVC2*, the gene that is mutated in EvC and Weyers, has been implicated in Hh signaling. However, it has remained unknown whether *Evc2* influences Hh signaling directly or in an indirect manner. The objective of this work was to understand the biochemical mechanisms that link *Evc2* to Hh signaling and to analyze how mutations in *Evc2* can lead to defective Hh signaling in the context of normal cilia. In particular, the work aimed at answering the following questions:

- 1.) The step at which *Evc2* is required has remained unknown. By using Hh reporter assays, imaging-based cilia trafficking assays, and biochemical assays for Hh pathway activation the step in Hh signaling that requires *Evc2* function had to be determined.
- 2.) It has been unknown whether *Evc2* directly interacts with Hh components. By using immunoprecipitation experiments it should be tested whether *Evc2* binds to any of the Hh proteins.
- 3.) Mutations in *EVC* and *EVC2* do not account for the totality of EvC and Weyers cases suggesting that other genes might be involved in the phenotypic manifestations of these diseases. Assuming that such genes might function together with *Evc2* an unbiased proteomic approach to identify *Evc2* binding proteins should be performed. Potential *Evc2* interaction proteins should be analyzed for their role in Hh signaling and their interplay with *Evc* and *Evc2*.
- 4.) The characteristics of the *Evc2* protein were largely unknown. The subcellular localization (both by imaging-based techniques and biochemical assays), protein topology, post-translational modifications, and protein stability should be determined.

5.) Evc2 $\Delta$ W, a mutant protein found in Weyers syndrome, was shown to be a dominant negative protein in Hh signaling. It should be determined what the molecular basis for this dominant negative effect is. Also, the difference between the molecular mechanisms causing the recessive EvC disorder and dominant Weyers disorder – both caused by mutations in Evc2 – should be analyzed.

## 2. MATERIALS AND METHODS

### 2.1 Materials

#### 2.1.1 Chemicals and Biochemicals

Smoothened Agonist (SAG)	Enzo Lifesciences, USA
20(S)-hydroxycholesterol	Steraloids Inc., USA
Cyclopamine	Toronto Research Chemicals, Canada
Cycloheximide	Sigma-Aldrich, Germany
Puromycin	Sigma-Aldrich, Germany
Hygromycin	Life Technologies, USA
Peptide: N-Glycosidase F	New England Biolabs, USA
Endoglycosidase H	New England Biolabs, USA
Dithiobis[succinimidyl propionate] (DSP)	Thermo Scientific Inc., USA
Dimethyl pimelimidate•2 HCl (DMP)	Thermo Scientific Inc., USA
n-dodecyl- $\beta$ -D-maltopyranoside (DDM)	Affymetrix Inc., USA
Deoxycholate (DOC)	Sigma-Aldrich, Germany
Sodium lauroyl sarcosinate (Sarkosyl)	Calbiochem, USA
Sodium dodecyl sulfate (SDS) 20% solution	BioRad, USA
Cholesteryl-hemisuccinate	Affymetrix Inc., USA
Tween-20	Sigma-Aldrich, Germany
Nonidet P40 Substitute	Affymetrix Inc., USA
Triton X-100	Sigma-Aldrich, Germany
SigmaFast Protease Inhibitor Cocktail	Sigma-Aldrich, Germany
Leupeptin	Sigma-Aldrich, Germany
Pepstatin	Sigma-Aldrich, Germany
Chymostatin	Sigma-Aldrich, Germany
Tris(2-carboxyethyl)phosphine (TCEP)	Thermo Scientific, USA

Other standard laboratory chemicals were purchased from Sigma-Aldrich (Germany), Merck (Germany), J.T.Baker/Covidien (USA), VWR International (USA), BioRad (USA), and Roche (Germany).

### 2.1.2 Solutions and Buffers

The buffers and solutions used in this study are listed with the description of the protocol in the Methods section below. In general, for the preparation of stock solutions and dilutions ultrapure Milipore-MiliQ water was used. Stock solutions were sterile-filtered through a 0.2  $\mu\text{m}$  filter prior to storage and usage. Glass bottles used for storage of stock solutions were sterilized in an autoclave with high-pressure saturated steam at 121 °C for 30 min.

### 2.1.3 Constructs

Mouse full-length Evc2 (NM\_145920.3) and Evc2 $\Delta$ W (a.a. 1-1176) were tagged with either a single FLAG tag or with a dual YFP-FLAG tag at the C-terminus. Mouse full-length Evc (NM\_021292.2) was tagged with a dual YFP-FLAG tag at the C-terminus. Mouse full-length Evcbp1 and Evcbp2 were both tagged with a single YFP-tag at the N-terminus. Cloning strategies were designed with Lasergene SeqBuilder software (DNASTAR, USA) and performed using standard cloning techniques including polymerase chain reaction (PCR), restriction enzyme digest, DNA ligation, and transformation in chemical competent *E.coli* bacteria (DH5 $\alpha$ ). Mutations were introduced in the full-length Evc2 or Smo constructs by inverse PCR (Ochman et al., 1988) or the QuikChange method (Agilent Technologies, USA). Oligonucleotides used for cloning of the constructs in this work were custom made by ElimBio (USA) and sequences are listed in the Appendix. All constructs were subjected to DNA sequencing (ElimBio, USA) and correct sequence was verified using the Lasergene SeqMan software (DNASTAR, USA).

The Evc2 siRNA resistant Evc2 construct was designed and synthesized by DNA2.0, USA. The construct for dominant-negative PKA was obtained from Addgene (#16716) and constructs encoding human Gli1, mouse Gli2, human Gli3, and HA-SuFu have

been described previously (Wang et al., 2000; Humke et al., 2010). Pawel Niawiadomski and Sohini Khan cloned the construct for dominant-negative Kif3a (unpublished reagent). Casey Hughes assisted with the cloning of the Evc2 mutant constructs.

#### 2.1.4 Cell lines

NIH/3T3 cells (mouse fibroblast cell line), C3H10T1/2 cells (mouse mesenchymal stem cell line), and IMCD3 cells (mouse inner medullary collecting duct cell line) were obtained from the American Type Culture Collection (ATCC). The stable cell lines expressing tagged Evcbp1, Evcbp2, Evc, Evc2 and Evc2 mutants were produced by site-specific recombination into a single site in the genome of 3T3 cells using the Flp-In system (Invitrogen/Life Technologies). Stable transductants were selected with 200 µg/ml Hygromycin. *Smo*<sup>-/-</sup>, *Smo*<sup>-/-</sup>;YFP-*Smo*, *Sufu*<sup>-/-</sup>, and *Sufu*<sup>-/-</sup>;SuFu mouse embryonic fibroblasts (MEFs) have been described previously (Svärd et al., 2006; Rohatgi et al., 2009; Humke et al., 2010). The Evc2-YFP;dnKif3a and Evc2-YFP;vector cell lines were generated by infecting Evc2-YFP cells with a retrovirus carrying dominant-negative Kif3a cloned into pRetroX-pTuner or a retrovirus carrying the empty pRetroX-pTuner vector. Stable transductants were selected in 2 µg/ml Puromycin. *Smo* deletion mutants were cloned into MSCV and stably expressed in *Smo*<sup>-/-</sup> cells using a retrovirus. Stable transductants were selected in 2 µg/ml Puromycin. See chapter 2.2.6 for details about the retroviral-based stable cell line production.

#### 2.1.5 Antibodies

Commercially available antibodies used in this work include polyclonal antibodies against Evc2 (rabbit polyclonal, sc-28393 from Santa Cruz Biotechnology, USA), GFP (for immunofluorescence: goat polyclonal, 600-101-215 from Rockland Immunochemicals, USA; for immunoblot: rabbit polyclonal, NB600-308 from Novus Biologicals, USA), LaminA, p38 (both rabbit polyclonal from Abcam, UK; ab26300 and ab7952 respectively), Gli3 (goat polyclonal, AF3690 from R&D Systems, USA), and mouse monoclonal antibodies against Gli1 (L42B10 from Cell Signaling

Technologies, USA), acetylated Tubulin, gamma Tubulin, and FLAGM2-HRP (all from Sigma-Aldrich, Germany; T6793, T6557, and A8592 respectively). Horseradish-peroxidase (HRP)-conjugated secondary antibodies used for immunoblotting were from Jackson Laboratories, USA. Secondary antibodies used for immunofluorescence coupled to the fluorophores Alexa488, Alexa594, and Alexa647 were from Invitrogen/Life Technologies, USA and those coupled to Atto425 (used for STED super-resolution microscopy) were from Rockland Immunochemicals, USA.

Polyclonal antisera against a fragment of mouse Arl13b (a.a. 208-428) was generated in guinea pigs as described in Caspary et al., 2007. Antibodies described previously include rabbit polyclonal anti-SmoN (Milenkovic et al., 2009), rabbit polyclonal anti-SmoC (Rohatgi et al., 2007), rabbit polyclonal anti-SuFu (Humke et al., 2010), GFP binding protein (GBP) (Rothbauer et al., 2008), rabbit polyclonal anti-IFT88 (Haycraft et al., 2005), rabbit polyclonal anti-Inv (Watanabe et al., 2003), rabbit serum anti-CEP164 (Graser et al., 2007), rabbit polyclonal anti-CEP290 (Chang et al., 2006), and guinea-pig polyclonal anti-Gli2 (Cho et al., 2008).

#### **2.1.6 Kits**

- QIAprep Plasmid Purification Mini Kit (Qiagen, Germany)
- QIAprep Plasmid Purification Maxi Kit (Qiagen, Germany)
- QIAQuick PCR Purification Kit (Qiagen, Germany)
- Zymoclean Gel DNA Recovery Kit (Zymo Research, USA)
- Pierce BCA Protein Assay Kit (Thermo Scientific, USA)
- SuperSignal West Femto Chemiluminescent Substrate (Thermo Scientific, USA)
- SuperSignal West Pico Chemiluminescence Substrate (Thermo Scientific, USA)
- Dual-Luciferase Reporter Assay Kit (Promega , USA)
- CDP-Star Chemiluminescence Reagent (Perkin Elmer, USA)
- QuikChange II Site-Directed Mutagenesis Kit (Agilent Technologies, USA)

### **2.1.7 Consumables**

Standard laboratory consumables including cell culture plates (21 cm<sup>2</sup>, 55 cm<sup>2</sup>, 148 cm<sup>2</sup>), multi-well (96-, 24-, 6-well) plates, disposable pipets (2 ml, 5 ml, 10 ml, 25 ml, 50 ml), filter devices (0.2 µm), centrifuge conical tubes (15 ml and 50 ml), pipet tips, and micro test tubes (PCR tubes, 0.6 ml, 1.5 ml, 2 ml, 5 ml) were from Fisher Scientific (USA) or E&K Scientific (USA). Consumables for microscopy such as cover glasses and microscopy slides were from VWR International (USA) and Fisher Scientific (USA). High performance cover glasses used for super-resolution microscopy were from Zeiss (Germany).

### **2.1.8 Instruments**

- Inverted epifluorescence microscope (DMI6000 with a high-sensitivity quantitative EM-CCD camera from Leica, Germany)
- Laser scanning confocal microscope (SP2 and SP5 from Leica Germany)
- Tissue culture fluorescence microscope (DMIL from Leica, Germany)
- Dissecting scope (Zeiss, Germany)
- Allegra X-15R centrifuge (Beckman Coulter, USA)
- Avanti J-E centrifuge (Beckman Coulter, USA)
- TL-100 ultracentrifuge (table-top) (Beckman Coulter, USA)
- Optima L-90K ultracentrifuge (Beckman Coulter, USA)
- Tecan Infinite M1000 plate reader (Tecan, Switzerland)
- Synergy H1 Hybrid multi-mode microplate reader (BioTek, USA)
- Cryostat Leica CM3050 (Leica, Germany)
- Nanodrop 2000C UV-Vis spectrophotometer (Thermo Scientific, USA)
- Ultrospec 2100pro UV-Vis spectrophotometer (GE Healthcare Biosciences, USA)
- 1300 Series A2 laminar flow hood (Thermo Scientific, USA)
- HeraCell 150i tissue culture incubator (Thermo Scientific, USA)

Other equipment used in this study was general lab equipment obtained from Thermo Scientific (USA) and VWR International (USA).

### **2.1.9 Software**

Microsoft Office (Excel, Word)

Adobe Illustrator CS2 (Graphic Design Software)

GraphPad Prism (Scientific Graphing and Statistics software)

ImageJ (Image processing program)

Leica Application Suite (LAS) (Confocal Imaging software)

AutoQuant (Deconvolution Software)

Metamorph (Microscopy Automation and Image Analysis Software)

Lasergene Suite (DNASTAR, USA)

Scaffold Viewer – Mass spectrometry visualization software (Proteome Software, USA)

## **2.2 Methods**

### **2.2.1 SDS polyacrylamide gel electrophoresis (SDS-PAGE)**

The separation of complex protein mixtures was performed using SDS-polyacrylamide gel electrophoresis according to Laemmli (Laemmli, 1970). For the SDS-PAGEs in this study a combination of 5 % stacking gel and 8 % Tris-glycine separating gel (see Table 1) was used to allow for the separation of proteins ranging in their molecular weights (MW) from ~35 to ~250 kDa. For the preparation of the polyacrylamide gels, mini format gel casters (Hoefer, USA) were used. Bis-Tris precast gels used for the separation of the samples from the tandem affinity purification and GST-Weyers affinity purification (paragraphs 2.2.11.2 and 2.2.11.3) were purchased from Life Technologies, USA.

Usually, equal amounts of protein were loaded in each well of a multi-well gel after resuspension in reducing SDS-loading buffer. Tris(2-carboxyethyl)phosphine (TCEP), which is a more stable (resistant to oxidation), odor-less, and more effective alternative to Dithiothreitol (DTT), was used as reducing agent. The SDS-PAGE was performed using a mini format vertical unit (Hoefer, USA) set to constant voltage (100 V) and ran for ~3 hours at RT.

Protein concentrations of extracts were determined using the Pierce BCA (bicinchoninic acid) protein Assay Kit (Thermo Scientific), a calorimetric assay compatible with the detergents used in this study. The kit was used according to the manufacturer's manual and samples were measured with a spectrophotometer at a wavelength of 562 nm relative to BSA standards of known concentrations.

Buffers and solutions:

5x SDS-sample buffer: 250 mM Tris-HCl pH 6.8  
 0.25% [v/v] bromophenol blue  
 50 % [v/v] glycerol  
 10% [v/v] SDS  
 → 50 mM TCEP was added freshly and the buffer was diluted 1:5 in protein extracts

SDS-PAGE running buffer: 25 mM Tris  
 192 mM glycine  
 0.1 % [v/v] SDS

	Stacking Gel (5%) – 4ml	Separating Gel (8%) – 10 ml
MiliQ-water	2.9 ml	5.3 ml
40 % Acrylamide <sup>1</sup>	0.5 ml	2 ml
1 M Tris pH 6.8	0.5 ml	-
1.5 M Tris pH 8.8	-	2.5 ml
20 % SDS	0.02 ml	0.05 ml
10 % Ammonium-persulfate (APS)	0.04 ml	0.1 ml
TEMED <sup>2</sup>	0.004 ml	0.006 ml

**Table 1:** Composition of stacking gels and separating gels used in this study. <sup>1</sup>37.5:1 ratio of acrylamide: bis-acrylamide; <sup>2</sup>Tetramethylethylenediamine.

**2.2.2 Immunoblotting and detection**

Western blotting - the transfer of proteins separated by SDS-PAGE from gel to membrane – was performed using the Criterion Blotter (BioRad, USA) according to the manufacturer's instructions. The transfer was performed using nitrocellulose membranes (BioRad, USA) for 2 hours at 110 V at 4°C in chilled transfer buffer. After completion of the transfer the successful binding of the proteins to the membrane was validated by Ponceau-S protein staining by incubation of the membrane in Ponceau-S solution (Sigma-Aldrich, Germany) for 2 min.

Proteins were detected using standard antibody detection techniques. In brief, membranes were incubated in blocking buffer for 30 min at RT, shaking. Primary antibodies were diluted in blocking buffer and incubated overnight at 4°C. Membranes were washed (3x 8 min in TBS-T) and then incubated with secondary antibodies coupled to horseradish peroxidase (HRP) diluted in blocking buffer for 1 hour at RT. After washing (3x 8 min in TBS-T) the HRP signal was detected in a dark room using film and an enhanced chemiluminescent substrate (ECL). Two substrates with different sensitivities were used depending on signal intensities: SuperSignal West Femto or Pico Chemiluminescent Substrate (both from Thermo Scientific, USA).

Buffers and solutions:

Transfer buffer:	12 mM Tris Base 96 mM glycine 10 % [v/v] methanol
Blocking buffer:	Tris-buffered saline (TBS) 0.01 % [v/v] Tween-20 5 % [w/v] milk powder
TBS-T:	Tris-buffered saline (TBS) 0.01 % [v/v] Tween-20

### **2.2.3 Antibody generation**

#### *2.2.3.1 Antigen production*

The intracellular domains of mouse Evc2 (a.a. 232-1220) or Evc (a.a. 461-1005) were expressed with an N-terminal Glutathione S-transferase- (GST) tag. A starter culture (in LB-medium) was inoculated with one colony of freshly transformed BL21 *E.coli* cells (Stratagene, USA), incubated overnight at 37°C, and diluted into 4 liters of culture the next morning. The expression was induced at OD<sub>600</sub> of 0.6 with 0.4 mM Isopropyl β-D-1-thiogalactopyranoside (IPTG) for 5 hours at RT. The cells were harvested by centrifugation (5,000xg, 20 min, 4°C) and the cell pellets were resuspended in lysis buffer, incubated for 1 hour at 4°C and homogenized by sonication. Inclusion bodies containing the antigens were pelleted by centrifugation (30,000xg, 15 min, 4°C) and washed once (PBS, 1% [v/v] Triton X-100, 10 mM β-

mercaptoethanol) with rigorous homogenization with a dounce homogenizer. Washed inclusion bodies were pelleted by centrifugation (20,000xg, 20 min, 4°C) and resuspended by dounce homogenization in 2xSDS loading buffer containing 100 mM DTT and incubated at 95°C for 10 min. Samples and a BSA standard were separated on a 8% SDS-PAGE in order to determine the concentration of the purified inclusion bodies. The antigens were separated by preparative SDS-PAGEs using single well combs. Following gel electrophoresis the gels were stained with GelCode Blue protein stain (more sensitive alternative to Coomassie Blue; Thermo Scientific, USA) and gel slices containing the antigen were cut out and stored at -80 °C.

Buffers and solutions:

LB-media:            1.0 % [w/v] tryptone  
                          0.5 % [w/v] yeast extract  
                          1.0 % [w/v] NaCl  
                          pH 7.0

Lysis buffer:        PBS  
                          2 mM MgCl<sub>2</sub>  
                          0.5 mg/ml Lysozyme  
                          1 % [v/v]  
                          1 mM AEBSF (protease inhibitor)  
                          1x protease inhibitor tables (Sigma-Aldrich)  
                          10 mM β-mercaptoethanol  
                          1 µg/ml DNase I

*2.2.3.2 Antiserum generation and antibody purification*

The antisera generation was performed by Cocalico Biologicals, USA by injection of the solubilized gel slices containing the antigens (see above). Antisera were affinity purified against the antigen containing a distinct tag from the GST-tagged version used for the immunization of the rabbits (in order to remove immunoglobulins recognizing the GST tag). Anti-Evc2W, the antibody that selectively recognizes full-length Evc2 but not Evc2ΔW, was generated by affinity purification of the antisera against the W-peptide alone.

#### **2.2.4 Cell culture**

Cell culture was performed under sterile working conditions in a laminar-flow hood. All liquids applied to cell culture were pre-warmed to 37°C prior to usage.

All the cell lines used in the present study were adherently growing cell lines. The cells were cultivated as monolayer cultures in regular cell culture medium in an atmosphere of 5 % CO<sub>2</sub> (in air) at a temperature of 37°C. Cells were grown on 55 cm<sup>2</sup> cell culture dishes in 10 ml medium and cells were subcultured at ~75% confluency. For subculturing, the medium was aspirated and the cells were rinsed once with Phosphate Buffered Saline (PBS). The addition of 0.05 % trypsin-EDTA (Life Technologies, USA) for 3-5 min allowed for the detachment of the cells. The trypsin activity was inactivated by addition of culturing media and cells were placed in new culture dishes at dilutions ranging from 1:3 to 1:10 depending on the cell line used. Cell cultures were maintained up to a passage number of 30. For plating cells at certain cell numbers the concentration of the cell suspension after trypsinization was determined using the Scepter 2.0 Handheld Automated Cell Counter (MiliQ, USA). For Hh assays cells were grown to confluence and incubated with serum starvation medium to allow for ciliation of the cells (Tucker et al., 1979). A detailed description of the Hh assays is given below (paragraph 2.2.7).

Regular cell culture medium: (all components are from Life Technologies, USA)

- Dulbecco's Modified Eagle Medium (DMEM) - high glucose
- 0.05 mg/ml penicillin
- 0.05 mg/ml streptomycin
- 2 mM GlutaMAX
- 1 mM sodium pyruvate
- 0.1 mM MEM nonessential amino acid supplement containing
- 10 % [v/v] fetal bovine serum (FBS) (HyClone).

Serum starvation medium: (all components are from Life Technologies, USA)

Dulbecco's Modified Eagle Medium (DMEM) - high glucose  
0.05 mg/ml penicillin  
0.05 mg/ml streptomycin  
2 mM GlutaMAX  
1 mM sodium pyruvate  
0.1 mM MEM nonessential amino acid supplement containing  
0.5 % [v/v] fetal bovine serum (FBS) (HyClone).

### 2.2.5 DNA transfection in mammalian cells

The transient transfection of cells was performed using Fugene6 transfection reagent (Roche, Germany). Cells were plated in regular growth medium lacking antibiotics (penicillin and streptomycin) 1 hour prior to transfection to allow the cells to adhere to the culture dish before transfection. The Fugene6 reagent was diluted in serum-free culture medium (Opti-MEM, Life Technologies, USA), incubated for 5 min at RT, followed by the addition of the construct of interest. The transfection mix was incubated for 30 min at RT before it was added drop-wise to the cells. Assays were performed 48 hours after transfection.

### 2.2.6 siRNA and esiRNA transfection

RNA interference (RNAi) is widely used to silence gene expression in living cells. It mimicks the naturally occurring mechanism in cells fighting double-stranded RNA, an intermediate product during the infection cycle of some viruses. In 2006, Andrew Fire and Craig C. Mello shared the Nobel Prize in Physiology or Medicine for their work on RNAi in *C. elegans*, which they had published in Nature in 1998 (Fire et al., 1998). The reagents for gene silencing used in this study are small interfering RNAs (siRNA), short double stranded RNA molecules which can be exogenously added to cells by transient transfection. The mechanism of gene down-regulation by siRNAs is described in Figure 8.

siRNA and esiRNA (endoribonuclease-prepared siRNAs) reagents for Evc2 (siRNA: SASI\_Mm\_01\_00106977; esiRNA: EMU014101), Smo (siRNA: SASI\_Mm\_02\_00346929, esiRNA: EMU047471) and non-targeting controls were obtained from Sigma-Aldrich, Germany. The siGENOME smart pool siRNA reagents

(a mix of 4 single siRNAs) for *Evcbp1* and *Evcbp2* were obtained from Thermo Scientific, USA.

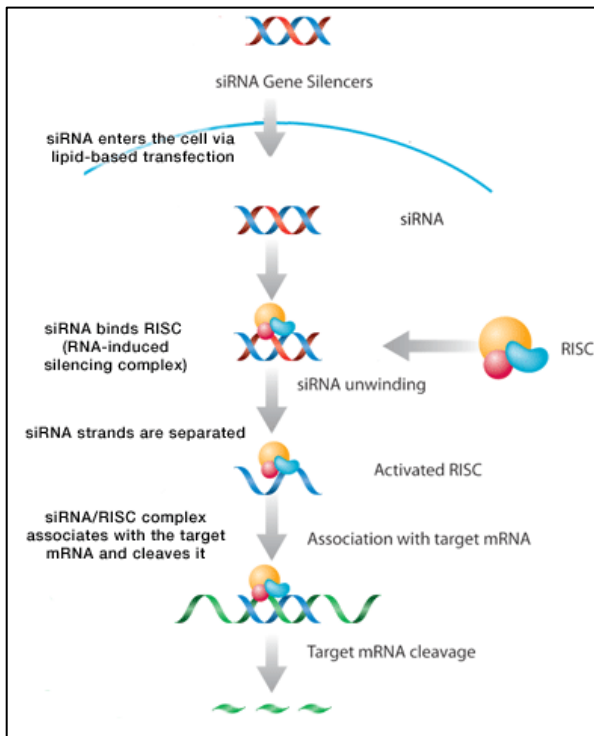


**Figure 8: Mechanism of siRNA-mediated silencing of target genes** (from Santa Cruz Biotechnology, USA).

NIH/3T3 cells were reverse transfected with 38-50 nM of siRNA or esiRNA using Lipofectamine RNAiMax (Life Technologies, USA) transfection reagent. The siRNA or esiRNA was diluted in serum-free medium (Opti-MEM, Life Technologies, USA) and incubated for 5 min at RT. The RNAiMax reagent was added, mixed, and the transfection mix was incubated for 25 min at RT. In the meantime, cells were trypsinized and diluted to the appropriate concentration. The transfection mix was added to the cell culture plate and the cell suspension was added on top. Assays were performed 48 hours after transfection.

### 2.2.7 Stable cell line production

The retroviral-based production of stable cell lines was performed as described in (Pear et al., 1993). The construct of interest cloned into MSCV (Smo-constructs) or pRetroX-pTuner (dnKif3a construct) was transfected in the virus-packaging cell line Bosc23 and 48 hours after transfection virus particles were harvested by collecting the medium. To increase the efficiency of infection 4 mg/ml polybrene was added to the virus-containing medium, which was subsequently filtered through a 0.22  $\mu$ m filter. The target cell line, in our case either *Smo*<sup>-/-</sup> MEFs or *Evc2*-YFP cells were infected with the virus-containing medium and the selection for positive transductants was started 48 hours after infection with 2 mg/ml puromycin. Single clones were combined and used as cell pools of positive expressing cells.

## 2.2.8 Assays for Hedgehog pathway activation

### 2.2.8.1 Luciferase-based Hh-reporter assay

For Hedgehog reporter assays cells were transiently transfected using Fugene6 with a mixture (4:1) of a firefly luciferase reporter driven by a Gli-responsive promoter and a constitutive renilla luciferase reporter (Sasaki et al., 1997) together with the construct of interest. Cells were grown to confluence and switched to medium containing 0.5 % FBS with pathway agonists or antagonists for 24 hours. Shh conditioned media (CM) was produced in 293T cells expressing full-length Shh as described in Taipale et al., 2000. In all cases SAG was used at 100 nM and Shh conditioned medium at a 1/4 dilution. Cells were lysed by incubation in lysis buffer for 45 min (shaking). The activity of both reporters was measured using the Dual-Luciferase Reporter Kit (Promega, USA) and read on a multi-well plate reader: The firefly luciferase was measured by addition of Luciferase Assay Reagent II (LARII). Quenching of firefly luciferase and activation of renilla luciferase was accomplished by adding Stop&Glo Reagent. The ratio of Gli-luciferase to renilla luciferase was used as a metric for Hh activity. In the graphs, each data point represents the mean of triplicate wells with error bars representing standard deviation (SD).

#### Buffers:

Lysis Buffer:	provided passive lysis buffer (5x) diluted 1:5 in MiliQ-water
LAR II Reagent:	provided Luciferase Assay Substrate resuspended in Luciferase Assay Buffer II
“Stop&Glo” Reagent:	provided “Stop&Glo” Substrate (50x) diluted 1:50 in “Stop&Glo” Buffer

### 2.2.8.2 *Gli1 protein expression*

Cells were grown to confluence in regular growth medium and then switched to medium containing 0.5 % [v/v] FBS with pathway agonists for 24 hours (unless indicated otherwise). In all cases SAG was used at 100 nM and Shh conditioned medium at a 1/4 dilution. Whole cell lysates were prepared in lysis buffer (50 mM Tris pH 7.4, 150 mM NaCl, 2 % [v/v] NP-40, 0.25 % [w/v] deoxycholate, 1 mM DTT, and 1X protease inhibitor tablets (Sigma-Aldrich, Germany)). The protein concentration of the cell lysates was determined using the BCA protein assay Kit (Thermo Scientific, USA) and 50 µg total protein were loaded per lane. Gel electrophoresis, transfer on nitrocellulose membranes, and Western detection were performed as described above.

### 2.2.8.3 *Alkaline phosphatase expression assay*

For the alkaline phosphatase expression assay (Hyman et al., 2009) C3H10T1/2 cells were transfected with siRNA reagents as described above, grown to confluence, and treated with SAG (100 nM) for 36 hours in medium containing 0.5 % [v/v] FBS. After lysis in lysis buffer for 45 min at 4°C alkaline phosphatase activity was measured using a multi-well plate reader and the CDP-Star chemiluminescence reagent (Perkin Elmer, USA). In the graphs, each data point represents the mean of triplicate wells with error bars representing standard deviation (SD).

#### Buffers and solutions:

Lysis buffer: 100 mM Tris pH 9.4  
250 mM NaCl  
25 mM MgCl<sub>2</sub>  
1% [v/v] Triton-X100

## 2.2.9 Immunofluorescence and Microscopy

### 2.2.9.1 Immunofluorescence of fixed cells

Cells were cultured on cover glasses in 24-well culture plates. After serum-starvation and treatment cells were fixed in 4 % [w/v] paraformaldehyde (PFA) in PBS for 10 min at RT and washed in PBS 3x 5 min. Fixed cells were incubated with blocking solution for 30 min at RT. Primary antibodies were diluted in blocking buffer and used to stain cells for 2 hours at RT or overnight at 4°C. After washing for 3x 5 min in PBS containing 0.1 % [v/v] Triton X-100 secondary antibodies were added in blocking buffer and incubated for 1 hour at RT in the dark. Stained cells were washed as above and mounted with DAPI-(nuclear stain) containing Mowiol anti-fade mounting medium (Nachtergaele et al., 2012).

#### Buffers and solutions:

Blocking solution:            PBS  
                                  1 % [v/v] normal donkey serum  
                                  10 mg/ml [w/v] bovine serum albumin (BSA)  
                                  0.1 % [v/v] Triton X-100

### 2.2.9.2 Mouse tissue preparation and cryo-sectioning

The mice used in this study were purchased from Charles River, USA. The mouse work was carried out at Stanford University Research Animal Facility II (RAFII) and was approved by IACUC (Institutional Animal Care and Use Committee, USA). Mice were euthanized by CO<sub>2</sub> asphyxia. E11.5 embryos were dissected from uteri under a dissecting scope in ice-cold PBS. Both embryos and kidneys from adult mice (P28) were washed in ice-cold PBS, fixed in 4% PFA in PBS for 3 hours at 4 °C and then equilibrated in 30 % Sucrose in PBS for 16 hours at 4 °C. The tissues were embedded in OCT and sectioned on a cryostat (Leica CM3050) with a 10 µm slice thickness. Sections were put on superfrost microscopy slides and were stored at -20 °C.

### *2.2.9.3 Immunofluorescence of mouse tissue sections*

Staining was performed as for cultured cells except that sections were incubated with primary antibody overnight at 4°C, the DAPI stain was performed for 10 min in PBS containing 0.1% Triton X-100 after secondary antibody incubation, and slides were mounted with Prolong Gold (Life Technologies, USA).

### *2.2.9.4 Microscopy*

Microscopy was performed on an inverted Leica SP2 or SP5 laser scanning confocal microscope or an inverted Leica DMIRE2 epifluorescence microscope. Epifluorescence images, taken as z-stacks, were deconvolved using AutoQuant deconvolution software. In all figures, cilia are oriented with their base to the left and their tip to the right. While markers of the cilia base are only shown in selected images, ciliary orientation was explicitly established using a basal body marker (gamma tubulin) in all cases. For super-resolution microscopy cells were seeded on #1.5H high precision cover glasses and processed for Immunofluorescence using secondary antibodies (Atto425 and Alexa488) compatible with 2-color STED. Images were taken as z-stacks on a Leica TCS STED CW system and deconvolved using the built-in Leica STED-2D-deconvolution software. For the quantitative analysis of fluorescence intensities, all images were obtained with identical gain, offset, and laser power settings.

### **2.2.10 Analysis of protein glycosylation**

Most proteins entering the lumen of the endoplasmic reticulum (ER) become glycosylated, most commonly by addition of the glycans to an Asparagine (N-glycans). During the directional movement of these proteins through the secretory pathway the attached oligosaccharide chains undergo massive remodeling, especially in the Golgi (Stanley, 2011). As the glycans mature they become either sensitive or resistant to highly specific glycosidases. The use of such glycosidases can be used to determine the localization of a protein along the secretory pathway (Freeze and Kranz, 2010). Two commonly used enzymes for this purpose are Peptide: N-Glycosidase F (PNGaseF) and Endoglycosidase H (EndoH). Proteins that have traversed the Golgi

apparatus remain sensitive to PNGaseF resulting in a faster mobility on a SDS-PAGE, but acquire resistance to EndoH (mobility unchanged). For the deglycosylation of proteins isolated by IP (Figure 24A) or in lysate (Figure 18A), samples were incubated overnight at 4°C with PNGaseF (1000U) or EndoH (1000U).

### **2.2.11 Subcellular fractionation**

Subcellular fractionation was used to separate cells into cytoplasmic, nuclear, and membrane fractions as described in Humke et al., 2010. The culture medium was removed by aspiration and the cells attached to the culture plate were washed in ice-cold PBS carefully to avoid the detachment of the cells. The PBS was removed and the cells were incubated for 10 min on ice with ice-cold hypotonic buffer (10 mM HEPES pH 7.9), which allows for the swelling of the cells facilitating subsequent homogenization steps. After swelling, homogenization buffer (=SEAT buffer) was added to the cells and the cells were then carefully scraped off the culture plate using a cell lifter (Corning, USA). Cells were homogenized by pushing through a 25G needle attached to a syringe for 15 times (1x = up and down). Nuclei were separated from the post-nuclear supernatant (PNS) by centrifugation at 900xg for 5 min at 4°C. Membranes were isolated from the PNS by centrifugation (95,000xg, 30 min, at 4°C). The nuclear pellet was extracted in nuclear extraction buffer and the membrane pellet in membrane extraction buffer (both for 1 hour at 4°C). All extracts were cleared by centrifugation (20,000xg, 30 min, at 4°C) prior to separation on a SDS-PAGE. For the use of the membrane extract for immunoprecipitations (IPs) the membrane lysate was subjected to centrifugation (95,000xg, 30 min, at 4°C) prior to use in IPs.

Buffers and solutions:

Swelling buffer:	10 mM HEPES, pH 7.9
Homogenization buffer (SEAT):	250 mM Sucrose 1 mM EDTA pH 8.0 10 mM triethanolamine/ acetic acid pH 7.4 10 µg/ml LPC-protease inhibitors 1x protease inhibitor tables (Sigma-Aldrich)
Nuclear extraction buffer:	20 mM HEPES pH 7.9 1 mM MgCl <sub>2</sub> 0.5 M NaCl 0.2 mM EDTA 20% [v/v] glycerol 1% [v/v] Triton X-100 1 mM DTT 10 µg/ml LPC-protease inhibitors 1x protease inhibitor tablets (Sigma-Aldrich)

Benzonase-Nuclease (Calbiochem, USA) was added to the final buffer (5 µl/ml) to prevent DNA smearing.

Membrane extraction buffer:	50 mM Tris at pH 8 150 mM NaCl 1% [w/v] n-dodecyl-β-D-maltopyranoside (DDM) 0.1 % [w/v] cholesteryl-hemisuccinate (CHS) 10 % [v/v] glycerol, 1 mM DTT 10 µg/ml LPC-protease inhibitors 1x protease inhibitor tablets (Sigma-Aldrich)
-----------------------------	---

## **2.2.12 Purification of protein complexes**

### *2.2.12.1 Immunoprecipitation*

#### *2.2.12.1.1 Preparation of anti-Evc, anti-Smo, and anti-Evc2 beads:*

For the isolation of Evc, Evc2, or Smo complexes the antibodies against those proteins (all rabbit polyclonal antibodies) were covalently coupled to Protein A Dynabeads (Life Technologies, USA) to prevent co-elution of the antibodies during the immunoprecipitation (IP) process. Dynabeads are magnetic particles designed for IP as they can easily be captured on a magnetic device making them a great alternative to sepharose beads. Dynabeads Protein A beads are Dynabeads

covalently coupled to Protein A, which specifically binds to the Fc region of immunoglobulins. Routinely, 100 µg of antibody were coupled to 400 µl of Dynabeads slurry. The antibody was diluted in conjugation buffer and added to Dynabeads (prewashed in conjugation buffer), and rotated for 1 hour at RT. Beads were equilibrated in crosslink buffer (-DMP) and the antibodies were covalently coupled to the matrix by using the crosslinker Dimethyl pimelimidate•2 HCl (DMP). Crosslinking was performed with 22 mM DMP for 30 min at RT in crosslink buffer. Washing the beads extensively with quenching buffer quenched the crosslinker and beads were stored in storage buffer at 4°C.

Buffers and solutions:

Conjugation buffer:	25 mM Citrate-phosphate buffer pH 5.0 0.1 % [v/v] NP-40
Crosslink buffer (-DMP):	200 mM Sodium-borate pH 9.0 0.1 % [v/v] NP-40
Quenching buffer:	200 mM Ethanolamine pH 8.5 200 mM NaCl 0.1 % [v/v] NP-40
Storage buffer:	200 mM Ethanolamine pH 8.5 200 mM NaCl 0.1 % [v/v] NP-40 10 % [v/v] glycerol 0.01 % [v/v] Sodium-azide 0.02

2.2.12.1.2 Preparation of anti-YFP beads:

For the purification of YFP-tagged proteins GFP binding protein (GBP) was used. GBP has been engineered as a specific binder for fluorescent proteins based on a 13-kDa GFP binding fragment derived from a llama single chain antibody and can be easily expressed in bacteria (Rothbauer et al., 2008). GBP (purified by Andres Lebenssohn) was coupled to Dynabeads M-270 Carboxylic Acid (Dynabeads-COOH). The mechanism for coupling GBP to Dynabeads-COOH involves the formation of amide bonds between primary amino groups of GBP and the carboxylic acid groups on the surface of the beads (Figure 9). Dynabeads-COOH were washed in Buffer A

and activated with 25 mg/ml EDC and 25 mg/ml Sulfo-NHS (diluted in Buffer A; both from Thermo Scientific, USA) for 15 min at 4°C. Beads were washed in coupling buffer and GBP was coupled to the activated beads for 30 min at 4°C. After quenching in quenching buffer overnight at 4°C, beads were stored in storage buffer.

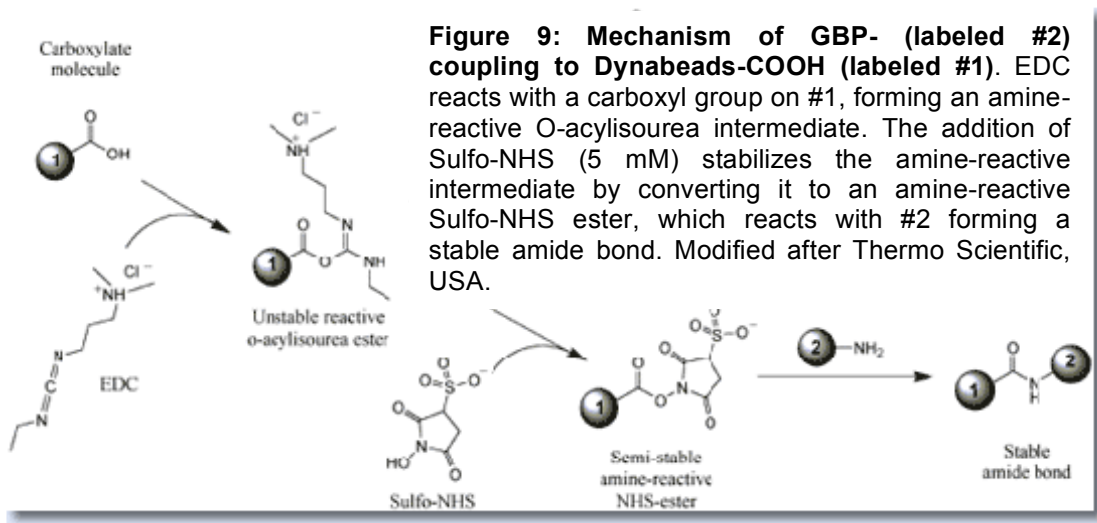
Buffers and solution:

Buffer A: 0.1 M MES pH 6.0  
0.5 M NaCl  
0.01 % [v/v] SDS

Coupling buffer: 0.1% [v/v] Tween-20 in PBS pH 7.4

Quenching buffer: 0.2 M Ethanolamine pH 8.5  
0.15 M NaCl  
0.1% [v/v] Tween-20

Storage buffer: Coupling buffer supplemented with 10 % [v/v] glycerol and 0.01 % [v/v] Sodium-azide



2.2.12.1.3 Co-Immunoprecipitation (IP) protocol:

IP is a standard assay used to purify an antigen from a complex mixture of soluble proteins and is a method routinely used to study protein complexes. The standard protocol includes 3 steps: Capturing the antigen on the antibody-matrix (in our case antibodies coupled to Dynabeads), washing to prevent non-specific binding of proteins to the matrix and the antibody, and elution of the bound protein complexes.

For the protocol used in this study either whole cell extracts or membrane extracts were incubated with antibodies covalently coupled to Dynabeads. The preparation of DSP-crosslinked whole cell lysates was prepared as described in paragraph 2.2.13 and the membrane extracts as in paragraph 2.2.10. Extracts were incubated with antibody-coupled beads overnight at 4°C, rotating. After washing the beads in IP-buffer, proteins were eluted in a reducing SDS-sample buffer. In all cases the SDS-eluate and aliquots of the sample prior (Input) and after (flow-through, FT) IP were loaded on a SDS-PAGE.

Buffers and solutions:

IP-buffer (for IPs from DSP-crosslinked lysates):

- 50 mM Tris pH 7.4
- 300 mM NaCl
- 2% [v/v] NP-40
- 0.25% [w/v] deoxycholate
- 10 µg/ml LPC-protease inhibitors
- 1x protease inhibitor tablets (Sigma-Aldrich)

IP-buffer (for IPs from membrane fractions):

- 50 mM Tris pH 8, 150 mM NaCl
- 1% [w/v] n-dodecyl-β-D-maltopyranoside (DDM)
- 0.1% [w/v] cholesteryl-hemisuccinate (CHS)
- 10% [v/v] glycerol
- 10 µg/ml LPC-protease inhibitors
- 1x protease inhibitor tablets (Sigma-Aldrich)

*2.2.12.2 Tandem-affinity purification (TAP)*

The TAP strategy has been developed by Rigaut et al., 1999 and is a method well suited for the identification of protein interaction partners. A target protein expressed with a dual tag, in our case FLAG-YFP, and associated proteins are purified in a two-step process. This allows for the recovery of highly purified protein complexes that can be subsequently identified by mass spectrometry.

For the large scale TAP strategy used to identify Evc2 interaction partners, membrane fractions of Evc2-YFP-FLAG cells (from 100x 148 cm<sup>2</sup> culture plates) were prepared according to the protocol described above and extracted in TAP-lysis buffer. The extract was incubated overnight with FLAGM2-Sepharose beads (Sigma-Aldrich, Germany). The beads were sequentially washed with TAP-Lysis buffer, TAP-Wash Buffer 1-2 and incubated in FLAG Elution buffer for 4 hours at 4°C. The first FLAG eluate was collected (FLAG-E1) and fresh FLAG elution buffer was applied and incubated with the beads for 1 hour at RT (FLAG-E2). FLAG-E1 and FLAG-E2 were combined and Evc2-FLAG-YFP complex were further purified by an anti-YFP IP for 2 hours at 4°C. The anti-YFP beads were washed with TAP-Wash Buffer 3 and proteins were eluted in reducing SDS-sample buffer containing 50 mM TCEP for 30 min at 37°C. Samples were separated on a 4-12 % Bis-Tris precast gel (Life Technologies, USA) and on SDS-PAGE. The gels were stained with GelCode Blue protein stain (Thermo Scientific, USA), prominent bands were cut in the laminar flow hood to prevent contamination with keratins and gel slices were analyzed by mass spectrometry (MS Bioworks, USA).

Buffers and solutions: SAG (100 nM) was maintained in all the buffers

TAP-Lysis buffer:	50 mM Tris pH 8.0 150 mM NaCl 1 % [w/v] n-dodecyl- $\beta$ -D-maltopyranoside (DDM) 0.1 % [w/v] cholesteryl-hemisuccinate (CHS) 1 mM EGTA pH 8.0 1 mM EDTA pH 8.0 10 % [v/v] glycerol, 1 mM DTT, 10 $\mu$ g/ml LPC, 1x protease inhibitor tablets (Sigma-Aldrich) 1 mM Sodium fluoride 1 mM Sodium vanadate 1 $\mu$ M Mycrocystin LR
TAP-Wash Buffer 1:	is the same as TAP-lysis buffer, but contains more NaCl (300 mM) and less detergent (0.1 % [w/v] DDM, 0.01 % [w/v] CHS)
TAP-Wash Buffer 2:	is the same as TAP-lysis buffer, but contains less detergent (0.1 % [w/v] DDM, and 0.01 % [w/v] CHS)
FLAG Elution Buffer:	is the same as TAP-Wash Buffer 2 substituted with 200 $\mu$ g/ml 3xFLAG peptide (Sigma-Aldrich, Germany).

### 2.2.12.3 Affinity Purification

#### 2.2.12.3.1 Matrix preparation

GST alone and the fragment of Evc2 missing in Evc2 $\Delta$ W (W-peptide) tagged with a N-terminal GST-tag were expressed in BL21 *E.coli* cells as described in paragraph 2.2.1. Cell pellets of 2x 1 liter cultures each were lysed in lysis buffer (incubation for 1 hour at 4°C, sonication) and extracts were cleared by centrifugation (100,000xg, 30 min, 4°C). Supernatants containing GST or GST-W-peptide were normalized to contain equal protein amounts and filtered through 0.2  $\mu$ m filters and lysates were applied to Glutathione Sepharose resin (GE Healthcare, USA), rotating for 2 hours at 4°C. After serial washing steps in wash buffer A and B the resin with bound GST or GST-W-peptide was stored at 4°C in storage buffer.

Buffers and solutions:

Lysis buffer:	50 mM Tris pH 8.0 500 mM NaCl 5 mM MgCl <sub>2</sub> 0.5 mg/ml Lysozyme 1 % [v/v] Triton X-100 10 mM DTT 10 µg/ml LPC 1x protease inhibitor tables (Sigma-Aldrich) 10 mM b-mercaptoethanol 1 µg/ml DNase I 10 % [v/v] glycerol
Wash buffer A:	PBS, 1 % [v/v] Triton X-100, 1 mM DTT
Wash buffer B:	PBS, 1 M NaCl, 1 mM DTT
Storage buffer:	PBS, 50 % [v/v] glycerol, 0.1 % [v/v] NP-40, 1 mM DTT

2.2.12.3.2 Affinity purification

NIH/3T3 cells (50x 148 cm<sup>2</sup> culture plates) were resuspended in lysis buffer and homogenized with a dounce homogenizer. Nuclei were removed by centrifugation (500xg, 5 min at 4°C) and the lysate was cleared by centrifugation (100,000xg, 30 min at 4°C) and filtration through a 0.2 µm filter. The extract was pre-cleared by incubation (in batch) with the GST resin for 1 hour at 4°C, gently rotating. The supernatant was removed and subsequently incubated with the GST-W-peptide resin overnight at 4°C, gently rotating. After washing in high salt washing buffer and low salt washing buffer both resins were eluted by sequential incubation with Sarkosyl elution buffer (2 times), High salt elution buffer (2 times), and Glutathione elution buffer (2 times). The eluates were concentrated using protein concentrator tubes (Thermo Scientific, USA) before separation on 4-12 % Bis-Tris precast gels (Life Technologies, USA). Gels were stained with GelCode Blue protein stain (Thermo Scientific, USA) and prominent bands were cut in a laminar flow hood to prevent contamination with keratins. Gel slices were send to mass spectrometry analysis performed by MS Bioworks, USA.

Buffers and solutions

Lysis buffer:	50 mM HEPES-KOH pH 7.4 150 mM KCl 0.2 % [v/v] NP-40 1 mM MgCl <sub>2</sub> 1 mM EDTA 1 mM EGTA 1 mM AEBSF (protease inhibitor) 10 µg/µl LPC-protease inhibitors 1x protease inhibitor tables (Sigma-Aldrich) 1 mM DTT 10 % [v/v] glycerol 10 µg/ml Cytochalasin D (inhibitor of actin polymerization)
High salt washing buffer:	same as lysis buffer, but contains more KCl (250 mM)
Low salt washing buffer:	same as lysis buffer, but contains no KCl
Sarkosyl elution buffer:	50 mM HEPES-KOH pH 7.4 100 mM NaCl 0.3 % [v/v] Sarkosyl 1 mM EDTA 1 mM DTT 10 % [v/v] glycerol
High salt elution buffer:	50 mM HEPES-KOH pH 7.4 2500 mM NaCl 1 mM EDTA 1 mM DTT 10 % [v/v] glycerol
Glutathione elution buffer:	50 mM Tris pH 8.0 150 mM NaCl 20 mM Glutathione 0.2 % [v/v] NP-40 1 mM DTT 10 % [v/v] glycerol

### 2.2.13 Mass spectrometry

The samples of the Evc2-TAP-purification and the GST-W-peptide affinity purification were sent as gel slices to MS Bioworks (Ann Arbor, USA) for mass spectrometry analysis where they were subjected to Trypsin digestion. Each gel digest was analyzed by nano LC/MS-MS. Data processing was performed using Mascot software (Matrix Science, USA) using the SwissProt mouse database.

### 2.2.14 DSP crosslink of cultured cells

Chemical crosslinking can be used to stabilize transient protein-protein interactions during IP experiments. In this study Dithiobis[succinimidyl propionate] (DSP; Lomants reagent) was exclusively used as crosslinker for this purpose as it is cell permeable and reversible. DSP contains an amine-reactive N-hydroxysuccinimide (NHS) ester at each end of an 8-carbon spacer arm. NHS esters react with primary amines of proteins and form stable amide bonds. The disulfide bond in the middle of the spacer arm can be cleaved by reducing agents such as DTT or TCEP, which makes it a reversible crosslink agent.

In order to crosslink proteins prior to IP, cells attached to the culture dish were washed with D-PBS (PBS, 1 mM CaCl<sub>2</sub>, 1 mM MgCl<sub>2</sub>) and incubated with 0.1 mM DSP in D-PBS for 30 min on ice. Following DSP inactivation (100 mM Tris pH 7.4, 30 min, on ice), cells were harvested and lysed in a DTT-free DSP-lysis buffer. After incubation of this extract with antibody-coupled beads, proteins were eluted and crosslinks were reversed with a reducing SDS-sample buffer containing 50 mM TCEP.

#### Buffers and solutions:

DSP-lysis buffer: 50 mM Tris pH 7.4  
150 mM NaCl  
2% [v/v] NP-40  
0.25% [w/v] deoxycholate  
10 µg/ml LPC  
1x protease inhibitor tablets (Sigma-Aldrich)

### 2.2.15 *In situ* proximity ligation assay

The proximity ligation *in situ* assay (PLA or DUOLINK™) allows for the visualization of protein-protein interactions in samples prepared for microscopy. A pair of oligonucleotide-labeled secondary antibodies (PLA probes) only generates a signal (by rolling circle amplification) if the two primary antibodies they are binding two (and thus the two proteins of interest) are in close proximity. The PLA signals can be then assigned to a specific location by microscopy.

For the PLA assay Evc2-YFP or Evc2 $\Delta$ W-YFP cells were treated with or without SAG (100 nM) for 2 hours prior to fixation in 4% PFA. Fixation, blocking, and incubation with primary antibodies (anti-SmoC and anti-YFP) was performed as described in paragraph 2.2.8.1. PLA probes were diluted in blocking buffer and incubated for 1 hour at 37°C. After washing in wash buffer A (3x 5 min) samples were incubated with ligation solution for 30 min at 37°C. The coverslips were washed (2x 2 min wash buffer A) and incubated with the amplification solution for 100 min at 37°C. After the final washing steps (2x 10 min wash buffer B, 1x 1 min 0.1x wash buffer B) the coverslips were dried and mounted with the supplied Duolink II mounting media. Images were taken at the Leica epifluorescence microscope. Quantitation was performed by counting the number of PLA signals (red dots in Figure 24D) that overlapped with the endogenous fluorescence of Evc2-YFP or Evc2 $\Delta$ W-YFP at cilia.

#### Buffers and solutions:

PLA-probes:	provided by the kit; dilute 1:5 in blocking solution (1 % [v/v] normal donkey serum, 10 mg/ml bovine serum albumin (BSA), 0.1 % [v/v] Triton X-100 in PBS)
Ligation solution:	provided by the kit; dilute 5x Ligation stock 1:5 in MiliQ-water and add Ligase at 1:40 dilution.
Amplification solution:	provided by the kit; dilute 5x Amplification stock 1:5 in MiliQ-water and add Polymerase at 1:80 dilution.
Wash buffer A:	provided by the kit; dissolve content of one pouch in 1 liter of MiliQ-water; store at 4°C.
Wash buffer B:	provided by the kit; dissolve content of one pouch in 1 liter of MiliQ-water; store at 4°C.

## 2.2.16 Data analysis

### 2.2.16.1 Microscopy

For the quantitative analysis of fluorescence intensities, all images were obtained with identical gain, offset, and laser power settings. To measure the fluorescence intensities of Smo, Gli2, Gli3, Evcbp1, and Evcbp2 at primary cilia the ImageJ imaging-software was used by outlining the cilium and using the integrated density function. Data were imported into GraphPad Prism for graphing and statistical analysis. To assess statistical significance one-way ANOVA with a Tukey post-test was used. In addition, median fluorescence data was compared with a Kruskal-Wallis test to avoid assumptions about the normality of the underlying distribution. There was no difference between the two tests. In all the graphs mean fluorescence intensity  $\pm$  confidence interval (CI) is plotted.

For the single-cell analysis of the ciliary localization of YFP-tagged Smo or Evc2 mutants (Figures 20 and 21) whole-cell YFP immunofluorescence intensity (taken as a measure of protein expression) was measured by outlining the entire cell and using the integrated density function of ImageJ. In the same cell, the localization of Smo or Evc2 was classified as absent, present in EvC Zone, or present throughout the whole cilium. The mean fluorescence derived from measurements of multiple cells reflects the average protein expression in the cell population.

### 2.2.16.2 Western blots

Films were scanned with the Epson Perfection V700 Photoscanner as grayscale TIFF files (600 dpi). Quantitative analysis of band intensities was performed with ImageJ using the gel lane tool and the data were transferred to GraphPad Prism for analysis. To calculate the fraction of GliFL in the nucleus or cytoplasm (Figure 15), we calculated the ratios  $N/(N+C)$  and  $C/(N+C)$ , where N and C are intensities of the GliFL band in nuclear and cytoplasmic fractions, respectively.

## 3. RESULTS

### 3.1 Evc2 is required for Hedgehog signaling at a step between Smoothened and PKA/SuFu

#### 3.1.1 The function of Evc2 in fibroblasts

In order to dissect the mechanistic role of Evc2 in Hedgehog (Hh) signaling NIH/3T3 mouse fibroblast cells were used. These cells are well suited for this purpose as they robustly activate Hh target genes such as *Gli1* when exposed to Hh ligands, demonstrate dynamic trafficking of Hh pathway components to cilia, and allow for facile genetic manipulation of pathway components for mechanistic studies (Rohatgi et al., 2009; Humke et al., 2010). In order to mimic the recessive EvC syndrome caused by loss-of-function mutations in both alleles of *Evc2*, cellular levels of Evc2 were reduced by RNA interference. NIH/3T3 cells were transiently transfected with an Evc2 siRNA and effects on target gene expression were assayed as an output of Hh activity. The siRNA-mediated depletion of Evc2 inhibited the Shh-triggered induction of Gli1, a direct Hh target gene (Figure 10A) similar to cells depleted of Smo. A general concern with RNA interference strategies is their specificity as off-target activity is often an issue. Thus, the following controls were used to exclude that off-target effects of the Evc2 siRNA are causing the reduction of Gli1 protein levels: the effect on Gli1 protein levels was dose-dependent (Figure 10B) and was also seen if an esiRNA (Endoribonuclease-prepared siRNA) against a distinct region in the Evc2 mRNA was used (Figures 10C and D). In addition, the effect can be rescued by the co-expression of a siRNA-resistant Evc2 construct, which was synthesized harboring mutations only within the Evc2 siRNA target sequence (on nucleotide level) leaving the amino acid sequence unaffected (Figure 10E).

Furthermore, the siRNA-mediated depletion of Evc2 inhibited the Hh-triggered induction of Gli1 in a different system than NIH/3T3 cells. C3H10T1/2 pluripotent mesenchymal cells respond to the Hh signal by differentiation into osteoblasts, which

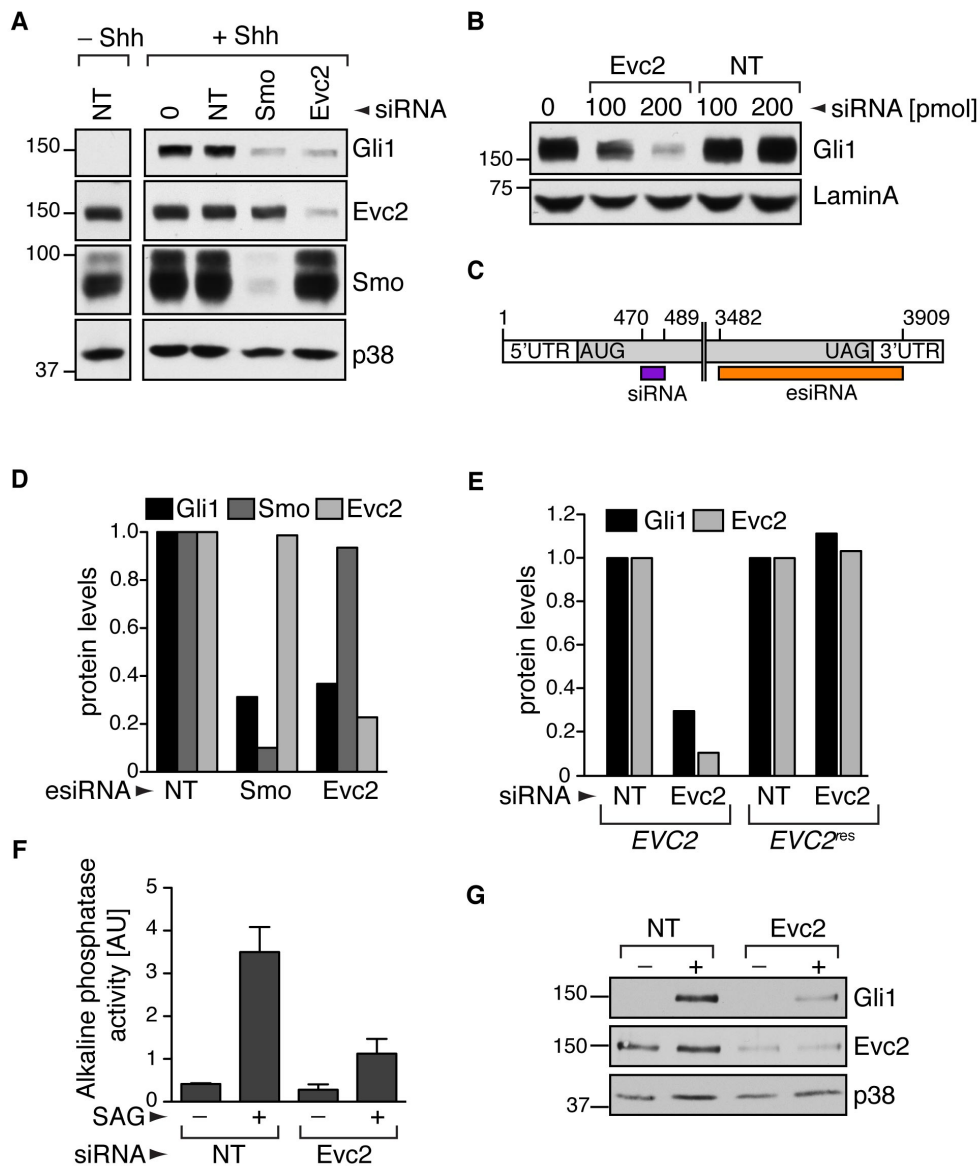


**Figure 10: Evc2 is a positive regulator in Hh signaling.** (A) Gli1 induction was used to measure Shh-triggered signaling in NIH/3T3 cells transfected with a non-targeting (NT) siRNA or siRNAs targeting Evc2 and Smo. (B) Dose-dependent effect of the Evc2 siRNA on Shh-induced Gli1 protein levels. (C) Distinct regions of the Evc2 mRNA targeted by the single siRNA used in A and B and the esiRNA used in D. (D) EsiRNAs against both Smo and Evc2 can block Shh-driven Gli1 induction compared to a NT control. The levels of Gli1, Evc2, and Smo protein were measured from an immunoblot (IB), normalized to a loading control (p38), and shown relative to levels in cells transfected with a NT control (set to 1.0). (E) Rescue of the Evc2 siRNA's inhibitory effect on Hh signaling by a siRNA-resistant Evc2 gene (*Evc2<sup>res</sup>*). NT or Evc2 siRNAs were transfected into cells stably expressing a wild-type Evc2 gene or an *Evc2<sup>res</sup>* gene. Gli1, Evc2, and p38 protein levels were measured from an IB after treatment with Shh. (F,G) The siRNA-mediated depletion of Evc2 from C3H10T1/2 cells blocks Hh signaling triggered by the Smo agonist SAG (36 hours). Hh signaling was measured in the same experiment by Gli1 induction (F) and by the differentiation of these cells into osteoblasts assayed by increase in alkaline phosphatase activity (mean  $\pm$ SD) after treatment with the Smo agonist SAG (36 hours) (G).

can be assayed by expression of alkaline phosphatase (Hyman et al., 2009). Consistent with the results found in NIH/3T3 cells, the siRNA-mediated depletion of Evc2 in C3H10T1/2 cells also blocked Gli1 induction as well as the Hh-induced differentiation into osteoblasts (Figures 10F and G).

In contrast to EvC, Weyers is a dominant syndrome caused by specific mutations that delete the last 43 amino acids (a.a.) at the C-terminus of Evc2, generating a dominant-negative protein that can inhibit Hh signaling (Valencia et al., 2009). Hereafter, this truncated protein is called Evc2 $\Delta$ W and the fragment missing in this protein is referred to as the Weyers peptide (W-peptide). In order to mimic the Weyers syndrome, NIH/3T3 fibroblast cell lines were generated stably expressing full-length Evc2 or Evc2 $\Delta$ W, each tagged with a dual YFP-FLAG tag. A schematic of both proteins and their domain structure including the TM domain close to the N-terminus is shown in Figure 11A. For the generation of these cell lines the FlpIn system from Invitrogen was used, which allowed for Flp recombinase mediated single, site-directed insertion of the Evc2 constructs. In these cell lines Evc2 and Evc2 $\Delta$ W are expressed at levels similar to endogenous Evc2 (Figure 11B). As predicted by the genetics of the Weyers syndrome, the expression of Evc2 $\Delta$ W produced a near-total block of Hh signaling stimulated by the direct Smo agonist SAG assayed by Gli1 induction (Figure 11C). To ensure that the large YFP-FLAG tag did not interfere with Evc2 function, the effect of Evc2 $\Delta$ W was confirmed in stable cell lines expressing Evc2 or Evc2 $\Delta$ W tagged with a single FLAG epitope (Figures 11A and D). Given their identical behavior, both sets of stable cell lines were used interchangeable and are referred to as Evc2 and Evc2 $\Delta$ W cells.

Taken together, both siRNA-based loss-of-function and dominant-negative expression confirmed the critical role of Evc2 in Hh signaling and established the Evc2 $\Delta$ W cell line as a relevant model for dissecting the mechanistic role of Evc2.

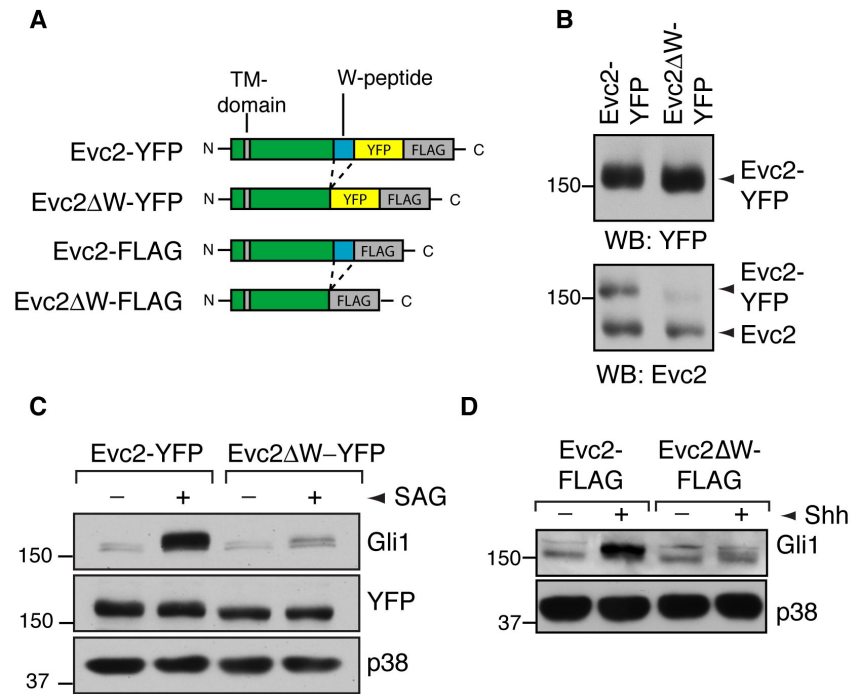


**Figure 11: Evc2ΔW is a dominant-negative protein in Hh signaling.** (A) Schematic of the Evc2 and Evc2ΔW proteins used to make stable cell lines. Evc2ΔW lacks the Weyers peptide (blue) at the C-terminus. TM = trans-membrane. (B) Evc2-YFP and Evc2ΔW-YFP were expressed at similar levels in stable cell lines (top, anti-YFP blot) and Evc2-YFP and endogenous Evc2 were present at similar levels (bottom, anti-Evc2 blot). Anti-Evc2 recognized Evc2ΔW-YFP poorly. (C) SAG (12 hours) induced Gli1 protein expression in Evc2-YFP cells but not in Evc2ΔW-YFP cells. (D) Shh-induced (16 hours) Gli1 protein levels were decreased in cell lines stably expressing Evc2ΔW-FLAG compared to Evc2-FLAG cells.

### 3.1.2 Evc2 is not required for cilia formation in fibroblasts

As cilia are critical for proper Hh signal transduction a likely explanation for the inhibitory effects of Evc2 depletion or Evc2ΔW expression on Hh signaling was a defect in cilia structure or function. However, neither the number of ciliated cells nor the lengths of cilia was affected in cells transfected with Evc2 siRNA or in cells expressing Evc2ΔW (Figures 12A-D). In addition, the functionality of cilia was tested by looking at the localization of three proteins known to localize and function in cilia in multiple systems: Ift88, Arl13b, and Inv (Pazour et al., 2000; Watanabe et al., 2003; Caspary et al., 2007). Immunofluorescence staining for all three proteins demonstrated indistinguishable localization in cilia of Evc2 and Evc2ΔW cells (Figures

12E-G). The interesting observation that inhibition of Evc2 function did not affect general cilia structure or function but yet severely inhibited Hh signaling, provided a unique opportunity to understand how a ciliopathy protein can regulate Hh signaling in the context of otherwise normal cilia.

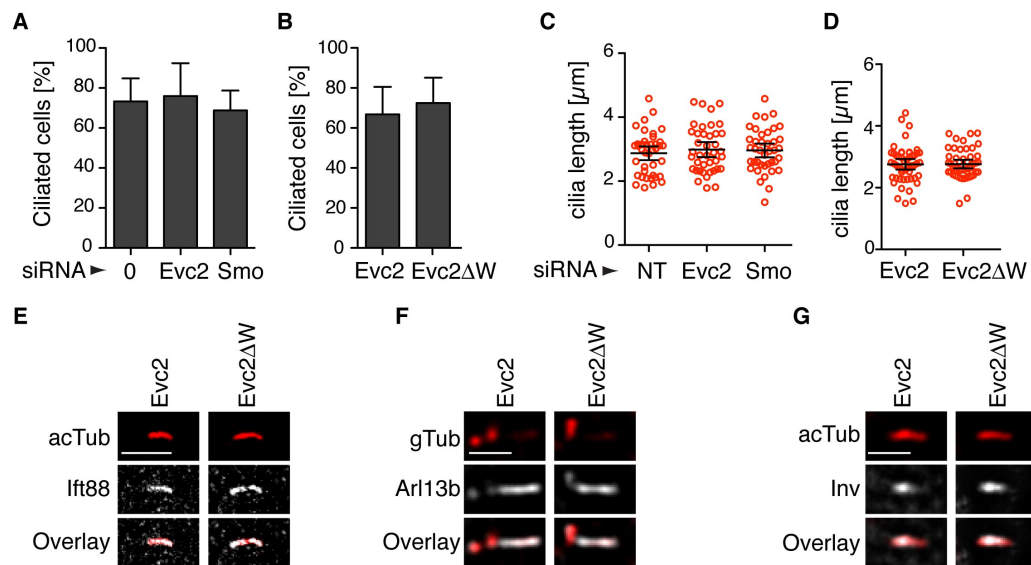


**Figure 12: Evc2 is not required for cilia formation and function in fibroblasts.** (A-D) The frequency of ciliation (A,B) and the lengths of cilia (C,D) were both unaffected in cells depleted of Evc2 by siRNA (A,C) or expression of Evc2ΔW (B,D). Bars in (A) and (B) indicate the mean ( $\pm$  SD) percentage of cells with cilia. Each red point in (C) and (D) represents a single cilium, and error bars indicate the mean length ( $\pm$  95% CI) with  $n=40$ . (E-G) Immunofluorescence (IF) was used to localize Ift88, Arl13b, and Inv (all white) relative to ciliary landmarks (red) in Evc2-YFP and Evc2ΔW-YFP cells. The ciliary axoneme was detected with anti-acetylated tubulin (acTub) and basal bodies with anti-gamma tubulin (gTub). Scale bar: 2.5  $\mu$ m.

### 3.1.3 Evc2 localizes to a novel compartment in the primary cilium

EvC and Weyers syndromes have been classified as ciliopathies on the basis of a report that both Evc2 and Evc localize to basal bodies of primary cilia (Blair et al., 2011). It was confirmed that both endogenous Evc2 and stably expressed Evc2-YFP localized in a punctate pattern near the base of the ciliary axoneme regardless of Hh pathway activity in NIH/3T3 fibroblasts (Figures 13A-D). In order to further characterize the sub-ciliary localization of Evc2-YFP its localization relative to a series of markers for known ciliary compartments such as the basal body, the transition zone (TZ), and the Inv compartment was analyzed. In contrast to the previous reports, Evc2 was clearly not localized at the basal body as determined by gamma tubulin staining (Figure 13D). Instead, it was found just distal to CEP164 and CEP290, both markers for the TZ (Graser et al., 2007; Craige et al., 2010). Consistent with Evc2 being a membrane protein (Figure 11A; see also Figure 31D) and analogous to some TZ proteins, Evc2 formed a ring-like collar around the axoneme as determined by super-resolution microscopy (Figure 13C). Evc, the second protein mutated in EvC syndrome and also a single-pass TM protein, precisely co-localized with Evc2 (Figure 13E). The distinct ciliary compartment where both Evc and Evc2 localized to was hereafter named the “EvC Zone”. The EvC Zone was defined as a region within the primary cilium that sits between – and is partially overlapping with – the TZ and the Inv compartment. This region is likely a general feature of primary cilia since endogenous Evc and Evc2 display a very similar localization pattern at the cilia base in other cell lines such as epithelial cells (IMCD3 cells) and mesenchymal cells (C3H10T1/2 cells) (Figure 13F). Importantly, the Evc and Evc2 staining pattern was also observed in primary tissues such as adult kidney and embryonic E11.5 limb mesenchyme (Figure 13G and H).

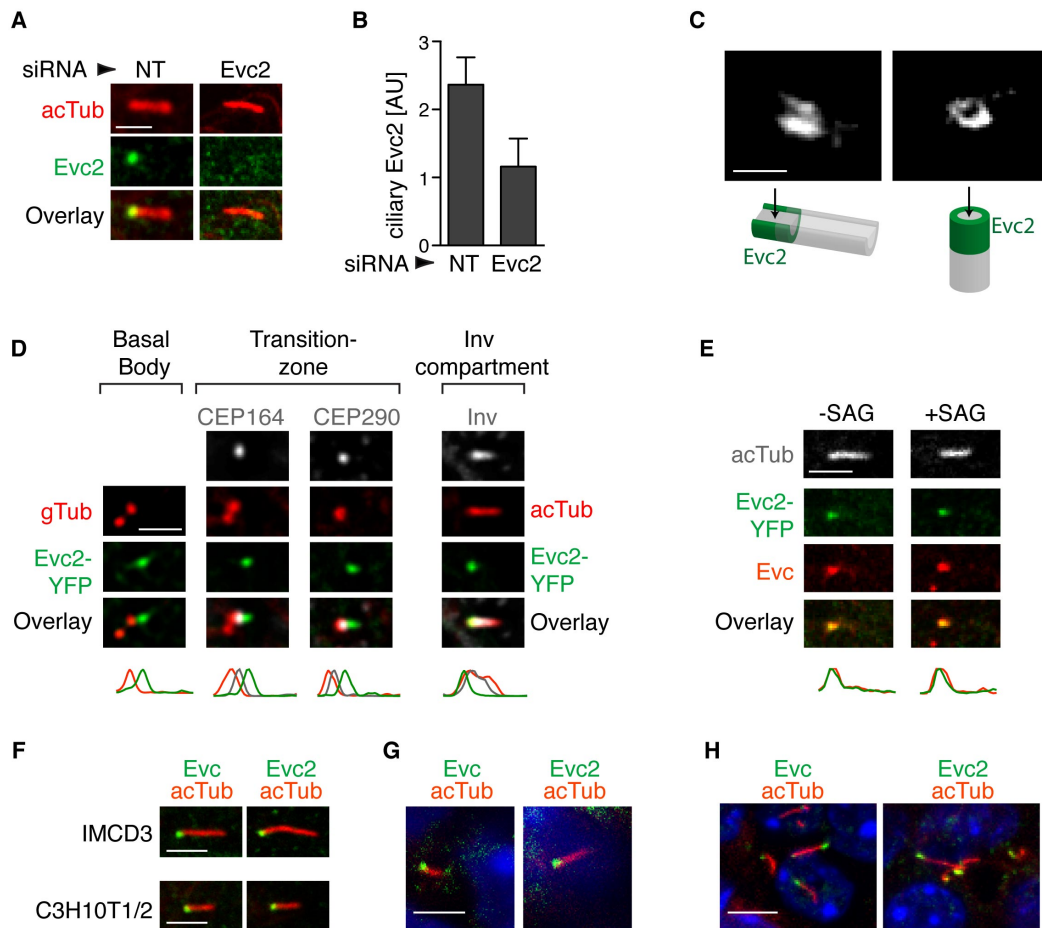


**Figure 13: Evc2 is localized at the EvC Zone in primary cilia.** (A) Localization of endogenous Evc2 (anti-Evc2, green) at cilia (red) marked by anti-acetylated tubulin (acTub) in NIH/3T3 cells. Mean ( $\pm$  95% CI,  $n=24$ ) Evc2 fluorescence at cilia from such images is shown in (B). Scale bar: 2.5  $\mu$ m. (C) Images of Evc2-YFP localization captured by STED microscopy. Scale bar 0.5  $\mu$ m. (D) Localization of stably expressed Evc2-YFP (anti-YFP, green) relative to markers of various ciliary compartments. Plots below the images indicate normalized fluorescent intensities for each of the channels along the cilium from base (left) to tip (right). Scale bar 2.5  $\mu$ m. (E) Localization of Evc2-YFP (green) and endogenous Evc (red) at cilia (white) in cells exposed to SAG (2 hours). Scale bar: 2.5  $\mu$ m. (F) Localization of endogenous Evc and Evc2 (both green) at cilia (red) in kidney epithelial (IMCD3) cells (top) and multipotent mesenchymal C3H10T1/2 cells (bottom). Scale bars: 2.5  $\mu$ m. (G,H) Localization of endogenous Evc and Evc2 (both green) at cilia (red) in sections from the hind limbs of E11.5 mouse embryos (G) or from the kidneys of postnatal (P28) mice (H). Nuclei in these tissues are stained with DAPI (blue). Cilia in (G) belong to mesenchymal cells of the developing limb and cilia in (H) belong to epithelial cells of tubules in the renal medulla. Scale bar: 2.5  $\mu$ m in (G) and 5  $\mu$ m in (H).

### 3.1.4 Identification of the step in Hedgehog signaling that requires Evc2

The step in Hh signaling impaired in EvC and Weyers was unknown. One possible explanation for the reduced Gli1 levels in Evc2 $\Delta$ W cells was a difference in either the expression level or the half-life of any of the Hh pathway components. In order to test whether this was the case Evc2 and Evc2 $\Delta$ W cells were treated with cycloheximide, which is a potent inhibitor of protein synthesis and a drug often used to determine a protein's half-life. The expression of Evc2 $\Delta$ W did not affect the levels of endogenous Evc2 or several key Hh pathway proteins (Figure 14A).

In order to identify the step in Hh signaling at which Evc2 is important, the pathway was activated at various levels and the effect of Evc2 $\Delta$ W expression was monitored. First, cells were treated with Shh, which activates the pathway at the level of Ptc1, and with SAG or 20-hydroxycholesterol, which both activate Smo (Chen et al., 2002; Nachtergaele et al., 2012). In all three cases, Evc2 $\Delta$ W blocked signaling (Figure 14B). Strikingly, Evc2 was also required for Hh signaling initiated by a constitutively active oncogenic mutant of Smo, SmoM2 (Figure 14C) (Xie et al., 1998). The precise signaling events downstream of Smo remain poorly understood, but depend on the negative regulators PKA and SuFu. Dominant-negative PKA (dnPKA) activated Hh target gene transcription to equal degrees in both Evc2 and Evc2 $\Delta$ W cells (Figure 14D). Mouse embryonic fibroblasts (MEFs) lacking SuFu (*Sufu*<sup>-/-</sup> cells) show high levels of Hh target gene transcription consistent with activated signaling (Svärd et al., 2006). Hh reporter gene activity in *Sufu*<sup>-/-</sup> cells was unaffected by the expression of either Evc2 or Evc2 $\Delta$ W; re-introduction of SuFu into these cells restored the dominant-negative effect of Evc2 $\Delta$ W (Figure 14E). Taken together these data suggest that Evc2 is important at a step in Hh signaling at the level or downstream of Smo and upstream of SuFu and PKA.

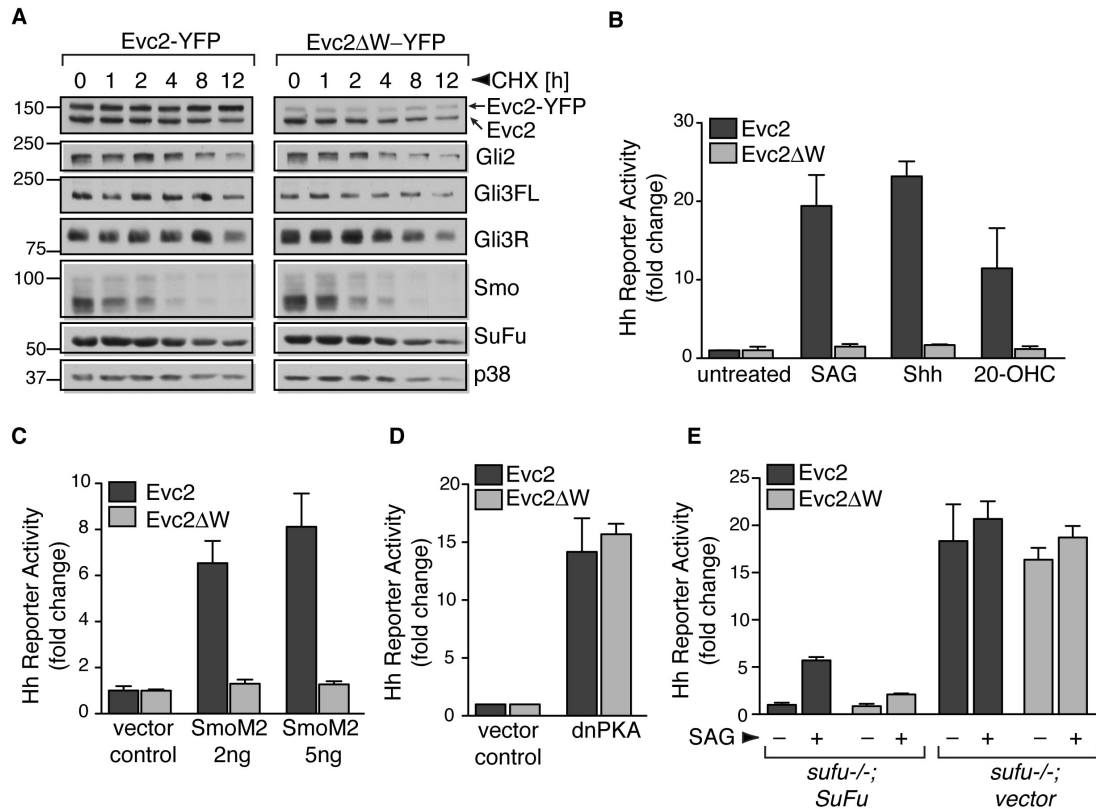


**Figure 14: Evc2 is required for Hh signaling at a step between Smo and PKA/SuFu.** (A) Levels of endogenous Evc2, Gli2, Gli3, SuFu, Smo, and the non-Hh protein p38 in Evc2-YFP and Evc2 $\Delta$ W-YFP stable cell lines at baseline (t=0) or after blockade of translation with cycloheximide (100  $\mu$ g/ml) for various periods of time. (B) Hh reporter activity in response to SAG, Shh, or 20-OHC (10  $\mu$ M) in cells stably expressing Evc2 or Evc2 $\Delta$ W. (C-D) Hh reporter activity measured in Evc2 or Evc2 $\Delta$ W cells transiently transfected with constitutively active SmoM2 (C) or dominant-negative PKA (dnPKA) (D). (E) Effect of Evc2 $\Delta$ W on Hh signaling (36 hours) in *Sufu*<sup>-/-</sup> MEFs or *Sufu*<sup>-/-</sup> MEFs rescued by the stable expression of SuFu.

Smo signaling influences the fate of the Gli transcription factors. Amongst the three Gli proteins, Gli2 and Gli3 are the immediate responders to the Hh signal. When the Hh signal is received, the production of the transcriptional repressor form (Gli3R) is turned off. Instead, full-length Gli2 (Gli2FL) and full-length Gli3 (Gli3FL) are converted to transcriptional activator proteins (GliA) that dissociate from SuFu in order to translocate into the nucleus to activate target genes (Humke et al., 2010). In order to test the effect of Evc2 $\Delta$ W expression on GliA and GliR formation subcellular fractionation of Evc2 and Evc2 $\Delta$ W cells was performed in order to determine the localization of the Gli proteins in the nucleus and the cytoplasm, respectively.

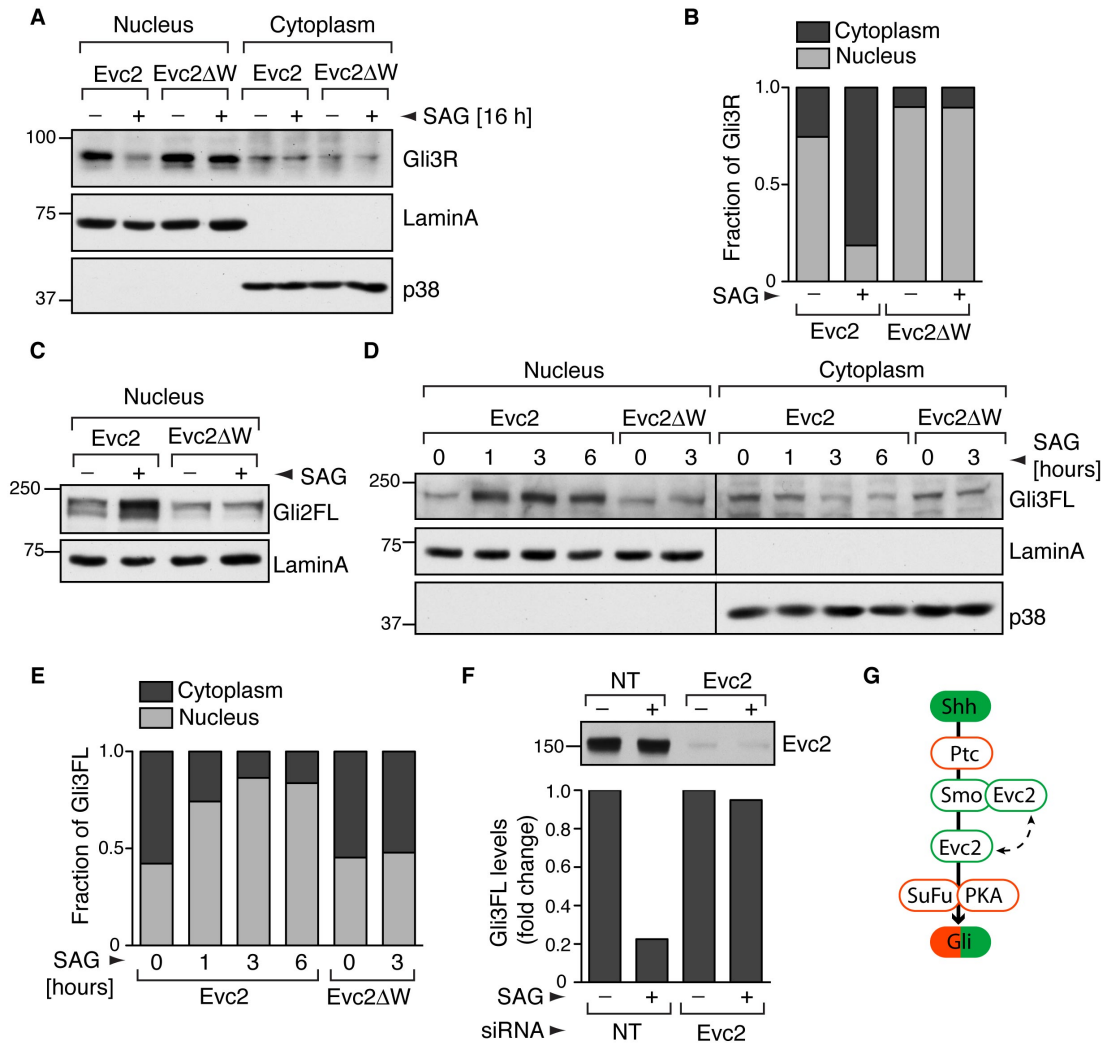


**Figure 15: Evc2 is required for the regulation of both Gli repressor and activator proteins.** (A) IB showing levels of the repressor form of Gli3 (Gli3R) in the cytoplasmic and nuclear fractions of Evc2 and Evc2ΔW cells left untreated or treated with SAG (16 hours). LaminaA and p38, markers of the nucleus and cytoplasm, demonstrate the purity of each fraction. (B) Bar graph showing the relative fraction of Gli3R in the cytoplasm and nucleus under the indicated conditions. (C) IB showing the levels of full-length Gli2 (Gli2FL) in the nucleus of cells after treatment with SAG (16 hours). IB (D) and bar graph (E) showing the levels of full-length Gli3 (Gli3FL) in the cytoplasm and nucleus of cells at various time points after addition of SAG (100 nM). (F) The SAG-induced (2 hours) dissociation of Gli3FL from SuFu, a hallmark of Gli3 activation, was assessed in cells treated with an Evc2 siRNA or a control NT siRNA. The amount of Gli3FL that co-precipitated with SuFu in an anti-SuFu IP was quantitated and plotted on the left graph. Dissociation of the Gli3-SuFu complex leads to a decrease in the amount of Gli3FL that co-precipitates with SuFu after treatment with SAG (left 2 bars). The Evc2 protein was efficiently depleted by the Evc2 siRNA but not the NT siRNA (right panel). (G) Evc2 functions at the level of Smo or at a step between Smo and SuFu/PKA. Positive and negative regulators are colored in green and red, respectively.

In the absence of signaling, both Evc2 and Evc2 $\Delta$ W cells had equal amounts of Gli3R in the nucleus, suggesting that Evc2 is not required for the conversion of Gli3FL to Gli3R (Figures 15A and B). However, Hh signaling was unable to extinguish Gli3R production in Evc2 $\Delta$ W cells (Figure 15A and B). In addition, all aspects of Hh-induced GliA formation were blocked in Evc2 $\Delta$ W cells: both Gli3FL and Gli2FL proteins failed to translocate from the cytoplasm to the nucleus in response to SAG in Evc2 $\Delta$ W cells (Figures 15C-E) and Gli3FL failed to dissociate from SuFu in Evc2-depleted cells (Figure 15F). Summarizing the above epistasis analysis, Evc2 is required at the level of or immediately downstream of Smo but upstream of PKA and SuFu (summarized in Figure 15G).

### **3.1.5 The role of Evc2 in trafficking Hh pathway proteins to primary cilia**

Smo accumulation in the primary cilia upon pathway activation is critical for its function. Given that Evc2 is critical for all aspects of Smo signaling, a role in the trafficking of Smo to primary cilia was very plausible. However, Smo accumulated in cilia normally in response to SAG in both Evc2 and Evc2 $\Delta$ W cells and in NIH/3T3 cells depleted of endogenous Evc2 by siRNA as determined by Smo immunofluorescence (Figures 16A-D).

Smo activation and accumulation in cilia is correlated with an increase in the levels of Gli2, Gli3, and SuFu at the tips of cilia, a step thought to be critical for the nuclear translocation of the Gli proteins (Kim et al., 2009; Tukachinsky et al., 2010). Since Evc2 function was not required for Smo translocation to the cilium but was yet important for GliA formation it was tested whether Evc $\Delta$ W expression affects Hh-induced cilia localization of Gli2, Gli3, and SuFu. It was found that the SAG-induced recruitment of endogenous Gli2, Gli3, and SuFu to the tips of cilia was reduced in Evc2 $\Delta$ W cells compared to Evc2 cells (Figures 17A-F). Thus, Evc2 is required to transduce Smo activation to the recruitment of SuFu and Gli proteins to the tips of primary cilia.

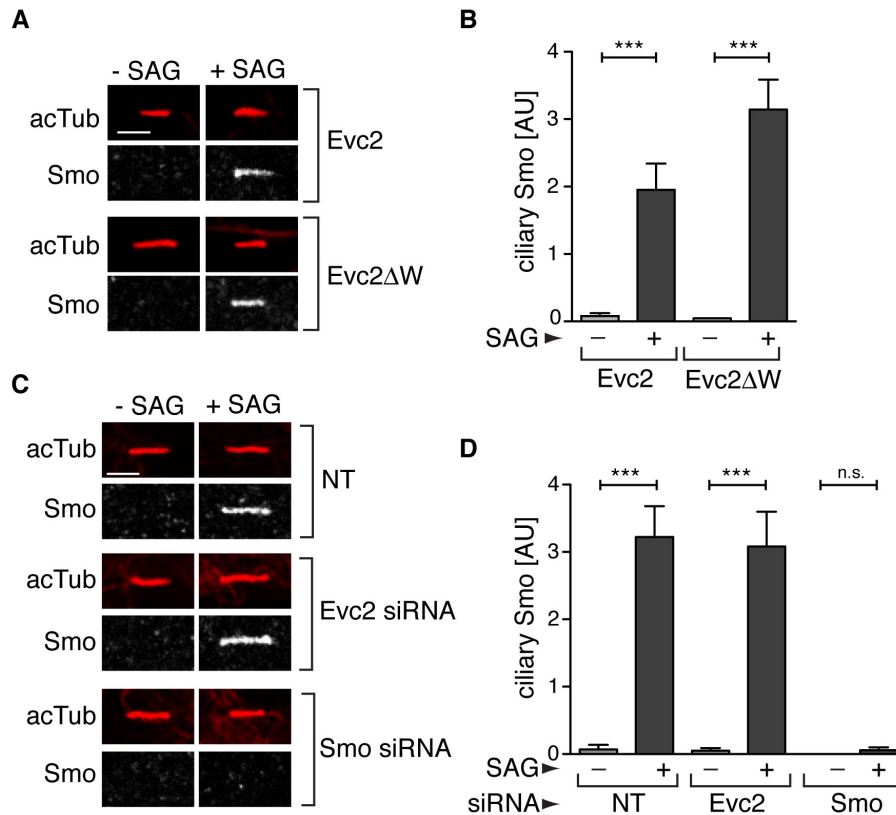


**Figure 16: Evc2 is not required for accumulation of Smo in primary cilia.** (A) Confocal images showing levels of endogenous Smo (in white) at representative cilia (red) from Evc2 and Evc2ΔW cells treated with or without SAG (4 hours). (B) Multiple cilia from such images were used to quantitate the mean ( $\pm$  95% CI) fluorescence of Smo (n=49) at cilia. Statistical test: one-way ANOVA with Tukey post-test;  $p < 0.001$  (\*\*\*) and  $p > 0.05$  (ns). Scale bars: 2.5  $\mu$ m. (C) IF was used to assess the SAG-induced (4 hours) accumulation of Smo (white) in cilia (red) of NIH/3T3 cells transfected with siRNAs against Evc2, Smo or a non-targeting (NT) control. (D) Multiple cilia from such images were used to quantitate the mean ( $\pm$  95% CI) fluorescence of Smo at cilia (n=50). AU = arbitrary unit of fluorescence intensity.

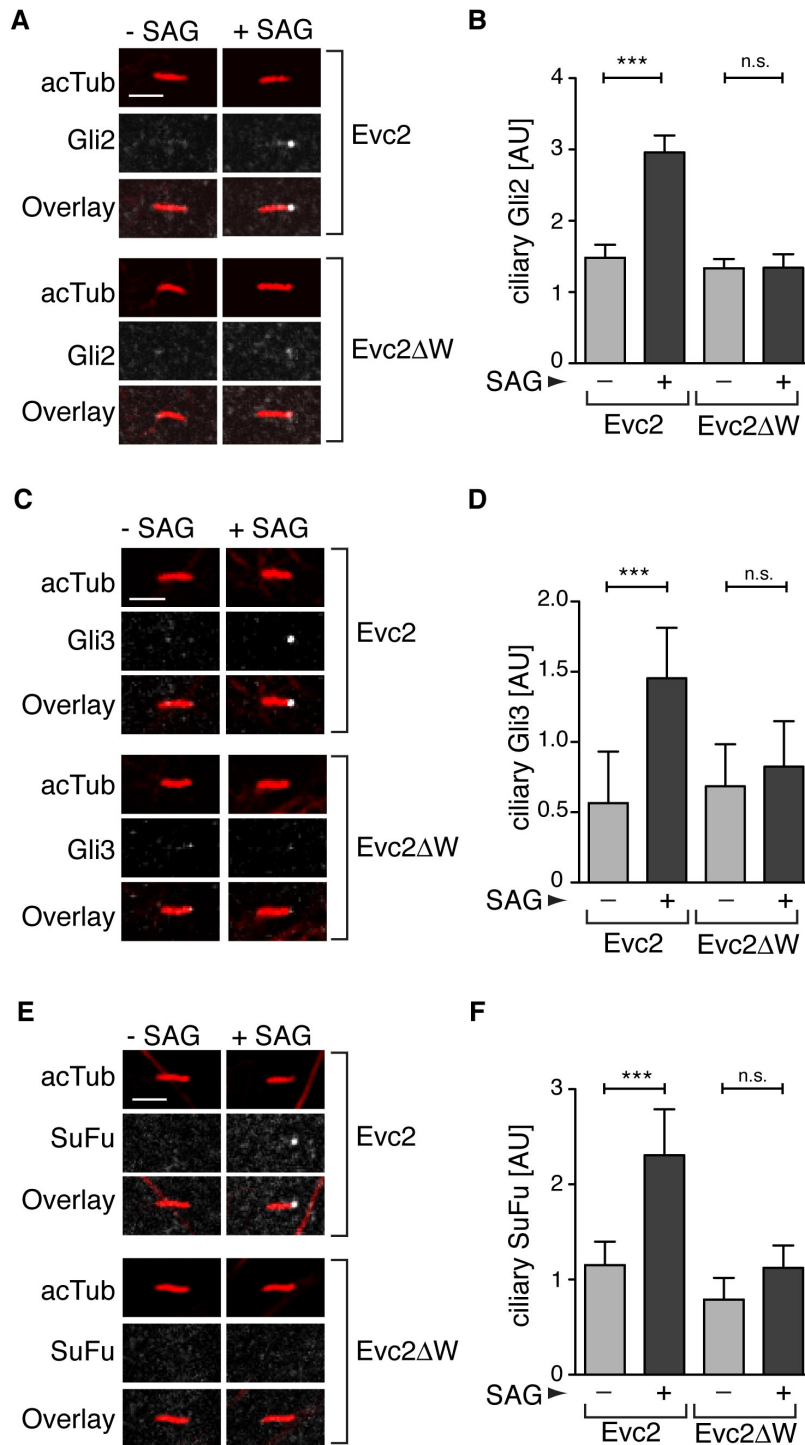


**Figure 17: Evc2 is required for the accumulation of Gli2, Gli3, and SuFu in cilia.** Confocal images showing levels of endogenous Gli2 (A), Gli3 (C), and SuFu (E) (all white) at representative cilia (red) from Evc2 and Evc2ΔW cells treated with or without SAG. Multiple cilia from such images were used to quantitate the mean ( $\pm$  95% CI) fluorescence of Gli2 (n=25) (B), Gli3 (n=22) (D), and SuFu (n=22) (F) at cilia. Treatment times were 4 hours for A, C, and 12h for E. Statistical test: one-way ANOVA with Tukey post-test;  $p < 0.001$  (\*\*\*) and  $p > 0.05$  (ns). Scale bars: 2.5  $\mu$ m. AU = arbitrary unit of fluorescence intensity.

## **3.2 The localization of Evc2 to the primary cilium is critical for its function**

### **3.2.1 The ciliary localization of Evc2 $\Delta$ W**

It is striking that the deletion of a small segment at the C-terminus of Evc2 converts it into a dominant-negative protein (see Figure 11) that can cause a human disease. To investigate the defect in Evc2 $\Delta$ W, protein trafficking of Evc2 $\Delta$ W itself was analyzed. Glycosylation patterns of membrane proteins can be used to infer their locations within the secretory pathway. Glycoproteins in pre-Golgi compartments are sensitive to digestion by both endo-beta-N-acetylglucosaminidase H (EndoH) and peptide:N-glycosidase F (PNGaseF). Proteins that have traversed the Golgi apparatus remain sensitive to PNGaseF but acquire resistance to EndoH. When treated with PNGaseF, Evc2 and Evc2 $\Delta$ W showed faster mobility, suggesting that they are both glycosylated (Figure 18A). Only a fraction of each protein, the fraction present in pre-Golgi compartments, was sensitive to EndoH (Figure 18A). Overall, the indistinguishable effects of EndoH and PNGaseF on Evc2 and Evc2 $\Delta$ W imply that both proteins are similarly distributed along the secretory pathway. Treatment with lambda-phosphatase did not result in a shift in mobility suggesting that neither of the two proteins is phosphorylated (Figure 18A).

While Evc2 $\Delta$ W traverses the core ER-Golgi pathway normally, it may not reach the primary cilium. Surprisingly, Evc2 $\Delta$ W was efficiently targeted to cilia, but its pattern of localization within the cilium was very different from wild-type Evc2. Instead of being concentrated in a punctate pattern at the EvC Zone, Evc2 $\Delta$ W-YFP was distributed along the entire length of the ciliary membrane independent of pathway activation (Figure 18B; compare to Figure 13E). This mis-localization was not caused by altered insertion in the ciliary membrane, as the topology of Evc2 $\Delta$ W was identical to Evc2 (cytoplasmic C-terminus and extracellular N-terminus) (Figure 18D).

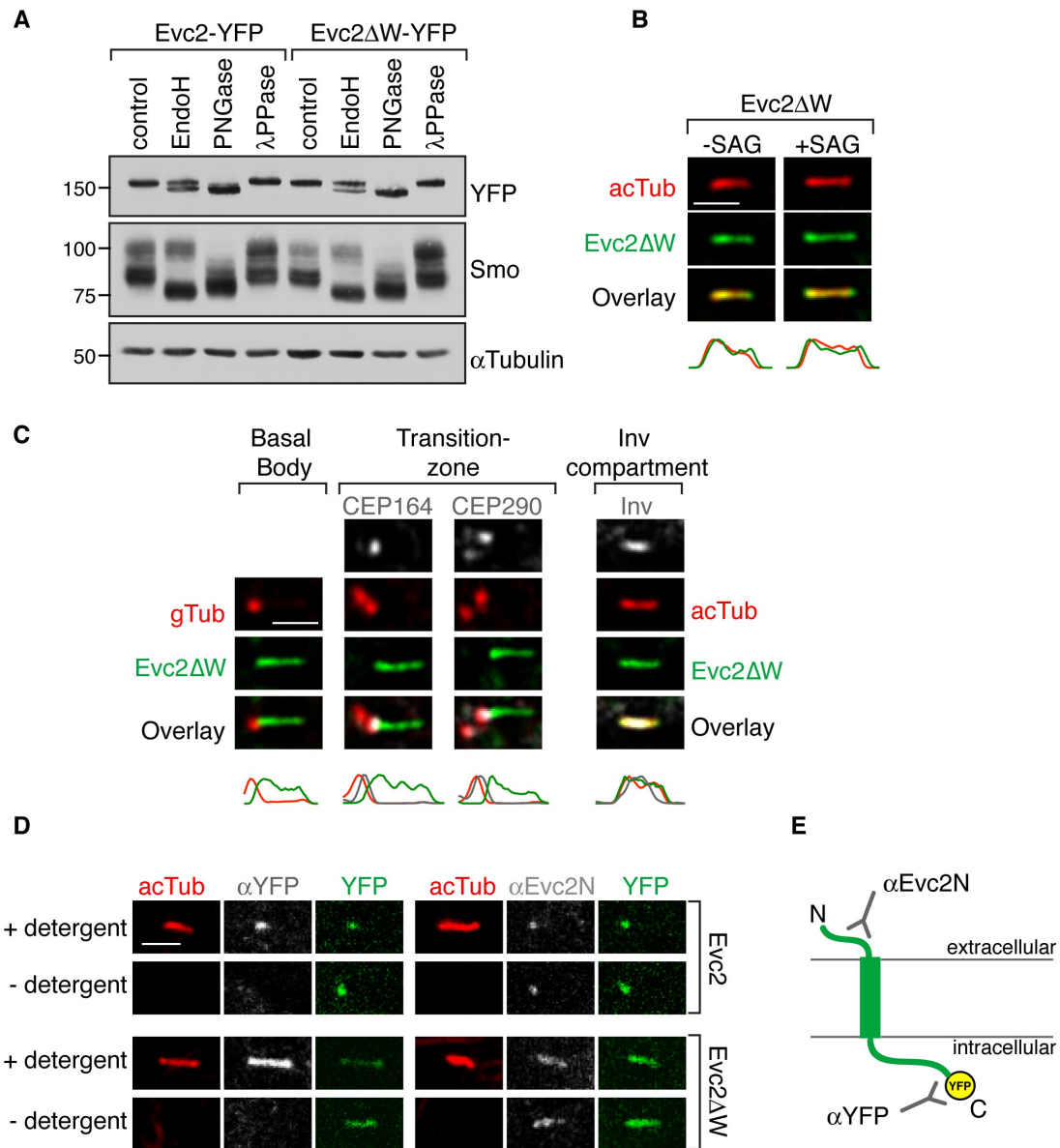


**Figure 18: Localization of Evc2ΔW is not restricted to the EvC Zone.** (A) IB showing the electrophoretic mobility of Evc2-YFP, Evc2ΔW-YFP, Smo or αTubulin (loading control) derived from Evc2-YFP and Evc2ΔW-YFP whole-cell extracts left untreated or treated with EndoH, PNGaseF, or lambda phosphatase (λPPase). The indistinguishable effects of EndoH and PNGaseF on Evc2 and Evc2ΔW imply that both proteins are similarly distributed along the secretory pathway. (B) Evc2ΔW-YFP (green) is localized along the entire length of cilia (red) in Evc2ΔW cells regardless of Hh signaling (2 hours). (C) Evc2ΔW-YFP localization relative to various ciliary compartments (compare to Figure 13D). (D,E) The topology of Evc2-YFP and Evc2ΔW-YFP was determined by IF of permeabilized (+ detergent, 0.1 % Triton X-100) or non-permeabilized cells (- detergent) using antibodies against the C-terminal YFP tag (anti-YFP) or the N-terminal domain (anti-Evc2N). The intrinsic YFP fluorescence (green) was used to demonstrate the presence of the YFP-tagged Evc2 proteins in all images. Anti-YFP only detects the YFP-tagged Evc2 proteins in permeabilized cells but anti-Evc2N detects the proteins in both permeabilized and non-permeabilized cells, demonstrating that the N-terminus is extracellular and the C-terminus is intracellular for both Evc2-YFP and Evc2ΔW-YFP (E).



Given that the W-peptide was required for EvC Zone localization, it was tested if it could target a different ciliary membrane protein to this compartment. YFP-tagged Smo (YFP-Smo) is known to localize along the entire length of the ciliary membrane when over-expressed in cells (Rohatgi et al., 2009). Remarkably, the W-peptide was sufficient to restrict Smo to the EvC Zone when fused to the C-terminus of YFP-Smo (Figures 20A-C). The FV motif was again critical because mutation of this motif in the W-peptide abrogated its ability to target Smo to the EvC Zone (Figure 20D). The W-peptide did not induce ciliary or EvC Zone localization when fused to a Smo

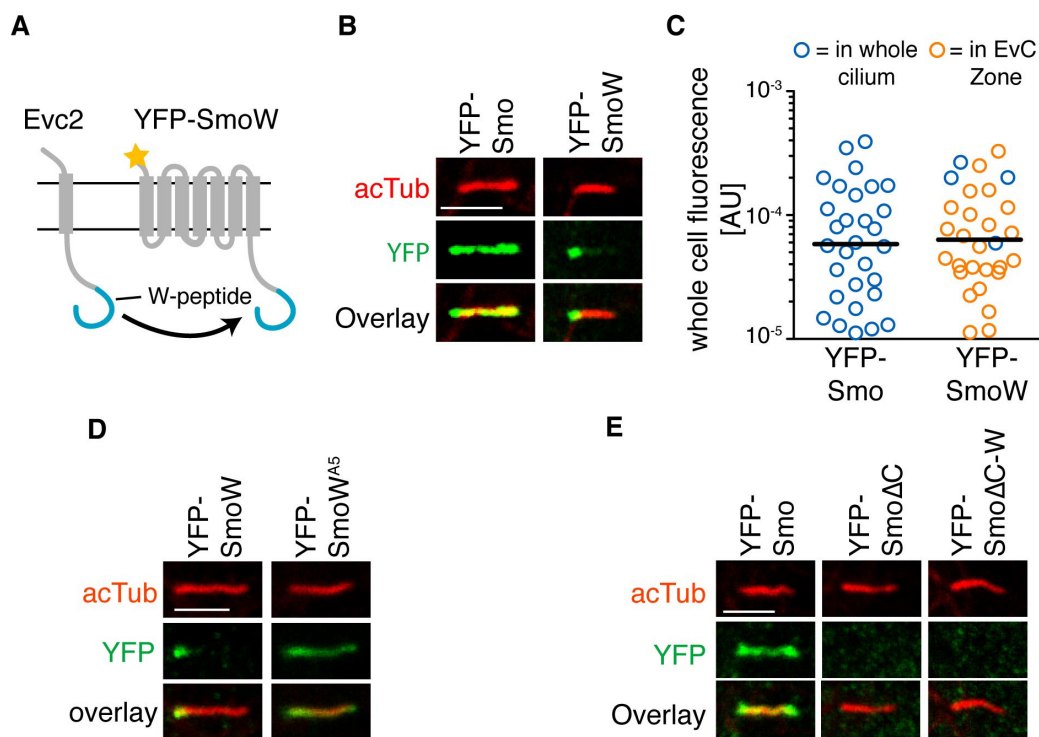


**Figure 20: A W-peptide/Smo fusion protein is restricted to the EvC Zone.** (A) YFP-SmoW was constructed by transferring the W-peptide (blue) from Evc2 to the C-terminus of YFP-Smo (=YFP-SmoW). Yellow star: YFP tag. (B) Localization of YFP-Smo and YFP-SmoW (green) at cilia (red) after transient expression in NIH/3T3 cells. YFP-SmoW localizes at the EvC zone as demonstrated in a separate experiment (not shown). (C) Localization of YFP-Smo and YFP-SmoW at the EvC Zone (orange) or the whole cilium (blue) in individual cells (circles) expressing varying amounts of the two proteins after transient transfection. Whole-cell YFP fluorescence is plotted for each cell; the black bar marks the mean fluorescence (or expression level) for each construct (n=30). (D) A mutant W-peptide carrying the A5 mutation that overlaps the FV motif (YFP-SmoWA5) cannot target Smo to the EvC Zone. (E) Ciliary localization (anti-YFP, all green) of transiently transfected YFP-Smo, YFP-Smo lacking the C-terminal cytoplasmic tail of Smo (YFP-SmoΔC), and YFP-SmoΔC fused to the W-peptide from Evc2 (YFP-SmoΔC-W). Fusion of the W-peptide failed to target SmoΔC to cilia. Scale bars: 2.5 μm.

truncation mutant (Smo $\Delta$ C) unable to localize to cilia (Figure 20E). Thus, the W-peptide deleted from Evc2 in patients with Weyers is not a cilia targeting signal, but rather a portable sequence that is both necessary and sufficient to mediate the localization of ciliary membrane proteins to the EvC Zone.

### **3.2.3 The localization of Evc2 mutants predicts their phenotype in Hh signaling**

So far the results suggested the intriguing idea that Evc2 $\Delta$ W is a dominant-negative protein in Weyers patients because it is dispersed throughout the ciliary membrane rather than being restricted to the EvC Zone. To ask if the ciliary localization of Evc2 $\Delta$ W was necessary for its dominant-negative phenotype, C-terminally truncated Evc2 proteins modeled based on recessive disease alleles found in EvC patients (Ruiz-Perez and Goodship, 2009; Valencia et al., 2009) were generated. In comparison to Evc2 $\Delta$ W (which lacks the C-terminal 43 a.a.), Evc2 $\Delta$ 1157-1220 and Evc2 $\Delta$ 1133-1220 lack slightly longer fragments spanning the C-terminal 64 and 88 a.a., respectively. Evc2 $\Delta$ 1157-1176 carries a 21 a.a. internal deletion within this region. Amongst these mutants, only Evc2 $\Delta$ 1157-1220 blocked Hh signaling (Figure 21A, i) and was targeted to cilia but distributed along the entire ciliary membrane, analogous to Evc2 $\Delta$ W (Figure 21A, iii and iv). In contrast, neither Evc2 $\Delta$ 1133-1220 nor Evc2 $\Delta$ 1157-1176 strongly blocked Hh signaling. The former was not targeted to cilia at all and the latter was appropriately restricted to the EvC Zone (Figure 21A). To further test the correlation between mis-localization along the entire ciliary membrane and the dominant-negative phenotype, a series of Evc2 mutants with varying effects on Hh signaling were examined. In each case, mutants restricted to the EvC Zone did not block Hh signaling while those dispersed along the entire cilium were dominant inhibitors of the pathway (Figure 21B). Alanine mutations overlapping the FV motif of the W-peptide that blocked Hh signaling (Evc2A4 and Evc2A5) also mis-localized Evc2 throughout the ciliary membrane (Figure 21B). The above correlations provide functional evidence that both targeting to the cilium and restriction to the EvC Zone are critical for the proper function of Evc2 in Hh signaling.

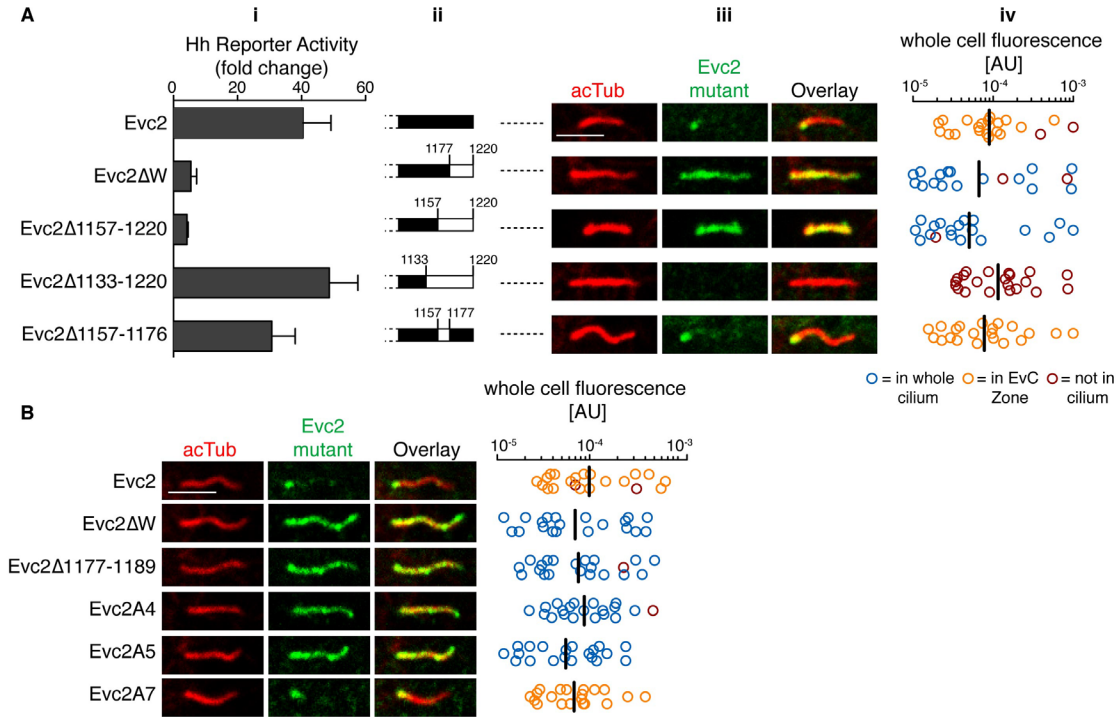


**Figure 21: The targeting of Evc2 to the Evc Zone is critical for its function.** (A) A series of Evc2-YFP deletion mutants (ii) were characterized for their effects on SAG-stimulated Hh-reporter activity (mean ±SD) (i) and for their localization in cilia (iii and iv). The localization of the Evc2 variants (green, anti-YFP) at cilia (red) was consistent across a range of expression levels in transiently transfected cells (graph in iv is drawn as in Figure 20C). (B) Ciliary localization of selected Evc2 mutants (green, anti-YFP) described in Figure 19 at cilia (red) of transiently transfected cells. n~20 for each construct. Scale bar: 2.5 μm.

### 3.3 The formation of a Hedgehog Signaling complex at the Evc Zone

#### 3.3.1 Evc2 associates with Smo in response to Hh signaling

Because Evc2 is required at a specific step in Hh signaling the binding of Evc2 to Hh pathway components that function at this step was analyzed. The binding experiments using immunoprecipitation (IP) were performed in Evc2-YFP cells, where both the Hh components and Evc2-YFP are expressed at endogenous levels (Figure 11B). To stabilize protein interactions during the detergent solubilization step required to extract Evc2 from membranes and to stabilize potentially very transient protein interactions, cells were treated with the membrane-permeable, reversible cross-linker Dithiobis[succinimidyl propionate] (DSP). DSP was added to intact cells and then inactivated prior to cell lysis to circumvent artifactual cross-linking during lysis and extraction. Evc2-YFP showed an interaction with Evc and with Smo, but not with Gli2, SuFu or PKA (Figure 22B). While the Evc2-Evc interaction was constitutive, the interaction between Evc2-YFP and Smo was only detectable when Hh signaling was activated by Shh or SAG (Figures 22B and C). To demonstrate the specificity of the Smo-Evc2 interaction, a panel of different antibodies against Smo and Evc2 (summarized in Figure 22A) were used to assay the interaction between YFP-Smo and Evc2 in extracts from *Smo*<sup>-/-</sup>;YFP-Smo MEFs (Rohatgi et al., 2009) without the use of a protein cross-linker. The Evc2-YFP-Smo interaction could be detected when endogenous Evc2 was isolated using an anti-Evc2 antibody or, in reciprocal IPs, when YFP-Smo was isolated using three different antibodies (Figures 22D-F). In order to test the binding of Hh proteins to Evc, Evc-YFP complexes were purified from a cell line stably expressing Evc tagged with a C-terminal YFP-tag (Evc-YFP). Consistent with the observation that Evc and Evc2 form a complex (Blair et al., 2011), an interaction between Smo and Evc could also be detected (Figure 22G). Taken together, these IP experiments confirmed the Hh-stimulated interaction between Smo and Evc and Evc2 and revealed that there is a direct link between those two ciliopathy proteins and Hh signaling.

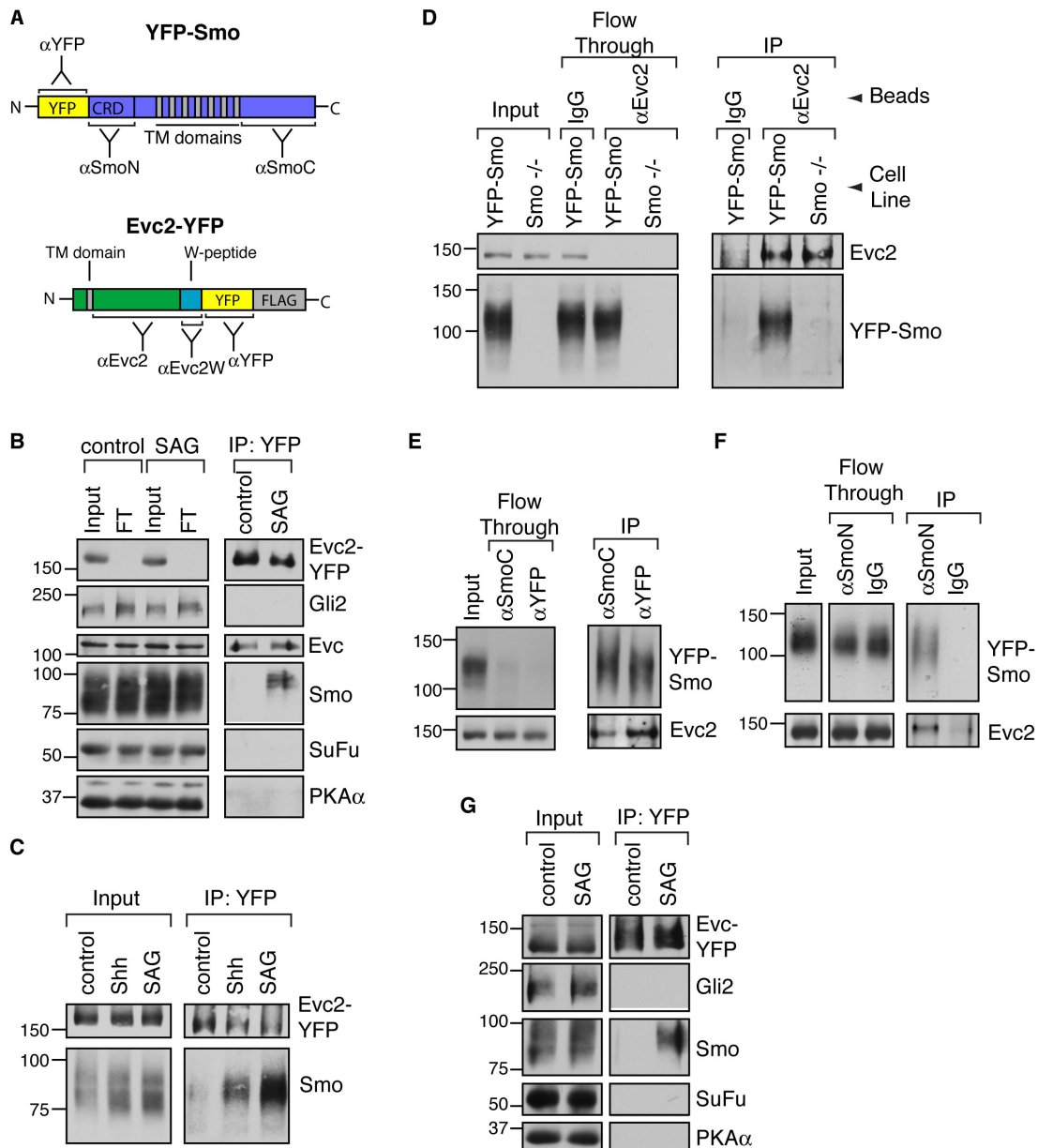


**Figure 22: Evc2 and Smo form a complex.** (A) Domain structures of YFP-Smo (which contains a N-terminal (extracellular) cysteine-rich domain (CRD) and seven transmembrane (TM) domains, Evc2-YFP-FLAG and Evc-YFP-FLAG. Brackets denote the epitopes for the antibodies used in the experiments shown in this Figure and in Figure 23. (B) Immunoblotting (IB) was used to assess the presence of Gli2, Evc, Smo, SuFu and PKA in anti-YFP immunoprecipitates (IP) from Evc2-YFP cells left untreated (control) or treated with SAG (2 hours). Input and flow-through (FT) samples show the amount of each protein in the whole extract before and after the IP respectively. In this panel and in panels (C) and (G) IPs were performed after whole cell crosslinking (DSP, 0.1 mM). (C) IBs showing the amount of endogenous Smo that co-precipitated with Evc2-YFP from cells left untreated or treated with SAG or Shh for 2 hours. (D) IB showing the amount of YFP-Smo that co-precipitated with anti-Evc2 beads or control IgG beads from extracts of *Smo*<sup>-/-</sup>:YFP-Smo cells or control *Smo*<sup>-/-</sup> cells treated with SAG. No cross-linker was used in this panel and in panels (E) and (F). Input and flow-through samples show the amount of each protein in the whole extract before and after the IP, respectively.

**Figure 22 (continued): Evc2 and Smo form a complex.** (E, F) IBs showing the amount of Evc2 that co-precipitated with YFP-Smo from extracts derived from Smo<sup>-/-</sup>;YFP-Smo cells treated with SAG. Extracts were incubated with anti-YFP and anti-SmoC beads (E) or with anti-SmoN and control rabbit IgG beads (F). (G) IBs showing the amounts of Gli2, Smo, SuFu, and PKA that co-precipitated with Evc-YFP from SAG-treated (2 hours) cells stably expressing the protein.

### 3.3.2 The dominant negative effect of Evc2 $\Delta$ W

Having established these interaction assays, they could be used to understand the molecular basis for the dominant-negative activity of Evc2 $\Delta$ W. One plausible explanation for the dominant negative effect was that Evc2 $\Delta$ W fails to bind to Smo or Evc. However, Evc2 $\Delta$ W could still bind to both Smo and Evc (Figures 23A and B). Unexpectedly, Evc2 $\Delta$ W-YFP showed an even stronger interaction with Smo and Evc than Evc2-YFP (Figure 23A). Thus, the interaction of Smo and Evc2 does not require the W-peptide. In addition, the W-peptide was not required for the binding of Evc2 to Evc (Figure 23B). Next, the ability of Evc2-YFP and Evc2 $\Delta$ W-YFP to form complexes with endogenous Evc2 was tested. Evc2-YFP was able to bind endogenous Evc2, suggesting that Evc2 can form homo-oligomers in cells (Figure 23C). This ability to multimerize was compromised by loss of the W-peptide, since Evc2 $\Delta$ W-YFP failed to bind endogenous Evc2 (Figure 23C). Consistent with these biochemical data, immunofluorescence experiments showed that Evc2 $\Delta$ W expression could displace endogenous Evc (Figure 23D), but not endogenous Evc2 (Figure 23E), from the EvC Zone and cause it to spread along the entire length of the cilium. Taken together, the data suggest that the critical biochemical defect in Evc2 $\Delta$ W is its inability to multimerize with endogenous Evc2. A summary of the interactions between Evc, Evc2, and Smo is summarized in Figure 23F.

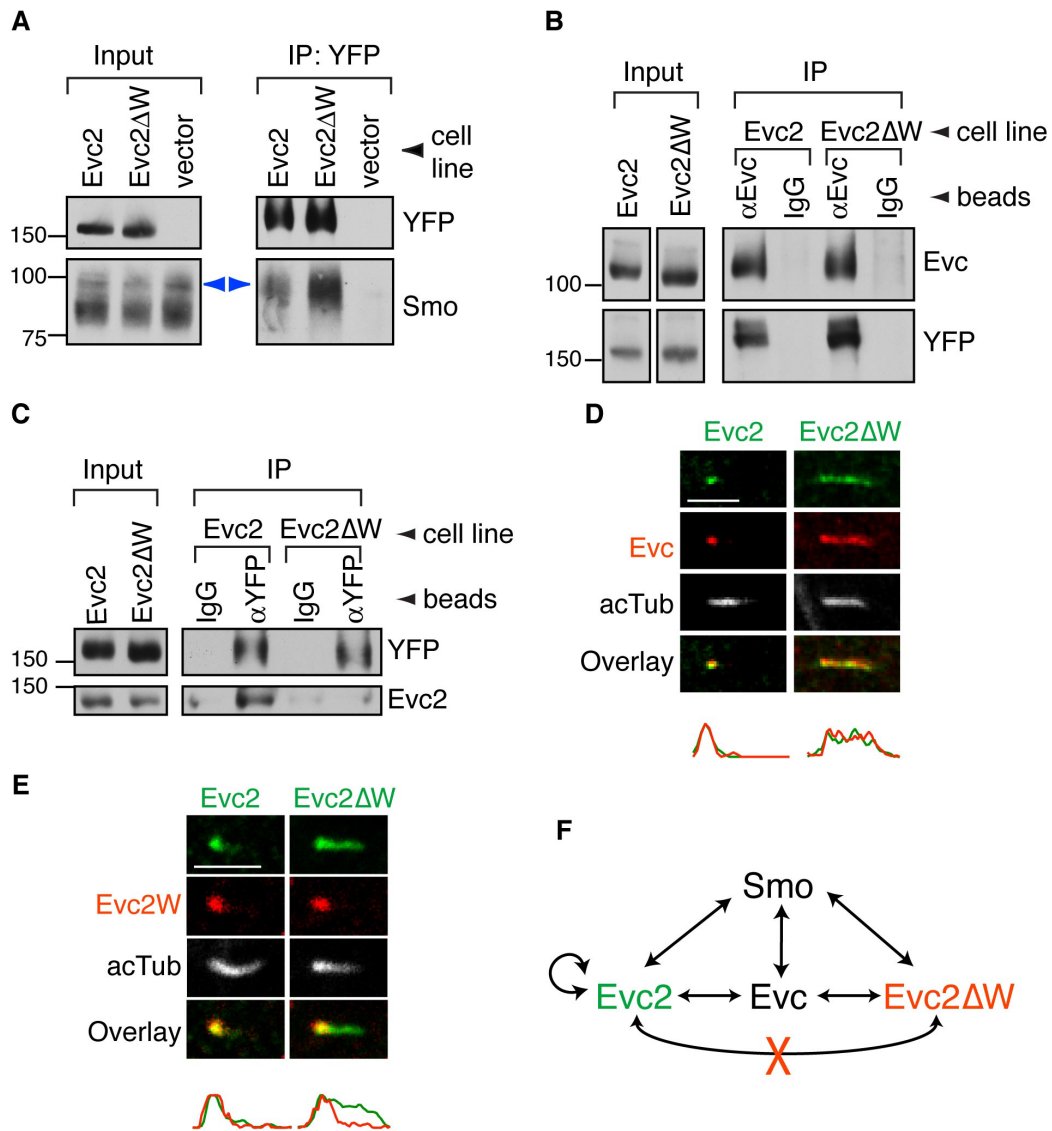


**Figure 23: Evc2ΔW binds to Smo and Evc, but fails to interact with Evc2.** (A) IBs showing the amount of Smo that co-precipitated with Evc2-YFP or Evc2ΔW-YFP from SAG-treated stable cell-lines. A control IP was performed from cells lacking a YFP-tagged Evc2 bait protein (vector control). Blue arrows denote the higher molecular weight fraction of Smo that associated with Evc2. See paragraph 3.3.3 (B) IBs showing the amount of Evc2-YFP and Evc2ΔW-YFP that co-precipitated with endogenous Evc from SAG-treated cells on anti-Evc beads or control IgG beads. (C) IBs showing endogenous Evc2 that co-precipitated with Evc2-YFP or Evc2ΔW-YFP using anti-YFP beads or control IgG beads from cells treated with SAG. (D) Localization of endogenous Evc (red) at cilia (white) in Evc2 and Evc2ΔW cells (anti-YFP, green). (E) An Evc2 antibody directed exclusively against the W-peptide (anti-Evc2W) was used to assess the ciliary localization of Evc2 (red) in Evc2-YFP and Evc2ΔW-YFP cells (anti-YFP, green). (F) Summary of the interactions between Evc2, Evc2ΔW, Evc, and Smo. While Evc2 can self-associate, Evc2ΔW cannot associate with Evc2. Scale bars: 2.5 μm.

### 3.3.3 Spatial restriction of the Smo-Evc2 interaction to primary cilia

During the interaction studies, it became clear that Evc2 selectively bound the fraction of total Smo that demonstrated slower mobility on SDS-PAGE (see for example Figure 23A), consistent with a post-Golgi glycosylation pattern. Indeed, Smo that co-precipitated with Evc2 and Evc2 $\Delta$ W was resistant to digestion with EndoH and sensitive to digestion with PNGaseF (Figure 24A), formally showing that it carried the glycosylation hallmark of transit through the Golgi. Thus, the Smo-Evc2 interaction was both induced by Hh signaling and spatially restricted to a post-Golgi compartment. The primary cilium was the most likely location for this interaction because Evc2 and Smo were co-localized in the EvC Zone after Hh pathway activation (Figure 24B). Consistent with the IP data (Figure 23A), Evc2 $\Delta$ W, which was distributed throughout the cilium, showed a greater degree of overlap with Smo in the cilium (Figure 24B). An *in situ* proximity ligation assay (DUOLINK™) demonstrated that Evc2 and Smo were located within 40 nm of each other at the cilium (Figures 24C-E).

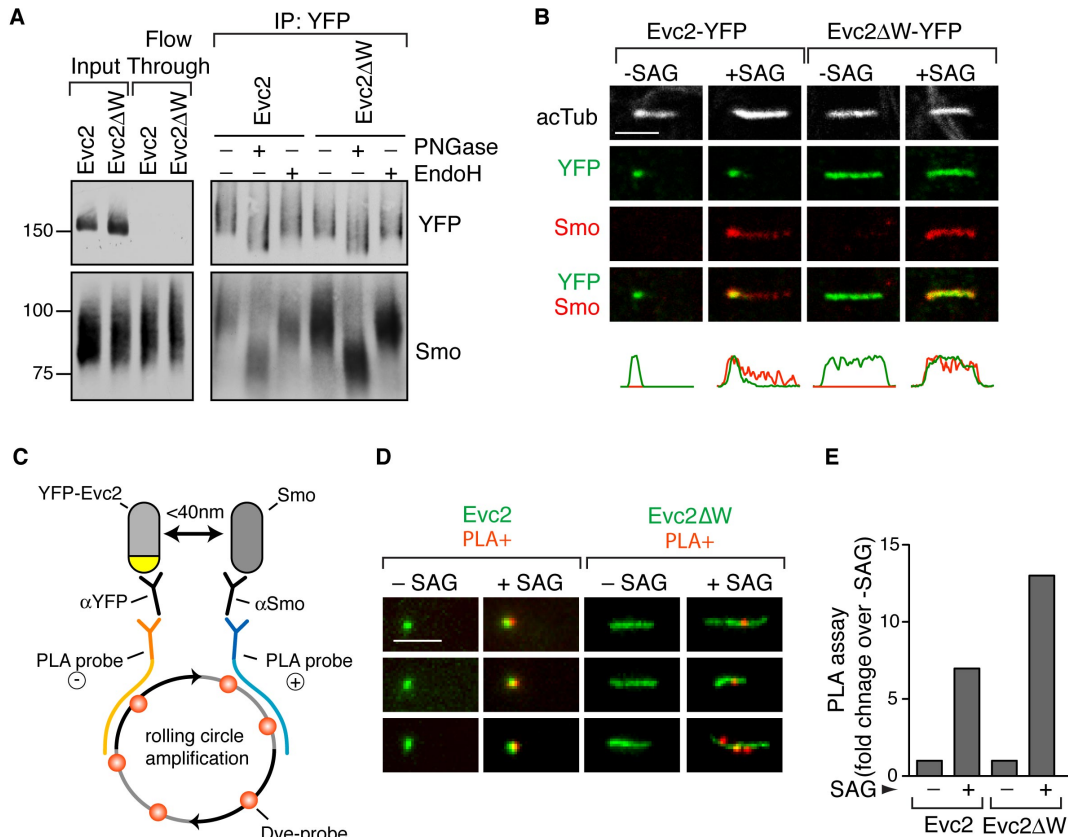


**Figure 24: Hh signaling induces the co-localization of Smo and Evc2 at primary cilia.** (A) IBs showing the electrophoretic mobility (6% SDS-PAGE) of endogenous Smo isolated in a complex with Evc2-YFP or Evc2ΔW-YFP after an overnight incubation with PNGaseF, EndoH, or a buffer control. Cells were treated with SAG followed by DSP (0.1 mM) before lysis. (B) Co-localization of Smo (red) and Evc2-YFP or Evc2ΔW-YFP (anti-YFP, green) at cilia (white) of stable cell lines left untreated or treated with SAG (4 hours). Scale bar: 2.5  $\mu\text{m}$ . (C) Schematic of the in situ proximity ligation assay (PLA, Duolink<sup>TM</sup>) used to assay the interaction between Smo and Evc2-YFP or Evc2ΔW-YFP. A positive PLA fluorescence signal marks a region where the two proteins of interest (Smo and Evc2 or Evc2ΔW) are in close proximity (<math><40\text{ nm}</math>). (D) Gallery of IF images showing overlap of the PLA signal (red dot) with the localization of Evc2-YFP or Evc2ΔW-YFP (both detected by endogenous green fluorescence) in cells left untreated or treated with SAG (2 hours). Scale bar: 2.5  $\mu\text{m}$ . Such images were used to quantitate the fold-change in the PLA signal at primary cilia (E).

Three independent strategies were used to determine whether cilia were indeed required for the interaction of Smo and Evc2. First, growth of cells in the presence of high serum, which is known to block ciliogenesis (Tucker et al., 1979), substantially inhibited the interaction between Smo and Evc2 (Figure 25A). Second, Evc2-YFP stable cell lines were generated expressing a dominant-negative fragment of the anterograde motor Kif3a (dnKif3a). In these cell lines the majority of cells lost cilia if compared to Evc2-YFP cells (Figure 25B). Consistently, the interaction between Smo and Evc2 was reduced in the dnKif3a expressing cells (Figures 25C and D).

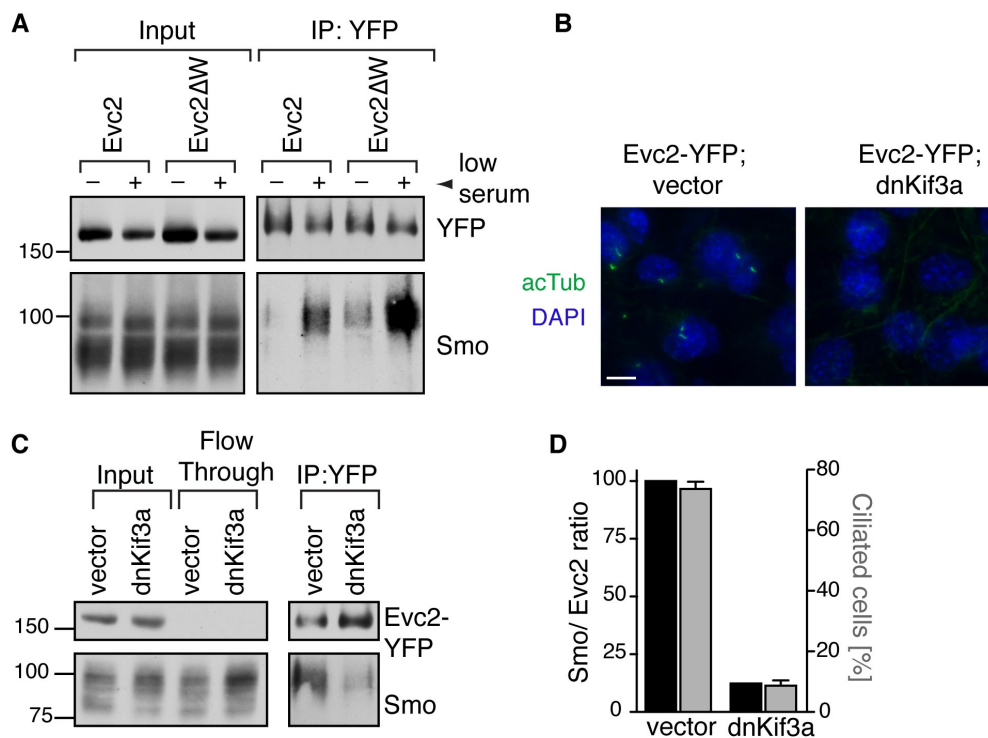


**Figure 25: Association of Evc2 and Smo at primary cilia.** (A) IBs showing the amount of endogenous Smo that co-precipitated with Evc2-YFP and Evc2 $\Delta$ W-YFP on anti-YFP beads from cells grown in high serum or in low serum (to efficiently induce ciliation) and exposed to SAG (2 hours). (B) The ciliation of Evc2-YFP cells expressing either dnKif3a (bottom) or a control vector (top) was assessed by anti-acTub staining (green). (C) IBs showing the association of endogenous Smo with Evc2-YFP in Evc2-YFP cells stably expressing dnKif3a (to ablate cilia) or cells expressing an empty control vector. (D) Quantification of (B) and (C): In dnKif3a or control cells, Smo-Evc2 association (left axis), expressed as the ratio of Smo pulled-down per unit of Evc2 based on the immunoblot from (C), is compared to the percentage of cells that form cilia based on multiple images such as the ones shown in (B) (right axis, mean  $\pm$  SD). DAPI stains the nuclei (blue); scale bar: 10  $\mu$ m.

Finally, cell lines were generated stably expressing various deletion mutants of Evc2, each tagged with a C-terminal YFP tag. A combination of IP experiments and immunofluorescence of these Evc2 mutants revealed that the interaction with Smo was abrogated by mutations that prevented the ciliary localization of Evc2 (Figures 26A and C). Similar results were obtained using cell lines stably expressing YFP-Smo deletion mutants. Only Smo mutants that localized to the cilium interacted with Evc2 (Figures 26B and C).

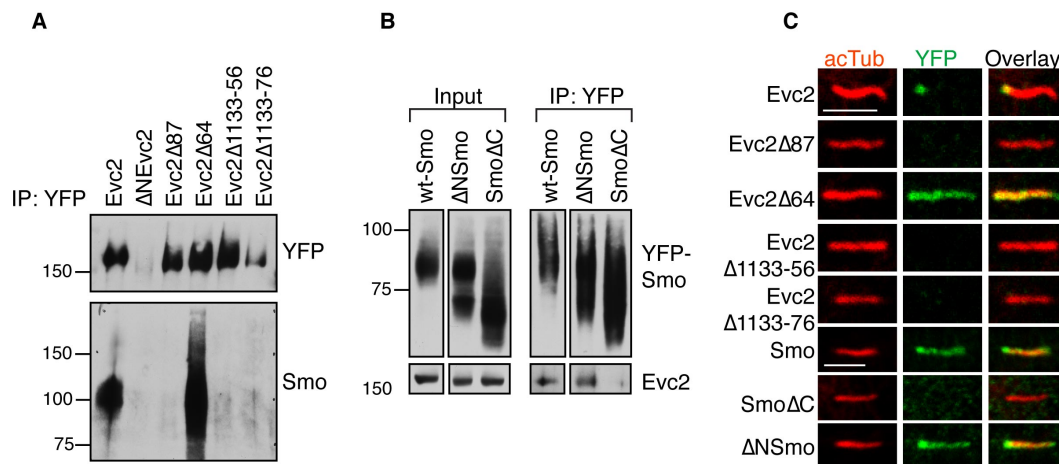


**Figure 26: Cilia localization of Evc2 and Smo is required for the formation of the Evc2-Smo complex.** (A) The indicated truncation mutants of Evc2 were stably produced as YFP fusions and tested for their ability to bind to endogenous Smo (A) using an anti-YFP IP and for their ability to localize in primary cilia (C) by anti-YFP IF. Only the Evc2 variants that localized in cilia (Evc2-YFP and Evc2Δ64-YFP) showed an interaction with Smo. A mutant lacking the N-terminal domain of Evc2 (ΔNEvc2-YFP) was not well expressed. (B) IBs showing the amounts of endogenous Evc2 that co-precipitated in an anti-YFP IP with wild-type YFP-Smo or with two YFP-Smo mutants lacking either the N-terminal extracellular domain (YFP-ΔNSmo) or the C-terminal intracellular tail (YFP-SmoΔC). Evc2 bound to YFP-Smo and YFP-ΔNSmo, both localized in cilia (C), but did not interact with YFP-SmoΔC, which failed to localize in cilia (C) despite being highly expressed (B).

### 3.3.4 Smo signaling in the EvC Zone

Smo can adopt either an active or an inactive conformation in cilia (Rohatgi et al., 2009). Both SAG, a Smo agonist, and cyclopamine, a Smo antagonist, can induce the accumulation of Smo in cilia. However, the association between Smo and Evc2 was only detected in cells treated with SAG but not in Cyclopamine treated cells (Figures 27A and B). Thus, the Smo-Evc2 interaction appears to be sensitive to both the integrity of the primary cilia and to the active conformation of Smo. Within the cilium, the EvC Zone is the most likely place where Smo and Evc2 associate. However, since Smo is often found throughout the ciliary membrane, an important question is precisely where in the cilium Smo activity is required to transduce the Hh signal. In order to answer this question the signaling activity of a Smo protein that was tethered to the EvC Zone by fusion of the W-peptide (YFP-SmoW, see Figure 20) was tested. If Smo activity is required at the tips of cilia, as proposed by some models (Goetz et al., 2009), YFP-SmoW should show less signaling activity compared to the wild-type YFP-Smo protein that localizes throughout the cilium. Instead, both with and without SAG, YFP-SmoW was ~2-fold more active than YFP-Smo, even though the former was present in cilia at ~2.6-fold lower levels (Figures 27C-E). Interestingly, the fusion of the W-peptide with a mutation in the FV-motif (YFP-SmoWAla5) did not show the increased Hh activity. Taken together, these results are consistent with the notion that Smo signaling at the cilium is compartmentalized in the EvC Zone and facilitated by association with Evc2.

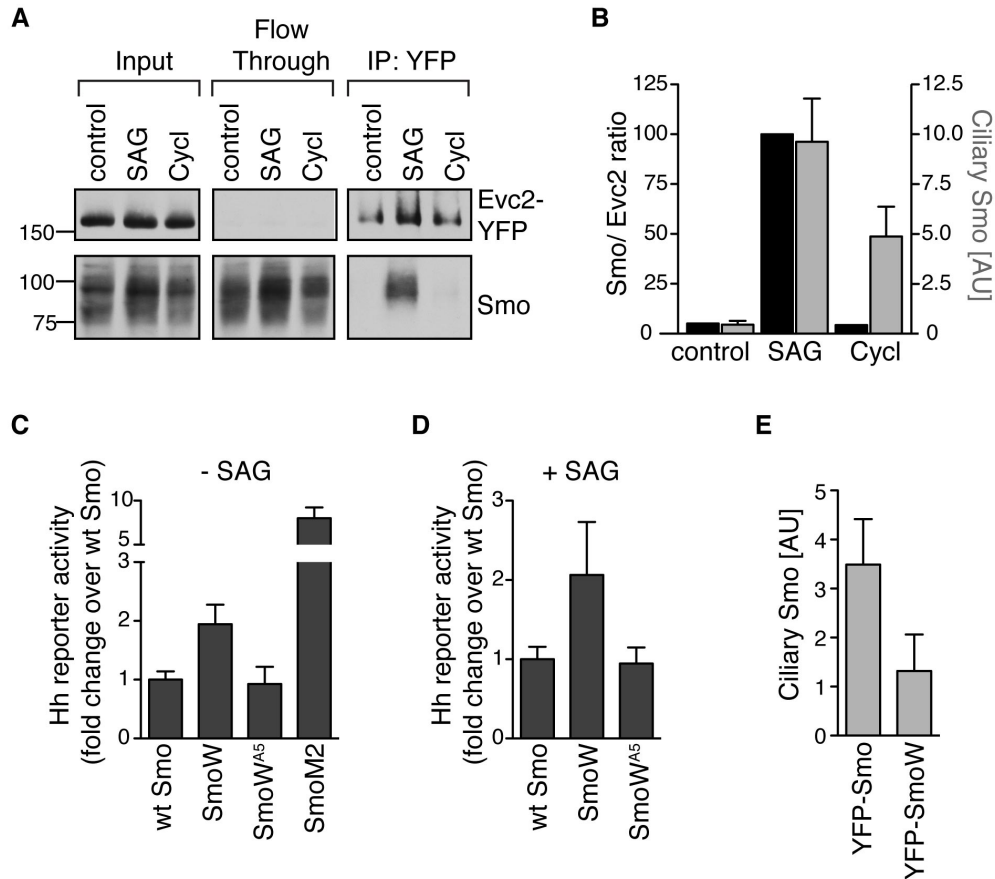


**Figure 27: Smo activity in the EvC Zone.** (A) IBs showing the association between Smo and Evc2-YFP in cells left untreated or treated with SAG or Cyclopamine (Cycl, 5  $\mu$ M) for 2 hours. (B) Quantification of (A): in control-, cyclopamine- or SAG-treated cells, Smo-Evc2 association (left axis) is compared to the intensity of Smo fluorescence (mean  $\pm$  95% CI) at cilia (right axis) from cells treated as in (A). (C,D) Mean ( $\pm$  SD) Hh reporter activity in cells transiently expressing YFP-Smo, YFP-SmoW, or YFP-SmoW<sup>A5</sup> left untreated or treated with SAG. In each case, data are shown relative to wild-type YFP-Smo. (D) Bar graph showing the mean ( $\pm$  95% CI; n=19) fluorescence of YFP-Smo or YFP-SmoW at cilia.

## 3.4 Identification of Evc2 binding partners

### 3.4.1 Purification of Evc2 complexes

After establishing a role for Evc2 as a positive regulator in the Hh signaling pathway a remaining question was how Evc2 transduces the Hh signal to the downstream effectors and whether there are other so far unknown proteins involved in this process. As a first step towards answering this question a comparative proteomic strategy using both affinity chromatography and Tandem Affinity Purification (TAP) was used to uncover the most specific and functionally important Evc2 interaction partners. The findings that Evc2 $\Delta$ W blocks Hh signaling and is localized to the cilium in a strikingly different pattern suggests that the last 43 a.a. (= W-peptide) of Evc2 are likely to regulate important protein interactions and that any proteins that bind differentially to Evc2 and Evc2 $\Delta$ W are likely to be functionally important. Thus, the W-peptide fused to Glutathione-S-Transferase (GST) (GST-W) was used as a bait to purify protein complexes specifically bound to the last 43 a.a. of Evc2 (Figure 28A). TAP-based purification of Evc2 complexes was performed using a cell line stably expressing Evc2 tagged with a dual YFP-FLAG tag (Evc2-YFP-FLAG), the same cell line as described and characterized in paragraph 3.1. The strategy of the TAP-based purification of Evc2 complexes is summarized in Figure 28B.

For the TAP experiment, membranes from Evc2-YFP-FLAG cells were prepared and extracted, Evc2-YFP-FLAG complexes were captured on anti-FLAG beads, eluted with free FLAG peptide and re-captured on anti-YFP beads. The eluate was then separated on a 4-12% Bis-Tris precast gel and a 8% SDS-PAGE and prominent bands relative to a GST-control were cut and proteins were analyzed by LC-MS/MS (Figure 29A).

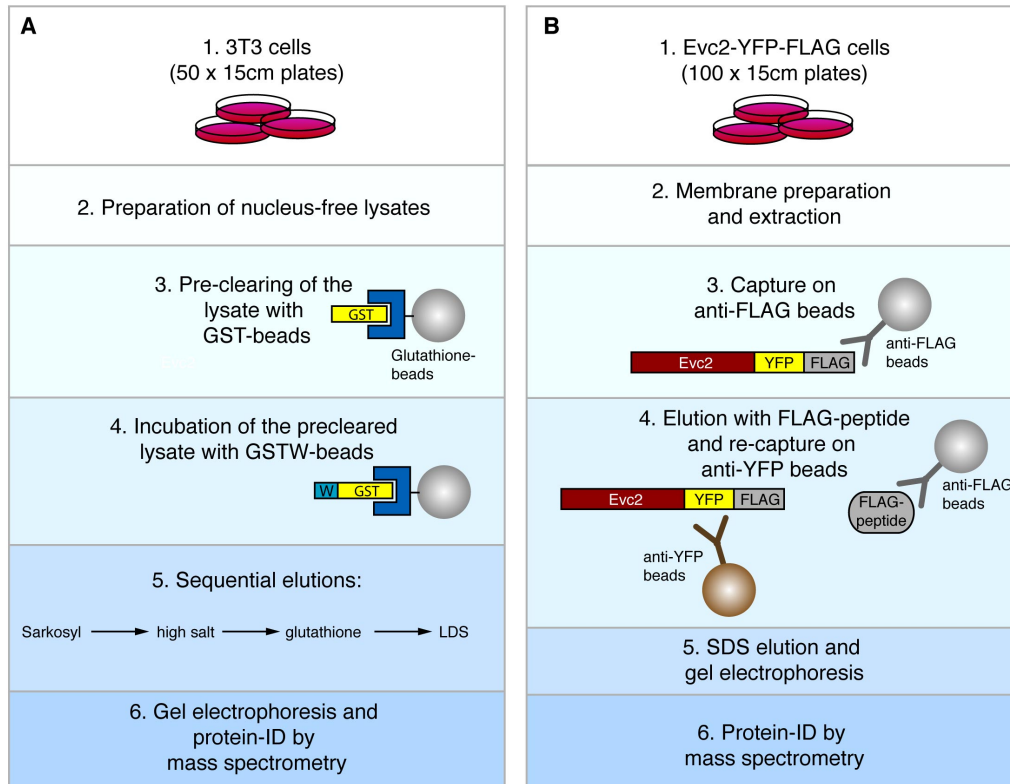


**Figure 28: Purification of Evc2 complexes.** (A,B) Experimental outline for the identification of Evc2 binding partners by affinity purification of GST-tagged Evc2 W-peptide (GST-W) from NIH/3T3 cell lysates (A) and for the tandem-affinity purification (TAP) approach for the identification of proteins associated with Evc2-YFP-FLAG (B). Details are provided in the materials and methods section.

As TAP experiments can only detect stable interactions due to the multiple washes and IP steps, affinity purification using a GST-W column was performed aiming for the detection of weaker interaction partners. For the W-peptide affinity purification (Figure 28A) a nuclear-free NIH/3T3 cell lysate was prepared and incubated with GST-bound resin in order to deplete the lysate of proteins “sticking” to the GST-tag. This pre-cleared lysate was subsequently incubated with the GST-W-resin. Protein complexes bound to the W-peptide were sequentially eluted with Sarkosyl, high salt, glutathione, and finally with lithium dodecyl sulfate (LDS). Each eluate was separated on a SDS-PAGE and prominent bands relative to the GST-control samples were cut and proteins were analyzed by LC-MS/MS (Figure 29B).

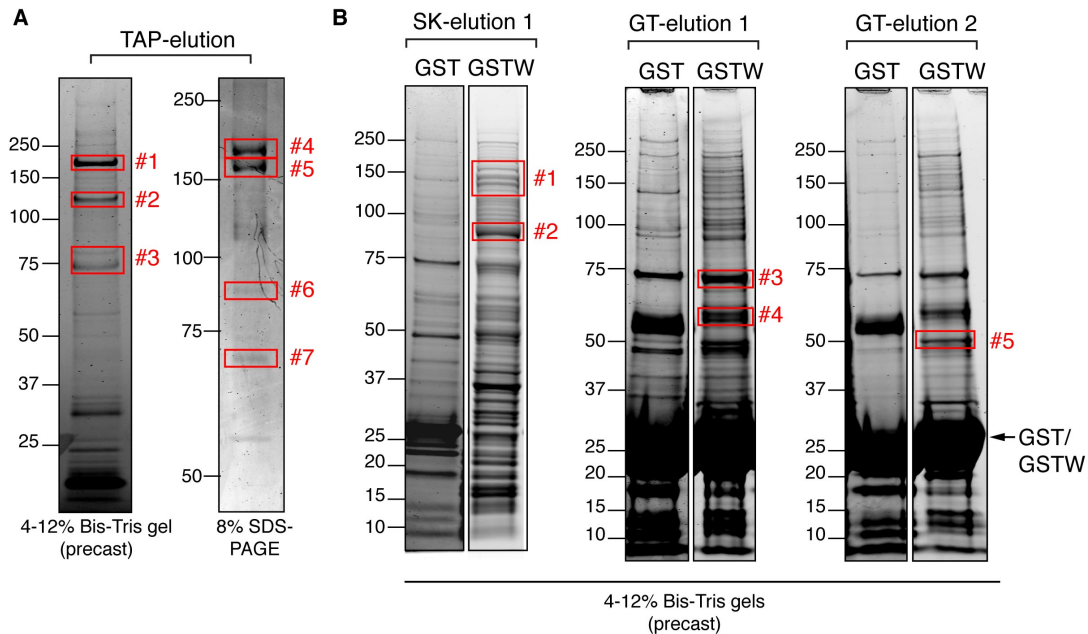


**Figure 29: GelCode Blue stained protein gels of Evc2-TAP and W-peptide affinity purification.** (A) The Evc2-TAP eluate was separated on two gels, a 4-12% Bis-Tris gel and a 8% Tris-Glycine gel. Both gels were stained and the indicated bands (#1-7) were cut and analyzed by mass spectrometry (LC-MS/MS). (B) Shown are stained gels of the Sarkysyl eluate 1 (SK-elution1) and the two Glutathione eluates (GT-elution 1 and 2) of the GST-tagged W-peptide (GSTW) resin and the GST control resin (GST). The indicated bands (#1-5) were cut and subjected to LC-MS/MS analysis. Arrows indicate the GST and GSTW fragment coming off the column during Glutathione elution.

### 3.4.2 Evcbp1 and Evcbp2 interact with Evc and Evc2

The identified proteins of the Evc2-TAP experiment and the GST-W affinity purification were analyzed separately by listing the proteins based on the number of unique peptides. A unique peptide is described as a peptide that exists only in one protein in the database analyzed, in our case the SwissProt mouse protein database. The lists of proteins identified in both experiments were also compared relative to each other with a focus on proteins identified in both experiments. In addition each of the two protein lists was compared to a recently published list of ciliary proteins (“ciliome”) of cultured mouse IMCD3 cells (Ishikawa et al., 2012).

The two most prominent hits in the two independent experiments were proteins of unknown function, named Evc2 binding protein 1 and 2 (Evcbp1 and Evcbp2). Evcbp1 was the top hit of the proteins identified in the TAP experiment with 52 unique

peptides and 74 % peptide coverage. Evcbp2 was identified as the second most abundant protein in the TAP experiment (51 unique peptides, 59 % peptide coverage) and was also identified in the GST-W affinity purification (3 unique peptides, 6 % peptide coverage). Interestingly, Evcbp1 was also identified in the “ciliome” of IMCD3 cells as a protein potentially localized to primary cilia (Ishikawa et al., 2012). Evcbp1 is a soluble protein with predicted molecular weight of 72 kDa. It contains three EF-hand domains (EF1-3), EF1 and EF2 are localized close to the N-terminus and EF3 close to the C-terminus (Figure 30A). An EF-hand is a structural helix-loop-helix  $\text{Ca}^{2+}$  binding motif found in a large family of calcium-binding-proteins with calmodulin being the most famous member of this family (Gifford et al., 2007). Evcbp1 is highly conserved among species and there are homologs in human, mouse, rat, zebrafish (*Danio rerio*) and the african clawed frog (*Xenopus laevis*). Evcbp2 has a predicted molecular weight of 86 kDa and contains two IQ-domains and two coiled-coil regions (Figure 30A). An IQ-domain is a seven-turn alpha-helix motif of approximately 25 a.a. in length with a consensus sequence of [I,L,V]QxxxRGxxx[R,K]. Interestingly IQ-domain containing proteins often interact with EF-hand containing proteins. An example of such an interaction is the binding of EF-hand containing Calmodulin to IQ-domain-repeats containing Myosins (Cheney and Mooseker, 1992; Bähler and Rhoads, 2002). Evcbp2 is conserved among various species and homologs of Evcbp2 can be found in mouse, human, rat, zebrafish, and the western clawed frog (*Xenopus tropicalis*).

In order to study Evcbp1 and Evcbp2 and to verify the binding to Evc2, two NIH/3T3 fibroblast cell lines were generated stably expressing full-length Evcbp1 or Evcbp2, each tagged with a N-terminal YFP-tag (YFP-Evcbp1 cells and YFP-Evcbp2 cells) (Figure 30A). The expression of the two proteins was confirmed by an anti-YFP immunoblot and both cell lines were Hh responsive as determined by SAG-induced Gli1 protein levels (Figure 30B). Anti-YFP IP experiments from these two cell lines were used to test binding to Evc2. Evc2 co-precipitated with both YFP-Evcbp1 and YFP-Evcbp2 independent of pathway activation (Figures 30C and D). Interestingly, also Evc co-precipitated with both proteins (Figure 30C and D). These IP experiment suggest the intriguing idea that Evc, Evc2, Evcbp1 and Evcbp2 form a complex.

However, additional biochemical experiments are needed to further characterize this complex and whether its formation is critical for Hh signal transduction.

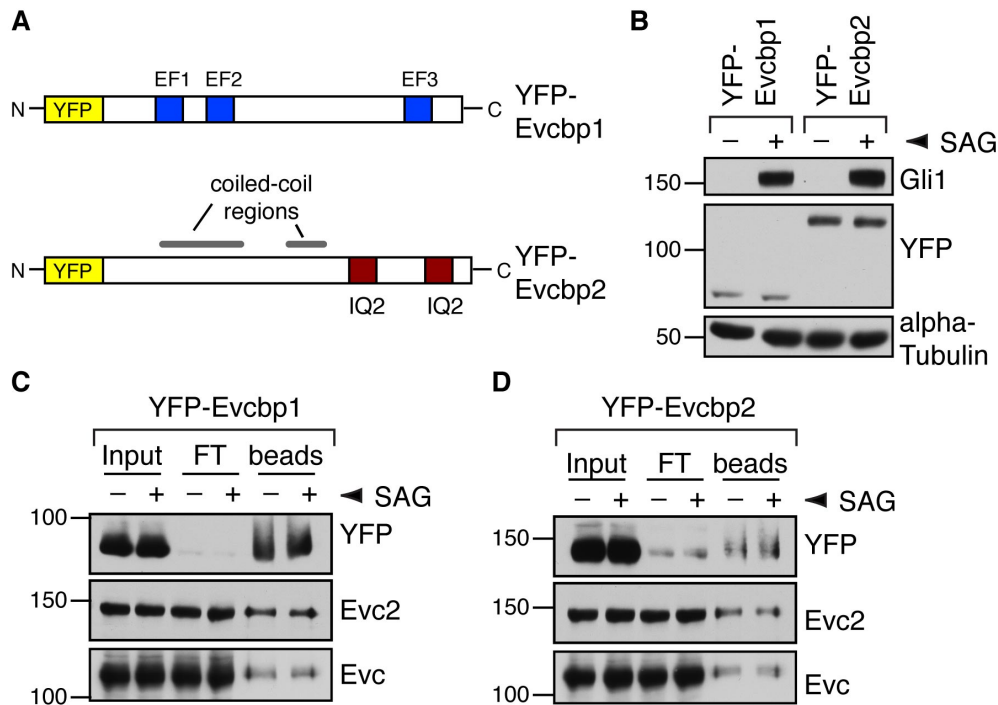


**Figure 30: Evcbp1 and Evcbp2 form a complex with Evc and Evc2.** (A) Schematic of the YFP-Evcbp1 and YFP-Evcbp2 proteins used to make stable cell lines. Evcbp1 contains 3 EF-hand domains (EF1-EF3). YFP-Evcbp2 contains 2 IQ-domains and 2 coiled-coil regions. (B) YFP-Evcbp1 is expressed at lower levels than YFP-Evcbp2 as determined by anti-YFP IB. Both cell lines are Hh responsive as determined by SAG-induced Gli1 protein expression. (C,D) IB of anti-YFP IPs showing the levels of Evc2 and Evc co-precipitating with YFP-Evcbp1 (C) and YFP-Evcbp2 (D), respectively. Input and flow-through (FT) samples show the amount of each protein in the whole extract before and after the IP, respectively.

### 3.4.3 Evidence for a role of Evcbp1 and Evcbp2 in Hedgehog Signaling

If Evcbp1 and Evcbp2 are part of a complex that is involved in Hh signaling one would predict that the two proteins co-localize with Evc2 and Evc in the EvC Zone of primary cilia. Indeed, both YFP-Evcbp1 and YFP-Evcbp2 were found to be ciliary proteins that co-localized with Evc and Evc2 in the EvC Zone independent of pathway activation (Figure 31A-C). Subcellular fractionation of YFP-Evcbp1 and YFP-Evcbp2 cells into cytoplasmic, nuclear, and membrane fraction revealed that Evcbp1 and Evcbp2 are predominantly found in the membrane fraction, further supporting the hypothesis that these proteins are associated with Evc and Evc2 (Figure 31D).

In order to test whether Evcbp1 and Evcbp2 are directly involved in Hh signaling both proteins were transiently expressed in NIH/3T3 cells followed by an Hh reporter assay. The SAG-induced expression of the Hh reporter gene was not altered in cells expressing either YFP-Evcbp1 or YFP-Evcbp2 (Figure 31E). Next, the effect of siRNA-mediated depletion of the two proteins on Hh signaling was tested. Both, Gli1 proteins levels and alkaline phosphatase activity were reduced to a level similar to Smo depletion in C3H10T1/2 cells transfected with either Evcbp2 or Evcbp1 siRNA (Figure 31F) suggesting that both proteins are required for proper Hh signal transduction. In summary the above results suggest that Evcbp1 and Evcbp2 are Evc- and Evc2 binding proteins, that are localized to the EvC Zone and are important for Hh signal transduction. Further experiments are needed to determine the role of these proteins within the Hh signaling cascade.

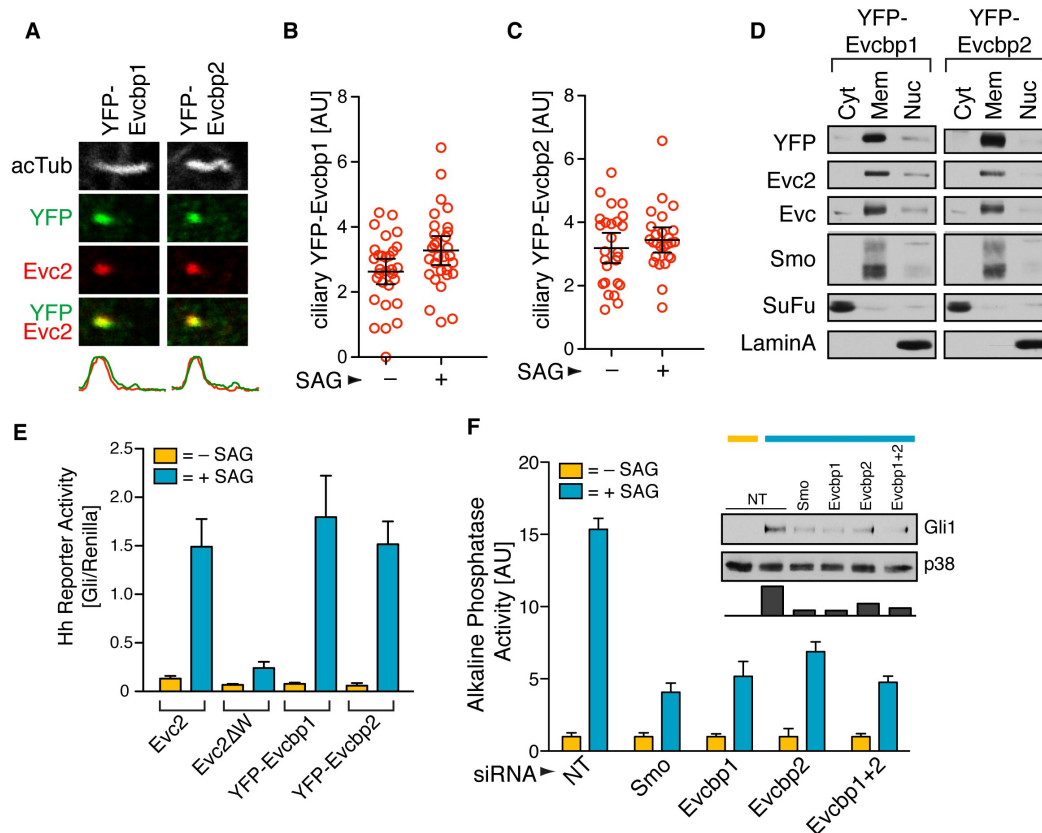


**Figure 31: Evcbp1 and Evcbp2 localize to the EvC Zone and are required for Hh signal transduction.** (A) Confocal images showing the localization of YFP-Evcbp1 and YFP-Evcbp2 (both in green, anti-YFP) at primary cilia (in white, anti-acTub). Both proteins co-localize with Evc2 (in red, anti-Evc2) in the EvC Zone. (B,C) Mean fluorescence intensities ( $\pm$  95% CI) of YFP-Evcbp1 and YFP-Evcbp2 at the cilium in the stable cell lines either left untreated or treated with SAG for 4 hours. (D) IBs of the subcellular fractionation of the YFP-Evcbp1 and YFP-Evcbp2 stable lines into cytoplasm (Cyt), membranes (Mem), and nuclei (Nuc) revealed that both proteins are membrane associated and thus are found in the same fraction as Evc, Evc2, and Smo. LaminA and SuFu are used as nuclear and cytoplasmic marker proteins, respectively. (E) Hh reporter activity was not affected (mean $\pm$ SD) in NIH/3T3 cells transiently transfected with YFP-Evcbp1 and YFP-Evcbp2. (F) The siRNA-mediated depletion of Evcbp1 and Evcbp2 from C3H10T1/2 cells blocks SAG-induced Hh signaling (36 hours). Hh signaling was measured in the same experiment by Gli1 induction (small inset) and by the differentiation of these cells into osteoblasts assayed by increase in alkaline phosphatase activity (mean  $\pm$ SD) after treatment with SAG (36 hours).

## **4. DISCUSSION AND FUTURE PERSPECTIVES**

The primary cilium has been called a “Hedgehog signal transduction machine” due to the requirement of this organelle for proper Hh signal transduction (Goetz et al., 2009). The input into this machine is the accumulation of Smo in the ciliary membrane and the output is activated Gli transcription factors that can transit to the nucleus and initiate the Hh transcriptional program. The present work sheds light on this mysterious step between Smo activation and Gli nuclear translocation by the discovery of an Evc2-Smo Hh signaling complex at the EvC zone of primary cilia.

### **4.1 Models for the function of Evc2 in Hedgehog signaling**

#### **4.1.1 Discussion**

Among the ciliopathy spectrum of human diseases that lead to defects in Hh signaling, EvC and Weyers are unique as they are characterized by ultra-structural normal cilia (Ruiz-Perez et al., 2000; Galdzicka et al., 2002; Takeda et al., 2002; Ruiz-Perez et al., 2003; Blair et al., 2011). Likewise, cilia formation and function is normal in cultured cells with impeded Evc2 function (Figure 12). Thus, phenotypes found in patients with EvC or Weyers, such as polydactyly or heart defects, cannot be attributed to defective cilia. Instead, the data presented in this work suggest that Evc2, the protein mutated in EvC or Weyers has a more direct role in Hh signaling: Evc2 is a positive regulator of the Hh pathway involved at a specific step between Smo and the negative regulators PKA and SuFu (Figure 15G). The Hh signal triggers the association of Evc2 with Smo and the formation of this Smo/Evc2 Hh signaling complex (HSC) at the primary cilium is required for the two canonical outputs of Smo activation - the inhibition of Gli3 repressor (GliR) formation and the induction of Gli2 and Gli3 activator formation (Figure 32). PKA and SuFu control both these outputs, promoting Gli3R formation and inhibiting Gli2/Gli3 activator formation (Wang et al., 2000; Chen et al., 2009; Humke et al., 2010). While the epistatic relationship between

PKA and SuFu is unclear, loss of either is sufficient to lead to full activation of Hh signaling (Hammerschmidt et al., 1996; Svärd et al., 2006; Tuson et al., 2011). However, PKA and SuFu show a critical difference in their dependence on cilia – the loss of PKA requires cilia to promote full Gli activation while cilia are dispensable for Gli activation produced by the complete loss of SuFu (Ocbina and Anderson, 2008; Chen et al., 2009; Jia et al., 2009). The activation of the Gli proteins seems to require two distinct steps, the reversal of PKA's effect on the Gli proteins and the cilia-dependent dissociation of Gli from SuFu. Evc2 is important for both of these aspects of Hh signaling mediated through Smo. Expression of dominant-negative PKA can fully induce a Hh-reporter gene in cells lacking Evc2 function (Figure 14D) and blocking Evc2-function reduces SuFu-dissociation from GliFL (Figure 15F).

In *Drosophila*, where cilia are not required for Hh signaling and the EVC2 gene is absent (Goetz et al., 2009; Blair et al., 2011), a critical step in Smo signaling is the recruitment of a Hh signaling complex (HSC) to the C-terminal tail of Smo. The core component of this complex is the motor protein Costal-2, which binds to the C-terminus of fly Smo (Jia et al., 2003; Barakat et al., 2010; Singh et al., 2011; Tzelepi et al., 2011). The molecular requirement for Evc2 most closely resembles that of kinesin family member 7 (Kif7), a kinesin that is the vertebrate homolog of Costal-2. Kif7 has also been implicated at the step between Smo and PKA/SuFu and, analogous to Evc2, Kif7 is required for the accumulation of Gli proteins at the tips of cilia in response to Hh signaling and for their subsequent activation (Endoh-Yamagami et al., 2009). Kif7 moves from the base to the tip of the cilium in response to Shh and has been proposed to carry Gli proteins to the tips of cilia (Cheung et al., 2009; Liem et al., 2009). Given the proximity of the EvC zone to the transition zone, the Smo-Evc2 complex may regulate the ability of Kif7 to traverse the cilia entry checkpoint selectively inhibiting the transport of SuFu and Gli to the tip of cilia, an event thought to be critical for dissociation of the complex and subsequent Gli activator formation (Tukachinsky et al., 2010).

However, it is also possible that Evc2 might not directly influence the known downstream effectors of Smo such as Kif7, SuFu, and PKA. None of the three proteins were found in the proteomic analysis of Evc2-complexes and neither SuFu

nor PKA were associated with Evc2-YFP (or Evc-YFP) in IP experiments (Figures 22). This suggests, that yet unidentified proteins might be involved in linking Smo/Evc2 with the downstream effectors PKA/SuFu/Gli. These proteins could be involved in processes mediated through Evc2 such as the inhibition of Kif7 function, the inhibition of PKA localization or function, or inhibiting the accessibility of Gli proteins to PKA.

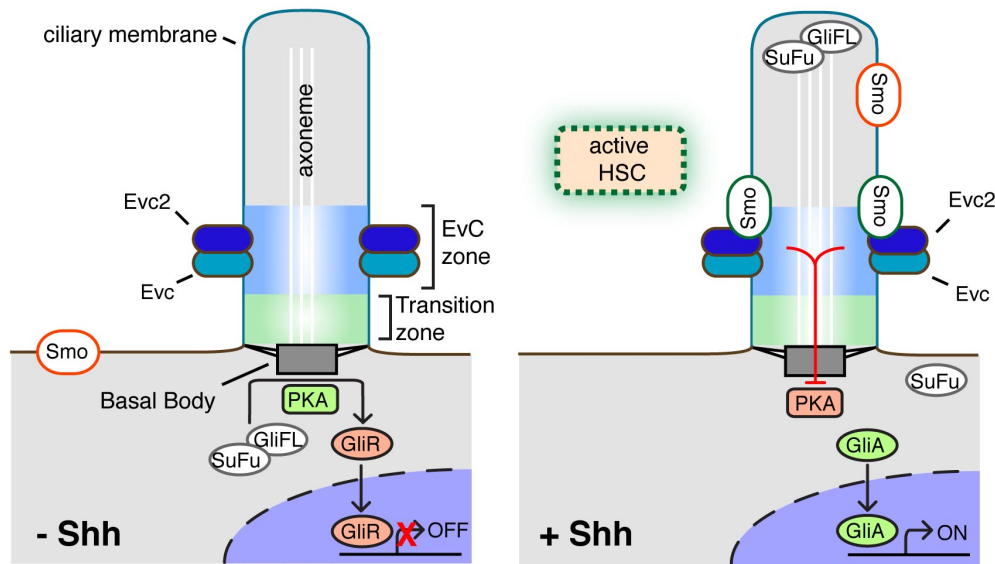


**Figure 32: A model for the function of Evc2 in Hh signaling.** In the absence of Shh (left), PKA channels Gli proteins towards the formation of transcriptional repressors (Gli3R) and away from the formation of Gli activators (GliA). Shh (right) promotes the association of Smo with Evc/Evc2 in the EvC Zone, leading to an active Hedgehog Signaling Complex (HSC) that relieves the negative effect of PKA on the Gli proteins. The Gli-SuFu complex translocates to the tip of the cilium, ultimately leading to the dissociation of SuFu, the nuclear translocation of the Gli proteins, and the transcription of target genes. Only the population of Smo at the EvC Zone participates in an active HSC. Active Smo is outlined in green, inactive Smo in red.

#### 4.1.2 Future Perspectives

Although Kif7 was not detected in the TAP experiment or the affinity purification, it should be subject of future studies to test the direct connection between Kif7 and Evc2. It should be tested whether Kif7 functions upstream or downstream of Evc2 in Hh signaling. As Kif7 is thought to be a negative regulator it would be interesting to analyze the effect of Kif7 knock-down in Evc2 $\Delta$ W cells. If Kif7 acts upstream of Evc2

the pathway should still be blocked. However, if Kif7 is required for Hh signal transduction downstream of Evc2 the siRNA-mediated depletion of Kif7 should reverse the dominant negative effect of Evc2 $\Delta$ W resulting in the activation of the Hedgehog pathway. In addition it could be tested whether Kif7 localization in primary cilia (Endoh-Yamagami et al., 2009) is altered in Evc2 $\Delta$ W cells.

Smo has the typical conformation of a G-protein coupled receptor and is thought to couple to the alpha subunits of heterotrimeric G-proteins in response to the Hh signal. In particular, the family of alpha subunits with inhibitory effects on adenylate cyclase (Gnai) are thought to couple to Smo (Hammerschmidt and McMahon, 1998; DeCamp et al., 2000; Barzi et al., 2011; Polizio et al., 2011). In fact, as part of a side project of this present thesis Gnai proteins were identified in a complex with Smo in a global proteomic screen for Smo binding partners. IP/western analysis confirmed the ligand-dependent association of Smo and Gnai (unpublished data). Although the regulatory connection between Gnai and Smo remains controversial (Low et al., 2008), one hypothesis of Smo signal transduction by Gnai involves the following steps: the Hh-induced activation of Gnai by Smo at the cilium, the inhibition of adenylate cyclase, the reduction of local cAMP levels consequently resulting in a decline of PKA activity. It would be interesting to test whether this aspect of PKA regulation is altered in Evc2 $\Delta$ W cells by testing the ability of Smo to bind to Gnai in Evc2 $\Delta$ W cells.

## **4.2 Evc2-binding proteins and their role in Hedgehog signaling**

### **4.2.1 Discussion and future perspectives**

The goal of the two unbiased mass spectrometry-based assays for the purification of Evc2-complexes and the identification of Evc2 binding partners was to shed light on the mechanism of Smo-Evc2 Hh signal transduction at the EvC zone. Among many interesting potential Evc2-binding proteins that were identified in the TAP and affinity purification of Evc2 complexes (not shown), Evcbp1 and Evcbp2 are two proteins that possibly function together with Evc2 in Hh signaling. Both proteins bind to Evc and

Evc2 and co-localize with Evc and Evc2 in the EvC Zone. Despite the fact that Evcbp1 and Evcbp2 are expected to be soluble proteins with no predicted membrane association and lacking TM domains, both proteins are found in membrane fractions of cultured cells. This suggests that the two proteins are associated with membrane proteins most likely Evc and Evc2. Most importantly, both proteins seem to be positive regulators of Hh signaling required for signal transduction downstream of Smo (Figure 31F). An intriguing model is that all four proteins (Evcbp1, Evcbp2, Evc, and Evc2) are part of a membrane-associated complex (“EvC complex”) that is located at the EvC Zone and required for Evc2-mediated Hh signal transduction.

Further experiments are needed to shed light on the details of the function of Evcbp1 and Evcbp2 in Hh signaling. For instance, it should be tested whether Evcbp1 and Evcbp2 are required at the same step in Hh signaling as Evc2 by using Hh reporter assays and imaging-based cilia trafficking assays of the Hh components. Further, it would be interesting to test whether Evcbp1 and Evcbp2 bind other Hh-proteins such as Smo, PKA, and SuFu. Evcbp2 was identified in the TAP experiment and the GST-W affinity purification experiment suggesting that this protein might bind to the last 43 a.a. of Evc2. Thus, it is predicted that Evcbp2 fails to interact with Evc $\Delta$ W and it would be interesting to test whether Evc $\Delta$ W can bind to Evcbp2 (and Evcbp1) and whether expression of Evc $\Delta$ W leads to the mis-localization of the two proteins along the ciliary axoneme similar to Evc (Figure 23).

In the present work it has been shown that Evc and Evc2 can bind to both Evcbp1 and Evcbp2. However, the detailed subunit architecture of the proposed EvC complex remains unclear and it would be interesting to test whether all four components interact with each other or not. This could be tested by knocking down each of the components individually and testing for the binding of the remaining three. A summary of the expected results from this strategy is depicted in Figure 33 using an Evc-IP as example.

In addition to the analysis of the composition of the EvC complex it would be interesting to test if the formation of this EvC complex requires the cilium, which of the components is important for the EvC Zone localization, and whether the localization of the complex to the EvC Zone is altered in Evc $\Delta$ W cells.

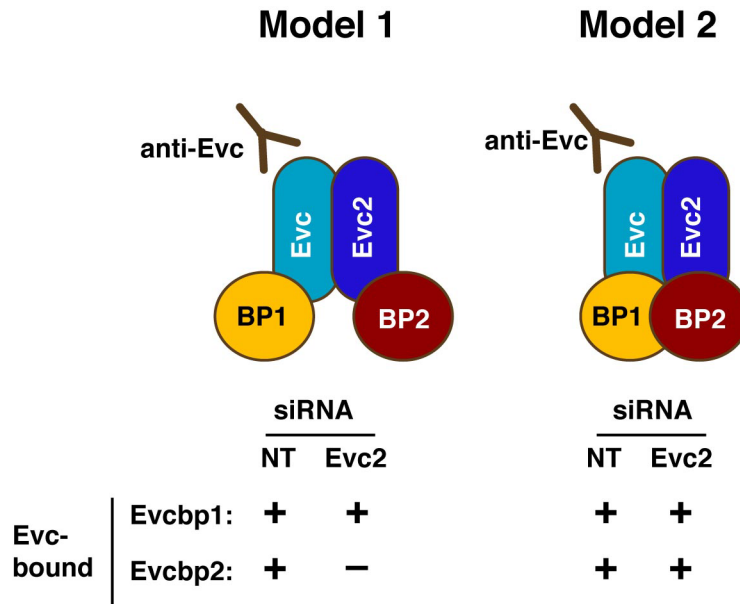


**Figure 33: Models for the subunit architecture of the EvC complex.** Shown are the two different models and a summary of the predicted outcome of an Evc-IP experiment in combination with Evc2 siRNA transfection. In cells transfected with a non-targeting siRNA (NT) both Evcbp1 and Evcbp2 are bound to Evc independent of the subunit architecture. Evc2 knockdown will allow distinguishing between the two models. If model 2 is correct Evcbp2 will still be bound to Evc, however if model 1 is correct the interaction between Evc and Evcbp2 will be lost.

Furthermore, it should be tested whether the binding of Evcbp1 and Evcbp2 to the EvC complex requires the IQ-domains of Evcbp2 or the EF-hand motifs of Evcbp1. An interesting aspect of the interactions of IQ-domain containing proteins and EF-hand proteins is that the formation of these complexes can be either  $Ca^{2+}$ -dependent or  $Ca^{2+}$ -independent (Bähler and Rhoads, 2002). Thus, it should be tested whether altering  $Ca^{2+}$  levels affects the binding of Evcbp1 and Evcbp2 to Evc and Evc2. Interestingly, changes in intracellular  $Ca^{2+}$  levels have been previously reported in the context of Hh signaling. In mouse embryonic stem cells (ES cells) and in rat gastric mucosal epithelial cells Shh treatment was shown to increase intracellular  $Ca^{2+}$  levels. This effect could be reversed by inhibition of Smo using cyclopamine (Osawa et al., 2006; Heo et al., 2007). Shh was also shown to acutely increase  $Ca^{2+}$  spike activity in the developing spinal cord (Belgacem and Borodinsky, 2011).

The observation of the membrane association of Evcbp1 and Evcbp2 suggests the idea that these proteins are linked to membranes through interaction with membrane

proteins, possibly Evc and Evc2. Knocking down Evc and/or Evc2 followed by subcellular fractionation can be used to test whether this membrane association is only mediated through Evc and Evc2 or whether other membrane proteins are involved.

Besides these proposed biochemical experiments it should also be considered to analyze the role of Evcbp1 and Evcbp2 in the developing embryo *in vivo*. It would be interesting to see whether *Evcbp1* and *Evcbp2* mutant mice display mainly skeletal abnormalities overlapping with those observed in EvC and Weyers patients (Baujat and Le Merrer, 2007) or whether the phenotypic spectrum includes distinct features. Mutations in *EVC* and *EVC2* only account for about 2/3 of cases of EvC suggesting that additional genes remain to be identified in this disorder. Thus, it would be of great interest to also sequence the *EVCBP1* and *EVCBP2* genes from patient samples with EvC, Weyers, or other skeletal dysplasias.

### **4.3 The EvC Zone is a new compartment within the primary cilium**

#### **4.3.1 Discussion**

In the present work a new region within the primary cilium was discovered which is distinct from the known ciliary sub-compartments including the basal body, the transition zone (TZ), and the Inv compartment. The EvC Zone sits between the TZ and the Inv compartment and is defined as the region in the primary cilium where Evc and Evc2 are located (Figure 13). The TZ can be morphologically distinguished in electron micrographs as a shift from the triple microtubules of the basal body to the doublet microtubules of the axoneme as well as by the presence of additional electron-dense structures (Czarnecki and Shah, 2012). Based on the evaluation of published EM images of primary cilia from various cell types, the EvC Zone seems to lack such structural determinants. Distal to the TZ, the ciliary axoneme is surrounded by the ciliary membrane, but no additional structural elements are visible that would allow for the distinction of the EvC Zone or the further distal localized Inv compartment. Thus, both the Inv compartment and the EvC Zone cannot be

distinguished by their morphology, but are characterized by the localization of specific proteins to these two regions (Watanabe et al., 2003).

The overlapping feature between these three sub-compartments of the primary cilium lays in the proteins localized to these regions, which have been shown to be involved in ciliopathies. In terms of the TZ this includes numerous proteins involved in many different ciliopathies leading to the model of the TZ as a signaling center (Czarnecki and Shah, 2012). The Inv compartment has mostly been implicated in nephronophthisis as the protein Inversin, after which the Inv compartment is named (Shiba et al., 2008), has been implicated in this ciliopathy (Otto et al., 2003). Interestingly, other proteins were shown to localize to this compartment that have also been linked to nephronophthisis such as Nphp3 and Nphp9 (Shiba et al., 2010). Similar to the Inv compartment and the TZ, the EvC Zone may represent an important signaling compartment in primary cilia, with implications for understanding ciliopathies.

An intriguing idea is that “cross-talk” between these adjacent zones provides a mechanism by which for example signaling events at the EvC Zone could impact trafficking decisions made at the TZ. What could be the candidates for this “cross-talk”? Among all the ciliopathies the EvC and Weyers syndromes, Short Rib Polydactyly Syndromes (SRPs), Jeune asphyxiating thoracic dystrophy (JATD), and Sensenbrenner Syndrome are skeletal disorders that belong to sub-class of ciliopathies characterized by significant phenotypic overlap (Huber and Cormier-Daire, 2012). Morphological features include short ribs, polydactyly, shortened long bones, and craniofacial defects. Today, 10 genes have been identified in these skeletal ciliopathies and many of the phenotypes can be attributed to defective chondrocyte cilia or aberrant Hh signaling (Huber and Cormier-Daire, 2012). Besides *EVC/EVC2* and *NEK1* (NIMA-related expressed kinase 1), many genes identified encode for proteins involved in intraflagellar transport (IFT). These genes include the dynein motor *DYNC2H* and *IFT122*, *IFT43*, *IFT80*, *WDR35* (WD repeat domain 35), *WDR19* (WD repeat domain19; encodes Ift144), and *TTC21B* (tetratricopeptide repeat domain 21B; encodes Ift139) (Beales et al., 2007; Dagoneau et al., 2009; Gilissen et al., 2010; Walczak-Sztulpa et al., 2010; Arts et al., 2011; Bredrup et al., 2011; Davis et al.,

2011). In addition to these ciliopathy genes a recent publication describes the interesting finding that *Ift25* (a IFT-B subunit) is dispensable for cilia formation, but is required for the signal-dependent transport of multiple Hh components. Mutations in the *IFT25* gene have not been identified in human ciliopathies yet, but the *Ift25* mouse phenotype includes clinical manifestations similar to those found in EvC (Keady et al., 2012).

#### **4.3.2 Future Perspectives**

Based on the phenotypic overlap between EvC and Weyers Syndromes with this subgroup of skeletal ciliopathies it would be interesting to test whether there is a direct biochemical connection between these proteins or whether mutations in these genes influence *Evc2* localization and function at the EvC Zone. Also, the localization of these proteins in *EvcΔW* cells or in cells depleted of endogenous *Evc2* could be tested. In addition to the analysis of these candidate proteins it would be also interesting to expand the spectrum of EvC Zone proteins by identifying other proteins localized to this region of the cilium. Approaches could include immunoprecipitation or tandem affinity purification experiments of known EvC proteins – such as *Evc*, *Evcbp1*, and *Evcbp2* – and the identification of these purified complexes by mass spectrometry. The role of these novel EvC Zone proteins in defining the EvC Zone, their interplay with the TZ and the Inv compartment, their involvement in Hh signaling, and their involvement in ciliopathies especially of skeletal dysplasias would be of great interest.

## **4.4 The biochemical basis for Ellis van Creveld and Weyers syndromes**

### **4.4.1 Discussion**

Targeting of Evc2 to the EvC Zone is accomplished by two hierarchical but separable steps – trafficking to the cilium followed by a second step that restricts Evc2 distribution to this region. The mutant Evc2 $\Delta$ W protein lacking 43 a.a at its C-terminus trafficks to the primary cilium but is not restricted to the EvC zone suggesting that the second step requires these 43 a.a. of the Evc2 protein, also called the W-peptide. Interestingly, the W-peptide is also a transferable sequence element allowing for the restriction of other ciliary proteins such as Smo to the EvC Zone (Figure 20). In addition, the two-step mechanism for Evc2 localization to the EvC Zone provides an explanation for the opposite modes of inheritance seen in recessive EvC and dominant Weyers disease (Figure 34). Mutant Evc2 proteins based on mutations found in EvC lacking slightly longer fragments at the C-terminus are non-functional because they fail to localize to cilia (Figure 21). Mutant mouse proteins implicated in Weyers interfere with Hh signaling because they are mis-localized throughout the ciliary membrane (Figures 18 and 21). In fact, every single mutant protein studied in the present work showed this correlation between mis-localization along the axoneme and dominant-negative effect in Hh signaling.

One particular mutant is an interesting example for this hypothesis. The murine Evc2 $\Delta$ 1157-1220 mutant was designed based on the human mutation c.3731dupT found in EvC patients (Valencia et al., 2009). In humans this frameshift mutation is predicted to introduce a non-sense codon leading to the production of a truncated protein (p.S1245VfsX20). However, a stop codon does not occur until 20 a.a after the non-sense codon. The murine Evc2 $\Delta$ 1157-1220, which is truncated at the position equivalent to the position of the non-sense codon in the human mutation, exhibited a dominant-negative effect unlike predicted by its involvement in recessive EvC syndrome. Why is the human c.3731dupT mutation a recessive EvC mutation and not a dominant Weyers mutation? The answer most likely lays in the additional 20 a.a present in the human mutant protein, which might lead to the degradation of the

protein or its mis-localization. Although not expected, the observed discrepancy between this EvC mutation and the dominant-negative effect further strengthens the hypothesis of a correlation between localization and dominant-negative effect described above. In accordance to the observed dominant negative effect the protein was spread out along the ciliary membrane similar to Evc2 $\Delta$ W (Figure 21).

What is the biochemical basis for the dominant-negative effect of the mutant Evc2 $\Delta$ W protein in Hh signaling? There is clearly a connection between the dominant-negative effect and the localization within the cilium. Like the wild-type protein Evc2 $\Delta$ W is capable of binding to Smo and Evc. Thus, these interactions do not require the W-peptide and a failure of binding to the two proteins is not the cause of the dominant-negative effect of Evc2 $\Delta$ W. However, while the wild-type Evc2 seems to form oligomers, Evc2 $\Delta$ W fails to bind to Evc2 suggesting that this defect might be the basis for the dominant-negative effect of this mutant protein (Figure 23). During the course

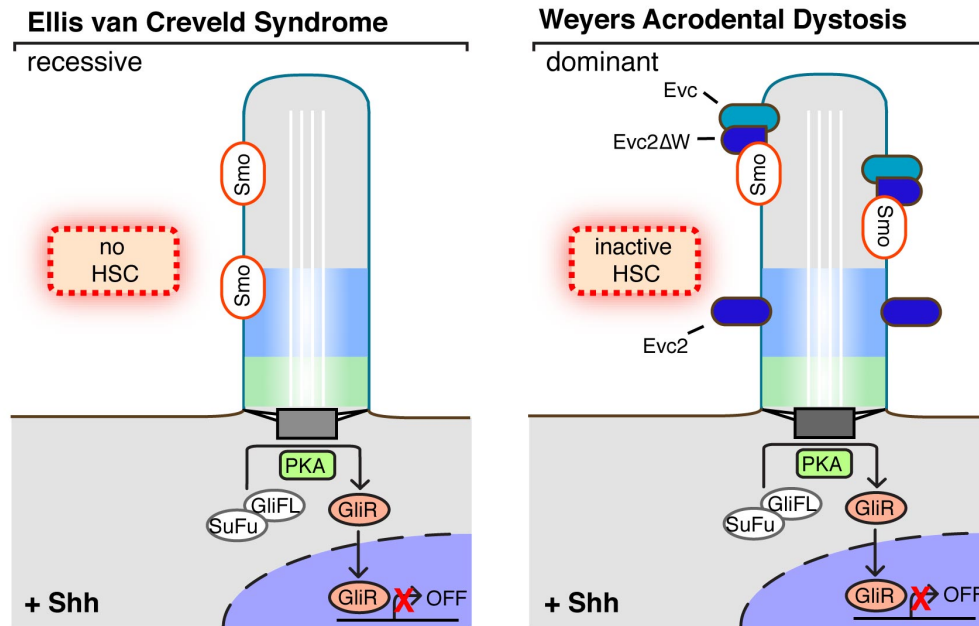


**Figure 34: Models of Hh signaling defects in Ellis van Creveld Syndrome (EvC) and Weyers Acrofacial Dysostosis (Weyers).** In the recessive EvC syndrome (left), mutant Evc2 proteins fail to localize in cilia, preventing the formation of an active HSC, leading to the repression of Hh target gene transcription. In the dominant Weyers syndrome, the mutant Evc2 $\Delta$ W protein is not confined to the EvC Zone, thus sequestering Smo and Evc in inactive complexes and preventing assembly of a functional HSC. In both cases Hh target gene expression is repressed. Compare to Figure 32. Active Smo is outlined in green, inactive Smo in red.

of the Smo-Evc2 immunoprecipitation experiments it was found that Evc2 $\Delta$ W bound significantly more Smo than wild-type Evc2 (Figure 23). Consistently, Smo showed a greater overlap with Evc $\Delta$ W than with Evc2 in immunofluorescence images (Figure 24). One plausible model for Evc2 $\Delta$ W's dominant negative effect is that due to its failure to multimerize with endogenous Evc2 in the EvC Zone, it sequesters Smo away from this zone preventing the activation of ciliary Smo, and eventually leading to the inhibition of the pathway.

#### **4.4.2 Future Perspectives**

The proposed Evc2 $\Delta$ W-sequestration model for the dominant negative effect can be tested by an immunoprecipitation experiment. If the model is correct there should be less Smo bound to endogenous Evc2 in Evc2 $\Delta$ W-YFP cells than in Evc2-YFP cells. A more general question is what distinguishes Evc2 complexes from Evc $\Delta$ W complexes. In order to determine whether overall complex sizes are different native gels or gel filtration could be used. In order to analyze the composition of the complexes a comparative proteomic approach such as SILAC (Stable Isotope Labeling with Amino Acids in Cell Culture) (Ong et al., 2002) could be applied as it would allow for the identification of interaction partners that are differentially bound to Evc2 or Evc $\Delta$ W. For SILAC, Evc2-YFP-FLAG and Evc2 $\Delta$ W-YFP-FLAG cells would be labeled with non-radioactive heavy and light isotopic forms of amino acids (distinguishable by mass spectrometry), respectively, and subjected to tandem affinity purification. The "heavy to light" ratio for a protein that selectively binds Evc2 over Evc2 $\Delta$ W will be biased towards the isotope used to label the Evc2-YFP-FLAG cells.

In addition, it would be interesting to shed light on the dominant negative effect of the murine Evc2 $\Delta$ 1157-1220 mutant (see discussion above). It could be tested whether the human mutant protein found in EvC patients (p.S1245VfsX20), which includes the additional 20 a.a., is a dominant negative protein and is distributed along the cilium. Also a murine version exactly mimicking the human mutant protein including the additional 20 a.a at the C-terminus should be synthesized and tested for both ciliary localization and dominant negative effect in a Hh reporter assay.

## 4.5 The tissue-specific role of Evc2 in Hedgehog signaling

### 4.5.1 Discussion and future perspectives

Smo is a core component of the Hh pathway and is absolutely required for Hh signaling in all tissues (Zhang et al., 2001). The present work and studies of other groups have found that Evc2 is critical for Hh signaling in cultured fibroblast cell lines and blocking Evc2 function leads to a drastic reduction of Hh pathway activation (Valencia et al., 2009; Blair et al., 2011) (Figures 10 and 11). However, it seems that Evc2 likely plays a more tissue-specific role in Hh signaling than for example Smo. In humans, loss-of-function mutations in EVC or EVC2, lead to EvC or Weyers syndrome characterized by clear Hh phenotypes in the skeleton, heart and oro-facial tissues (Ruiz-Perez and Goodship, 2009). A fascinating question is why the loss of Evc2 in humans does not produce Hh phenotypes in other tissues, notably the nervous system. At least in humans, this tissue specificity cannot be explained by a redundancy between EVC and EVC2 because rare patients carrying a deletion that eliminates both genes do not show more severe phenotypes (Temtamy et al., 2008). One explanation for the tissue specificity could be that a different protein or mechanism takes over the function of Evc or Evc2 in tissues such as the nervous system. This hypothesis is based on the observation that neither EVC nor EVC2 are expressed in the mouse neural tube during development (Takeda et al., 2002; Ruiz-Perez et al., 2007). Unfortunately, there is no *Evc2* loss-of-function mouse model for either EvC or Weyers syndrome, which would allow for more detailed analysis of tissue-specific Hh-signaling defects. Blair et al. used *Evc2*<sup>-/-</sup> MEFs in their study, but the publication of the *Evc2*<sup>-/-</sup> mouse phenotype is still to be awaited (Blair et al., 2011).

## **4.6 Evc2 as a potential drug target in Hedgehog-related cancers**

### **4.6.1 Discussion**

Activating Smo mutations are one of the most common mechanisms by which the Hh pathway is induced in cancer and it is not surprising that Smo is the main drug target in the treatment of Hh-related cancers (Lin and Matsui, 2012). In the present work Evc2 was identified as being critical for Smo signaling at the primary cilium and is also required for signaling by the Smo mutant SmoM2 (W535L in human Smo), a constitutively active oncoprotein originally identified in basal cell carcinoma (BCC) (Xie et al., 1998). The ability of therapeutic reagents to inhibit SmoM2 is commonly used as a metric to predict their effectiveness in oncogenic Hh signaling (Taipale et al., 2000; Wu et al., 2012). Thus, the requirement of Evc2 for SmoM2 signaling does not only highlight the critical role of Evc2 in Smo signal transduction, but also implies that Evc2 may qualify as a drug target for the treatment of Hh-related cancers. The observation that Evc2 might be required in certain tissues only, further suggests the possibility of interrupting Smo signaling in tissue-selective manner by targeting Evc2 rather than Smo itself.

### **4.6.2 Future Perspectives**

In the present work it was shown that a Smo/W-peptide fusion protein that is restricted to the EvC Zone is more active in an Hh reporter assay compared to the wild-type protein (Figure 27) suggesting that the localization of Smo to the EvC Zone is required for its function. It would be interesting to test whether the restriction of the Smo/W-peptide fusion protein depends on Evc2. If this is the case, the activity of SmoW should be blunted in cells transfected with an Evc2 siRNA. In addition, it would be interesting to test whether the constitutively active SmoM2 mutant is restricted to the EvC Zone or more generally whether the localization of SmoM2 is altered in cells transfected with Evc2 siRNA or Evc $\Delta$ W expression.

In order to test for the involvement of Evc2 in Hh-induced cancers patient samples or tissue derived from mouse models should be analyzed for Evc2 expression. In addition, it would be exciting to test the additive survival benefit of Evc $\Delta$ W expression

in a mouse xenograft model of an Hh-related cancer such as medulloblastoma (Kim et al., 2010b). In terms of the development of potential therapeutics interfering with Evc2 function one could test whether the targeting of the extracellular N-terminal fragment of Evc2 with a monoclonal antibody has a function blocking effect. This strategy is broadly used as immunotherapy for the treatment of many cancers as it targets the receptors involved in the formation of these cancers (Galluzzi et al., 2012).

## 5. SUMMARY

Primary cilia are non-motile cell surface protrusions found on most cells in our bodies and are important signaling centers during development. A number of human diseases, called “ciliopathies”, are caused by defects in cilia structure or function. Patients suffering from these syndromes display pleiotropic phenotypes affecting nearly all organ systems, highlighting the profound role of primary cilia in human physiology. A subset of the phenotypes seen in ciliopathy patients can be attributed to defective Hedgehog (Hh) signaling, a signaling pathway that critically depends on primary cilia as most Hh pathway proteins are localized to primary cilia. The ciliary localization of the Hh components is dynamically influenced by the Hh ligands such as Sonic Hedgehog (Shh). While considerable work has focused on the phenotypic consequences of defects in cilia and on the localization of signaling proteins in cilia, the biochemical mechanisms driving signal transduction at cilia remain poorly understood and only few biochemical interactions have been described between ciliopathy proteins and core components of the Hh pathway.

The present study aimed at investigating the biochemical mechanisms how two ciliopathies, Ellis van Creveld Syndrome and Weyers Acrofacial Dysostosis that are characterized by ultra-structurally normal cilia, lead to defects in Hh signaling. Evc2, a ciliary protein that is defective in these ciliopathies, was found to associate with the Hh protein Smo after activation of the pathway. The formation of this Smo-Evc2 complex is under rigorous spatial control, being restricted to a distinct ciliary compartment, which was named the “EvC Zone”. Mutant Evc2 proteins that localize in cilia but are displaced from the EvC Zone are dominant inhibitors of Hh signaling. Disabling Evc2 function blocks Hh signaling at a specific step between Smo and the downstream regulators Protein Kinase A and Suppressor of Fused, preventing activation of the Gli transcription factors. Thus, the Smo-Evc2 signaling complex at the EvC Zone is required for Hh signal transmission and elucidates the molecular basis of Ellis van Creveld Syndrome and Weyers Acrofacial Dysostosis.

## 6. ZUSAMMENFASSUNG

Bei primären Zilien handelt es sich um Membranfortsätze eukaryotischer Zellen, deren Funktion im Gegensatz zu motilen Zilien in der Signalaufnahme und Signalvermittlung besteht. Als „Zell-Antennen“ spielen sie eine wichtige Rolle für die Entwicklung vieler Organismen und Funktionsstörungen des primären Ziliums können zu schwerwiegenden Krankheiten, den so genannten Ziliopathien, führen. Einer Vielzahl der Symptome von Ziliopathie-Patienten liegt eine Störung des Hedgehog (Hh)-Signalwegs zu Grunde, da viele Komponenten dieses Signalweges in Zilien lokalisiert sind und daher die Hh Signaltransduktion nur in intakten Zilien stattfinden kann. In den vergangenen Jahren konzentrierte sich die Forschung in diesem Feld vor allem auf die phänotypische Charakterisierung von Ziliendefekten und die Identifizierung von Zilien-lokalisierten Signalproteinen. Die biochemischen Mechanismen, die den Ziliopathien zu Grunde liegen sind unklar und keinerlei biochemische Interaktionen zwischen Hh Proteinen und Ziliopathie-Proteinen konnten bislang gefunden werden.

Im Zuge der vorliegenden Doktorarbeit sollten die biochemische Grundlagen der beiden Ziliopathien Ellis van Creveld Syndrom (EvC) und Weyers Acrofaciale Dysostosis (Weyers) untersucht werden. Im Unterschied zu anderen Ziliopathien zeichnen sich diese beiden Krankheiten durch die Besonderheit aus, dass die Zilien sowohl strukturell als auch funktional normal sind. Innerhalb dieser Doktorarbeit konnte gezeigt werden, dass Evc2 – ein Protein, welches in Patienten mit EvC und Weyers mutiert ist – mit dem Hh Protein Smoothed (Smo) interagiert. Die Bildung dieses so genannten „Hedgehog Signal Komplexes“ (HSK) wird durch den Hh Liganden Shh ausgelöst und ist lokal auf eine Region innerhalb des Ziliums beschränkt. Bei dieser Region handelt es sich um ein zuvor unbekanntes Sub-Kompartiment am distalen Ende des primären Ziliums, das auf Grund der spezifischen Lokalisierung von Evc und Evc2 als EvC Zone bezeichnet wurde. Es konnte gezeigt werden, dass Evc2-Mutanten, die zwar im Zilium lokalisiert sind aber nicht auf die „EvC Zone“ beschränkt sind, einen dominant-negativen Effekt auf den

Hh Signalweg ausüben. Evc2 ist ein positiver Regulator innerhalb des Hh Signalweges, der seine Funktion zwischen Smo und den beiden negativen Regulatoren Proteinkinase A und Suppressor of Fused ausübt und daher für alle Aspekte der Signaltransduktion durch Smo benötigt wird. Mit Hilfe der erworbenen Kenntnis über Evc2 und durch die Analyse verschiedenster Evc2-Mutanten konnten außerdem die molekularen Mechanismen die zu den beiden Ziliopathien Ellis van Creveld Syndrom und Weyers Acrofaciale Dysostosis führen, entschlüsselt werden.

## 7. ABBREVIATIONS

a.a.	amino acid
acTub	acetylated tubulin
AEBSF	4-(2-Aminoethyl) benzenesulfonyl fluoride hydrochloride
Arl13b	ADP-ribosylation factor-like protein 13B
BCC	basal cell carcinoma
bp	base pairs
BSA	bovine serum albumine
C	cytoplasmic
CHS	cholesteryl hemisuccinate
CI	confidence interval
DAPI	4',6-diamidino-2-phenylindole
DDM	n-dodecyl $\beta$ -D-maltoside
DMP	dimethyl pimelimidate
DN	dominant-negative
DNA	deoxyribonucleic acid
DSP	dithiobis succinimidyl propionate
DTT	dithiothreitol
E	embryonic day
EDC	1-ethyl-3-(3-dimethylaminopropyl)carbodiimide
EDTA	ethylene diamine tetraacetic acid
EGTA	ethylene glycol tetraacetic acid
EndoH	endoglycosidase H
ER	endoplasmic reticulum
esiRNA	endoribonuclease-prepared siRNA
EvC	Ellis van Creveld Syndrome
Evc	Ellis van Creveld (protein)
Evc2	Ellis van Creveld syndrome 2 (protein)

FBS	fetal bovine serum
FT	flow through
g	g-force
GBP	GFP binding protein
GFP	green fluorescent protein
Gli	GLI-Kruppel family member
GliA	Gli activator
GliFL	Gli full-length
GliR	Gli repressor
GST	glutathione S-transferase
gTub	gamma Tubulin
HCl	hydrogen chloride
Hh	Hedgehog
IB	immunoblot
IF	immunofluorescence
IFT	intraflagellar transport
Ig	immunoglobulin
Inv	Inversin
IP	immunoprecipitation
IPTG	isopropyl $\beta$ -D-1-thiogalactopyranoside
KCl	potassium chloride
kDa	1000 Dalton
LB	Luria Broth
LPC	Leupetin-Pepstatin-Chymostatin
MEF	mouse embryonic fibroblasts
MgCl <sub>2</sub>	magnesium chloride
min	minute(s)
MW	molecular weight
N	nuclear
NaCl	sodium chloride
NP-40	Nonidet P-40

P	postnatal day
PAGE	polyacrylamide gelelectrophoresis
PBS	phosphate-buffered saline
PCR	polymerase chain reaction
PFA	paraformaldehyde
PKA	Protein kinase A
PLA	Proximity ligation assay
PNGase	Peptide-N-glycosidase F
PNS	postnuclear supernatant
Ptch1	Patched 1
RNA	ribonucleic acid
RT	room temperature
SAG	Smoothed agonist
SD	standard deviation
SDS	sodium dodecyl sulfate
Shh	Sonic Hedgehog
siRNA	Small interfering RNA
Smo	Smoothed
STED	stimulated emission depletion microscopy
SuFu	Suppressor of Fused
Sulfo-NHS	N-hydroxysulfosuccinimide
TAP	tandem affinity purification
TBS	tris-buffered saline
TCEP	Tris(2-carboxyethyl)phosphine
TM	trans membrane
TZ	transition zone
v/v	volume per volume
W-peptide	Weyers-peptide
w/v	weight per volume
Weyers	Weyers Acrofacial Dysostosis
YFP	yellow fluorescent protein

## 8. REFERENCES

- Anderson, R.G. (1977). Biochemical and cytochemical evidence for ATPase activity in basal bodies isolated from oviduct. *The Journal of Cell Biology* 74, 547–560.
- Ansley, S.J., Badano, J.L., Blacque, O.E., Hill, J., Hoskins, B.E., Leitch, C.C., Kim, J.C., Ross, A.J., Eichers, E.R., Teslovich, T.M., et al. (2003). Basal body dysfunction is a likely cause of pleiotropic Bardet-Biedl syndrome. *Nature* 425, 628–633.
- Arts, H.H., Bongers, E.M.H.F., Mans, D.A., van Beersum, S.E.C., Oud, M.M., Bolat, E., Spruijt, L., Cornelissen, E.A.M., Schuurs-Hoeijmakers, J.H.M., de Leeuw, N., et al. (2011). C14ORF179 encoding IFT43 is mutated in Sensenbrenner syndrome. *J. Med. Genet.* 48, 390–395.
- Bai, C.B., Auerbach, W., Lee, J.S., Stephen, D., and Joyner, A.L. (2002). Gli2, but not Gli1, is required for initial Shh signaling and ectopic activation of the Shh pathway. *Development* 129, 4753–4761.
- Barakat, M.T., Humke, E.W., and Scott, M.P. (2010). Learning from Jekyll to control Hyde: Hedgehog signaling in development and cancer. *Trends Mol Med* 16, 337–348.
- Barzi, M., Kostrz, D., Menendez, A., and Pons, S. (2011). Sonic Hedgehog-induced proliferation requires specific G $\alpha$  inhibitory proteins. *J. Biol. Chem.* 286, 8067–8074.
- Baujat, G., and Le Merrer, M. (2007). Ellis-van Creveld syndrome. *Orphanet J Rare Dis* 2, 27.
- Bähler, M., and Rhoads, A. (2002). Calmodulin signaling via the IQ motif. *FEBS Lett.* 513, 107–113.
- Beales, P.L., Bland, E., Tobin, J.L., Bacchelli, C., Tuysuz, B., Hill, J., Rix, S., Pearson, C.G., Kai, M., Hartley, J., et al. (2007). IFT80, which encodes a conserved intraflagellar transport protein, is mutated in Jeune asphyxiating thoracic dystrophy. *Nat. Genet.* 39, 727–729.
- Belgacem, Y.H., and Borodinsky, L.N. (2011). Sonic hedgehog signaling is decoded by calcium spike activity in the developing spinal cord. *Proc. Natl. Acad. Sci. U.S.A.* 108, 4482–4487.
- Bitgood, M.J., Shen, L., and McMahon, A.P. (1996). Sertoli cell signaling by Desert hedgehog regulates the male germline. *Current Biology* 6, 298–304.
- Blair, H.J., Tompson, S., Liu, Y.-N., Campbell, J., MacArthur, K., Ponting, C.P., Ruiz-Perez, V.L., and Goodship, J.A. (2011). Evc2 is a positive modulator of Hedgehog signalling that interacts with Evc at the cilia membrane and is also found in the

nucleus. *BMC Biology* 9, 14.

Bredrup, C., Saunier, S., Oud, M.M., Fiskerstrand, T., Hoischen, A., Brackman, D., Leh, S.M., Midtbø, M., Filhol, E., Bole-Feysot, C., et al. (2011). Ciliopathies with skeletal anomalies and renal insufficiency due to mutations in the IFT-A gene WDR19. *Am. J. Hum. Genet.* 89, 634–643.

Buttitta, L., Mo, R., Hui, C.-C., and Fan, C.-M. (2003). Interplays of Gli2 and Gli3 and their requirement in mediating Shh-dependent sclerotome induction. *Development* 130, 6233–6243.

Caspary, T., García-García, M.J., Huangfu, D., Eggenschwiler, J.T., Wyler, M.R., Rakeman, A.S., Alcorn, H.L., and Anderson, K.V. (2002). Mouse Dispatched homolog1 is required for long-range, but not juxtacrine, Hh signaling. *Current Biology* 12, 1628–1632.

Caspary, T., Larkins, C.E., and Anderson, K.V. (2007). The graded response to Sonic Hedgehog depends on cilia architecture. *Developmental Cell* 12, 767–778.

Chang, B., Khanna, H., Hawes, N., Jimeno, D., He, S., Lillo, C., Parapuram, S.K., Cheng, H., Scott, A., Hurd, R.E., et al. (2006). In-frame deletion in a novel centrosomal/ciliary protein CEP290/NPHP6 perturbs its interaction with RPGR and results in early-onset retinal degeneration in the rd16 mouse. *Hum. Mol. Genet.* 15, 1847–1857.

Chen, J.K., Taipale, J., Young, K.E., Maiti, T., and Beachy, P.A. (2002). Small molecule modulation of Smoothed activity. *Proc. Natl. Acad. Sci. U.S.A.* 99, 14071–14076.

Chen, M.H., Wilson, C.W., Li, Y.J., Law, K.K.L., Lu, C.S., Gacayan, R., Zhang, X., Hui, C.C., and Chuang, P.T. (2009). Cilium-independent regulation of Gli protein function by Sufu in Hedgehog signaling is evolutionarily conserved. *Genes Dev.* 23, 1910–1928.

Cheney, R.E., and Mooseker, M.S. (1992). Unconventional myosins. *Curr. Opin. Cell Biol.* 4, 27–35.

Cheung, H.O.L., Zhang, X., Ribeiro, A., Mo, R., Makino, S., Puvion-Randall, V., Law, K.K.L., Briscoe, J., and Hui, C.C. (2009). The Kinesin Protein Kif7 Is a Critical Regulator of Gli Transcription Factors in Mammalian Hedgehog Signaling. *Science Signaling* 2, ra29–ra29.

Chiang, C., Litingtung, Y., Harris, M.P., Simandl, B.K., Li, Y., Beachy, P.A., and Fallon, J.F. (2001). Manifestation of the limb prepattern: limb development in the absence of sonic hedgehog function. *Developmental Biology* 236, 421–435.

Chiang, C., Litingtung, Y., Lee, E., Young, K.E., Corden, J.L., Westphal, H., and Beachy, P.A. (1996). Cyclopia and defective axial patterning in mice lacking Sonic

hedgehog gene function. *Nature* 383, 407–413.

Cho, A., Ko, H.W., and Eggenschwiler, J.T. (2008). FKBP8 cell-autonomously controls neural tube patterning through a Gli2- and Kif3a-dependent mechanism. *Developmental Biology* 321, 27–39.

Christ, A., Christa, A., Kur, E., Lioubinski, O., Bachmann, S., Willnow, T.E., and Hammes, A. (2012). LRP2 is an auxiliary SHH receptor required to condition the forebrain ventral midline for inductive signals. *Developmental Cell* 22, 268–278.

Cole, D.G. (2003). The intraflagellar transport machinery of *Chlamydomonas reinhardtii*. *Traffic* 4, 435–442.

Cooper, A.F., Yu, K.P., Brueckner, M., Brailey, L.L., Johnson, L., McGrath, J.M., and Bale, A.E. (2005). Cardiac and CNS defects in a mouse with targeted disruption of suppressor of fused. *Development* 132, 4407–4417.

Coppieters, F., Lefever, S., Leroy, B.P., and De Baere, E. (2010). CEP290, a gene with many faces: mutation overview and presentation of CEP290base. *Hum. Mutat.* 31, 1097–1108.

Corbit, K.C., Aanstad, P., Singla, V., Norman, A.R., Stainier, D.Y.R., and Reiter, J.F. (2005). Vertebrate Smoothed functions at the primary cilium. *Nature* 437, 1018–1021.

Corcoran, R.B., and Scott, M.P. (2006). Oxysterols stimulate Sonic hedgehog signal transduction and proliferation of medulloblastoma cells. *Proc. Natl. Acad. Sci. U.S.A.* 103, 8408–8413.

Craige, B., Tsao, C.C., Diener, D.R., Hou, Y., Lechtreck, K.F., Rosenbaum, J.L., and Witman, G.B. (2010). CEP290 tethers flagellar transition zone microtubules to the membrane and regulates flagellar protein content. *The Journal of Cell Biology* 190, 927–940.

Creanga, A., Glenn, T.D., Mann, R.K., Saunders, A.M., Talbot, W.S., and Beachy, P.A. (2012). Scube/You activity mediates release of dually lipid-modified Hedgehog signal in soluble form. *Genes Dev.* 26, 1312–1325.

Czarnecki, P.G., and Shah, J.V. (2012). The ciliary transition zone: from morphology and molecules to medicine. *Trends Cell Biol.* 22, 201–210.

Dagoneau, N., Goulet, M., Geneviève, D., Sznajder, Y., Martinovic, J., Smithson, S., Huber, C., Baujat, G., Flori, E., Tecco, L., et al. (2009). DYNC2H1 mutations cause asphyxiating thoracic dystrophy and short rib-polydactyly syndrome, type III. *Am. J. Hum. Genet.* 84, 706–711.

Davenport, J.R., and Yoder, B.K. (2005). An incredible decade for the primary cilium: a look at a once-forgotten organelle. *Am. J. Physiol. Renal Physiol.* 289, F1159–

F1169.

Davis, E.E., Zhang, Q., Liu, Q., Diplas, B.H., Davey, L.M., Hartley, J., Stoetzel, C., Szymanska, K., Ramaswami, G., Logan, C.V., et al. (2011). TTC21B contributes both causal and modifying alleles across the ciliopathy spectrum. *Nat. Genet.* **43**, 189–196.

DeCamp, D.L., Thompson, T.M., de Sauvage, F.J., and Lerner, M.R. (2000). Smoothed activates Galphai-mediated signaling in frog melanophores. *J. Biol. Chem.* **275**, 26322–26327.

Delous, M., Baala, L., Salomon, R., Laclef, C., Vierkotten, J., Tory, K., Golzio, C., Lacoste, T., Besse, L., Ozilou, C., et al. (2007). The ciliary gene RPGRIP1L is mutated in cerebello-oculo-renal syndrome (Joubert syndrome type B) and Meckel syndrome. *Nat. Genet.* **39**, 875–881.

Digilio, M.C., Marino, B., Ammirati, A., Borzaga, U., Giannotti, A., and Dallapiccola, B. (1999). Cardiac malformations in patients with oral-facial-skeletal syndromes: clinical similarities with heterotaxia. *Am. J. Med. Genet.* **84**, 350–356.

Dlugosz, A., Agrawal, S., and Kirkpatrick, P. (2012). Vismodegib. *Nat Rev Drug Discov* **11**, 437–438.

Dwyer, J.R., Sever, N., Carlson, M., Nelson, S.F., Beachy, P.A., and Parhami, F. (2007). Oxysterols are novel activators of the hedgehog signaling pathway in pluripotent mesenchymal cells. *J. Biol. Chem.* **282**, 8959–8968.

Echelard, Y., Epstein, D.J., St-Jacques, B., Shen, L., Mohler, J., McMahon, J.A., and McMahon, A.P. (1993). Sonic hedgehog, a member of a family of putative signaling molecules, is implicated in the regulation of CNS polarity. *Cell* **75**, 1417–1430.

Ellis, R.W., and van Creveld, S. (1940). A Syndrome Characterized by Ectodermal Dysplasia, Polydactyly, Chondro-Dysplasia and Congenital Morbus Cordis: Report of Three Cases. *Arch. Dis. Child.* **15**, 65–84.

Endoh-Yamagami, S., Evangelista, M., Wilson, D., Wen, X., Theunissen, J.-W., Phamluong, K., Davis, M., Scales, S.J., Solloway, M.J., de Sauvage, F.J., et al. (2009). The mammalian Cos2 homolog Kif7 plays an essential role in modulating Hh signal transduction during development. *Curr. Biol.* **19**, 1320–1326.

Fire, A., Xu, S., Montgomery, M.K., Kostas, S.A., Driver, S.E., and Mello, C.C. (1998). Potent and specific genetic interference by double-stranded RNA in *Caenorhabditis elegans*. *Nature* **391**, 806–811.

Follit, J.A., Li, L., Vucica, Y., and Pazour, G.J. (2010). The cytoplasmic tail of fibrocystin contains a ciliary targeting sequence. *The Journal of Cell Biology* **188**, 21–28.

Follit, J.A., Tuft, R.A., Fogarty, K.E., and Pazour, G.J. (2006). The intraflagellar

transport protein IFT20 is associated with the Golgi complex and is required for cilia assembly. *Mol. Biol. Cell* *17*, 3781–3792.

Freeze, H.H., and Kranz, C. (2010). Endoglycosidase and glycoamidase release of N-linked glycans. *Curr Protoc Immunol Chapter 8*, Unit8.15.1–Unit8.15.25.

Galdzicka, M., Patnala, S., Hirshman, M.G., Cai, J.-F., Nitowsky, H., Egeland, J.A., and Ginns, E.I. (2002). A new gene, EVC2, is mutated in Ellis-van Creveld syndrome. *Mol. Genet. Metab.* *77*, 291–295.

Galluzzi, L., Vacchelli, E., Fridman, W.H., Galon, J., Sautès-Fridman, C., Tartour, E., Zucman-Rossi, J., Zitvogel, L., and Kroemer, G. (2012). Trial Watch: Monoclonal antibodies in cancer therapy. *Oncoimmunology* *1*, 28–37.

Geng, L., Okuhara, D., Yu, Z., Tian, X., Cai, Y., Shibazaki, S., and Somlo, S. (2006). Polycystin-2 traffics to cilia independently of polycystin-1 by using an N-terminal RVxP motif. *Journal of Cell Science* *119*, 1383–1395.

Gerdes, J.M., Davis, E.E., and Katsanis, N. (2009). The vertebrate primary cilium in development, homeostasis, and disease. *Cell* *137*, 32–45.

Gherman, A., Davis, E.E., and Katsanis, N. (2006). The ciliary proteome database: an integrated community resource for the genetic and functional dissection of cilia. *Nat. Genet.* *38*, 961–962.

Gifford, J.L., Walsh, M.P., and Vogel, H.J. (2007). Structures and metal-ion-binding properties of the Ca<sup>2+</sup>-binding helix-loop-helix EF-hand motifs. *Biochem. J.* *405*, 199–221.

Gilissen, C., Arts, H.H., Hoischen, A., Spruijt, L., Mans, D.A., Arts, P., van Lier, B., Steehouwer, M., van Reeuwijk, J., Kant, S.G., et al. (2010). Exome sequencing identifies WDR35 variants involved in Sensenbrenner syndrome. *Am. J. Hum. Genet.* *87*, 418–423.

Gilula, N.B., and Satir, P. (1972). The ciliary necklace. A ciliary membrane specialization. *The Journal of Cell Biology* *53*, 494–509.

Goetz, S.C., and Anderson, K.V. (2010). The primary cilium: a signalling centre during vertebrate development. *Nat. Rev. Genet.* *11*, 331–344.

Goetz, S.C., Ocbina, P.J.R., and Anderson, K.V. (2009). The primary cilium as a Hedgehog signal transduction machine. *Methods Cell Biol.* *94*, 199–222.

Graser, S., Stierhof, Y.D., Lavoie, S.B., Gassner, O.S., Lamla, S., Le Clech, M., and Nigg, E.A. (2007). Cep164, a novel centriole appendage protein required for primary cilium formation. *The Journal of Cell Biology* *179*, 321–330.

Gundersen, G.G., and Bulinski, J.C. (1986). Microtubule arrays in differentiated cells

contain elevated levels of a post-translationally modified form of tubulin. *Eur. J. Cell Biol.* **42**, 288–294.

Hahn, H., Wicking, C., Zaphiropoulos, P.G., Gailani, M.R., Shanley, S., Chidambaram, A., Vorechovsky, I., Holmberg, E., Uden, A.B., Gillies, S., et al. (1996). Mutations of the human homolog of *Drosophila* patched in the nevoid basal cell carcinoma syndrome. *Cell* **85**, 841–851.

Hammerschmidt, M., and McMahon, A.P. (1998). The effect of pertussis toxin on zebrafish development: a possible role for inhibitory G-proteins in hedgehog signaling. *Developmental Biology* **194**, 166–171.

Hammerschmidt, M., Bitgood, M.J., and McMahon, A.P. (1996). Protein kinase A is a common negative regulator of Hedgehog signaling in the vertebrate embryo. *Genes Dev.* **10**, 647–658.

Haycraft, C.J., Banizs, B., Aydin-Son, Y., Zhang, Q., Michaud, E.J., and Yoder, B.K. (2005). Gli2 and Gli3 Localize to Cilia and Require the Intraflagellar Transport Protein Polaris for Processing and Function. *PLoS Genet* **1**, e53.

Heo, J.S., Lee, M.Y., and Han, H.J. (2007). Sonic hedgehog stimulates mouse embryonic stem cell proliferation by cooperation of Ca<sup>2+</sup>/protein kinase C and epidermal growth factor receptor as well as Gli1 activation. *Stem Cells* **25**, 3069–3080.

Hu, Q., Milenkovic, L., Jin, H., Scott, M.P., Nachury, M.V., Spiliotis, E.T., and Nelson, W.J. (2010). A septin diffusion barrier at the base of the primary cilium maintains ciliary membrane protein distribution. *Science* **329**, 436–439.

Huangfu, D., and Anderson, K.V. (2005). Cilia and Hedgehog responsiveness in the mouse. *Proc. Natl. Acad. Sci. U.S.a.* **102**, 11325–11330.

Huangfu, D., Liu, A., Rakeman, A.S., Murcia, N.S., Niswander, L., and Anderson, K.V. (2003). Hedgehog signalling in the mouse requires intraflagellar transport proteins. *Nature* **426**, 83–87.

Huber, C., and Cormier-Daire, V. (2012). Ciliary disorder of the skeleton. *Am. J. Med. Genet.* **160**, 165–174.

Hui, C.-C., and Angers, S. (2011). Gli proteins in development and disease. *Annu. Rev. Cell Dev. Biol.* **27**, 513–537.

Humke, E.W., Dorn, K.V., Milenkovic, L., Scott, M.P., and Rohatgi, R. (2010). The output of Hedgehog signaling is controlled by the dynamic association between Suppressor of Fused and the Gli proteins. *Genes Dev.* **24**, 670–682.

Hyman, J.M., Firestone, A.J., Heine, V.M., Zhao, Y., Ocasio, C.A., Han, K., Sun, M., Rack, P.G., Sinha, S., Wu, J.J., et al. (2009). Small-molecule inhibitors reveal multiple strategies for Hedgehog pathway blockade. *Proc. Natl. Acad. Sci. U.S.a.* **106**, 14132–

14137.

- Insinna, C., Pathak, N., Perkins, B., Drummond, I., and Besharse, J.C. (2008). The homodimeric kinesin, Kif17, is essential for vertebrate photoreceptor sensory outer segment development. *Developmental Biology* 316, 160–170.
- Ishikawa, H., and Marshall, W.F. (2011). Ciliogenesis: building the cell's antenna. *Nat. Rev. Mol. Cell Biol.* 12, 222–234.
- Ishikawa, H., Thompson, J., Yates, J.R., III, and Marshall, W.F. (2012). Proteomic Analysis of Mammalian Primary Cilia. *Current Biology* 22, 414–419.
- Izzi, L., Lévesque, M., Morin, S., Laniel, D., Wilkes, B.C., Mille, F., Krauss, R.S., McMahon, A.P., Allen, B.L., and Charron, F. (2011). Boc and Gas1 each form distinct Shh receptor complexes with Ptch1 and are required for Shh-mediated cell proliferation. *Developmental Cell* 20, 788–801.
- Jenkins, P.M., Hurd, T.W., Zhang, L., McEwen, D.P., Brown, R.L., Margolis, B., Verhey, K.J., and Martens, J.R. (2006). Ciliary targeting of olfactory CNG channels requires the CNGB1b subunit and the kinesin-2 motor protein, KIF17. *Current Biology* 16, 1211–1216.
- Jékely, G., and Arendt, D. (2006). Evolution of intraflagellar transport from coated vesicles and autogenous origin of the eukaryotic cilium. *Bioessays* 28, 191–198.
- Jia, J., Kolterud, A., Zeng, H., Hoover, A., Teglund, S., Toftgård, R., and Liu, A. (2009). Suppressor of Fused inhibits mammalian Hedgehog signaling in the absence of cilia. *Developmental Biology* 330, 452–460.
- Jia, J., Tong, C., and Jiang, J. (2003). Smoothed transduces Hedgehog signal by physically interacting with Costal2/Fused complex through its C-terminal tail. *Genes Dev.* 17, 2709–2720.
- Johnson, J.-L.F.A., Hall, T.E., Dyson, J.M., Sonntag, C., Ayers, K., Berger, S., Gautier, P., Mitchell, C., Hollway, G.E., and Currie, P.D. (2012). Scube activity is necessary for Hedgehog signal transduction in vivo. *Developmental Biology* 368, 193–202.
- Johnson, R.L., Rothman, A.L., Xie, J., Goodrich, L.V., Bare, J.W., Bonifas, J.M., Quinn, A.G., Myers, R.M., Cox, D.R., Epstein, E.H., et al. (1996). Human homolog of patched, a candidate gene for the basal cell nevus syndrome. *Science* 272, 1668–1671.
- Karhadkar, S.S., Bova, G.S., Abdallah, N., Dhara, S., Gardner, D., Maitra, A., Isaacs, J.T., Berman, D.M., and Beachy, P.A. (2004). Hedgehog signalling in prostate regeneration, neoplasia and metastasis. *Nature* 431, 707–712.
- Keady, B.T., Samtani, R., Tobita, K., Tsuchya, M., San Agustin, J.T., Follit, J.A., Jonassen, J.A., Subramanian, R., Lo, C.W., and Pazour, G.J. (2012). IFT25 links the

signal-dependent movement of Hedgehog components to intraflagellar transport. *Developmental Cell* 22, 940–951.

Keating, G.M. (2012). Vismodegib: in locally advanced or metastatic Basal cell carcinoma. *Drugs* 72, 1535–1541.

Kee, H.L., Dishinger, J.F., Blasius, T.L., Liu, C.-J., Margolis, B., and Verhey, K.J. (2012). A size-exclusion permeability barrier and nucleoporins characterize a ciliary pore complex that regulates transport into cilia. *Nature Publishing Group* 14, 431–437.

Kim, J., Kato, M., and Beachy, P.A. (2009). Gli2 trafficking links Hedgehog-dependent activation of Smoothened in the primary cilium to transcriptional activation in the nucleus. *Proc. Natl. Acad. Sci. U.S.a.* 106, 21666–21671.

Kim, J., Lee, J.E., Heynen-Genel, S., Suyama, E., Ono, K., Lee, K., Ideker, T., Aza-Blanc, P., and Gleeson, J.G. (2010a). Functional genomic screen for modulators of ciliogenesis and cilium length. *Nature* 464, 1048–1051.

Kim, J., Lee, J.J., Kim, J., Gardner, D., and Beachy, P.A. (2010b). Arsenic antagonizes the Hedgehog pathway by preventing ciliary accumulation and reducing stability of the Gli2 transcriptional effector. *Proc. Natl. Acad. Sci. U.S.a.* 107, 13432–13437.

Klotz, C., Dabauvalle, M.C., Paintrand, M., Weber, T., Bornens, M., and Karsenti, E. (1990). Parthenogenesis in *Xenopus* eggs requires centrosomal integrity. *The Journal of Cell Biology* 110, 405–415.

Ko, H.W., Liu, A., and Eggenschwiler, J.T. (2009). Chapter 17 - Analysis of Hedgehog Signaling in Mouse Intraflagellar Transport Mutants (Elsevier).

Konno, A., Setou, M., and Ikegami, K. (2012). Ciliary and flagellar structure and function-their regulations by posttranslational modifications of axonemal tubulin. *Int Rev Cell Mol Biol* 294, 133–170.

Kozminski, K.G., Johnson, K.A., Forscher, P., and Rosenbaum, J.L. (1993). A motility in the eukaryotic flagellum unrelated to flagellar beating. *Proc. Natl. Acad. Sci. U.S.a.* 90, 5519–5523.

Krauss, S., Concordet, J.P., and Ingham, P.W. (1993). A functionally conserved homolog of the *Drosophila* segment polarity gene *hh* is expressed in tissues with polarizing activity in zebrafish embryos. *Cell* 75, 1431–1444.

Laemmli, U.K. (1970). Cleavage of structural proteins during the assembly of the head of bacteriophage T4. *Nature* 227, 680–685.

Lee, J.E., Silhavy, J.L., Zaki, M.S., Schroth, J., Bielas, S.L., Marsh, S.E., Olvera, J., Brancati, F., Iannicelli, M., Ikegami, K., et al. (2012). CEP41 is mutated in Joubert syndrome and is required for tubulin glutamylation at the cilium. *Nat. Genet.* 44, 193–

199.

Lei, Q., Zelman, A.K., Kuang, E., Li, S., and Matise, M.P. (2004). Transduction of graded Hedgehog signaling by a combination of Gli2 and Gli3 activator functions in the developing spinal cord. *Development* *131*, 3593–3604.

Lepage, T., Cohen, S.M., Diaz-Benjumea, F.J., and Parkhurst, S.M. (1995). Signal transduction by cAMP-dependent protein kinase A in *Drosophila* limb patterning. *Nature* *373*, 711–715.

Liem, K.F., Ashe, A., He, M., Satir, P., Moran, J., Beier, D., Wicking, C., and Anderson, K.V. (2012). The IFT-A complex regulates Shh signaling through cilia structure and membrane protein trafficking. *The Journal of Cell Biology* *197*, 789–800.

Liem, K.F., He, M., Ocbina, P.J.R., and Anderson, K.V. (2009). Mouse Kif7/Costal2 is a cilia-associated protein that regulates Sonic hedgehog signaling. *Proc. Natl. Acad. Sci. U.S.a.* *106*, 13377–13382.

Lin, F., Hiesberger, T., Cordes, K., Sinclair, A.M., Goldstein, L.S.B., Somlo, S., and Igarashi, P. (2003). Kidney-specific inactivation of the KIF3A subunit of kinesin-II inhibits renal ciliogenesis and produces polycystic kidney disease. *Proc. Natl. Acad. Sci. U.S.a.* *100*, 5286–5291.

Lin, T.L., and Matsui, W. (2012). Hedgehog pathway as a drug target: Smoothened inhibitors in development. *Onco Targets Ther* *5*, 47–58.

Liu, A. (2005). Mouse intraflagellar transport proteins regulate both the activator and repressor functions of Gli transcription factors. *Development* *132*, 3103–3111.

Low, W.-C., Wang, C., Pan, Y., Huang, X.-Y., Chen, J.K., and Wang, B. (2008). The decoupling of Smoothened from Galphai proteins has little effect on Gli3 protein processing and Hedgehog-regulated chick neural tube patterning. *Developmental Biology* *321*, 188–196.

Maity, T., Fuse, N., and Beachy, P.A. (2005). Molecular mechanisms of Sonic hedgehog mutant effects in holoprosencephaly. *Proc. Natl. Acad. Sci. U.S.a.* *102*, 17026–17031.

May, S.R., Ashique, A.M., Karlen, M., Wang, B., Shen, Y., Zarbalis, K., Reiter, J., Ericson, J., and Peterson, A.S. (2005). Loss of the retrograde motor for IFT disrupts localization of Smo to cilia and prevents the expression of both activator and repressor functions of Gli. *Developmental Biology* *287*, 378–389.

Mazelova, J., Astuto-Gribble, L., Inoue, H., Tam, B.M., Schonteich, E., Prekeris, R., Moritz, O.L., Randazzo, P.A., and Deretic, D. (2009). Ciliary targeting motif VxPx directs assembly of a trafficking module through Arf4. *Embo J.* *28*, 183–192.

McKusick, V.A. (2000). Ellis-van Creveld syndrome and the Amish. *Nat. Genet.* *24*,

203–204.

McMahon, A.P., Ingham, P.W., and Tabin, C.J. (2003). Developmental roles and clinical significance of hedgehog signaling. *Curr. Top. Dev. Biol.* 53, 1–114.

McMillan, R., and Matsui, W. (2012). Molecular Pathways: The Hedgehog Signaling Pathway in Cancer. *Clin Cancer Res.*

Milenkovic, L., Scott, M.P., and Rohatgi, R. (2009). Lateral transport of Smoothed from the plasma membrane to the membrane of the cilium. *The Journal of Cell Biology* 187, 365–374.

Molla-Herman, A., Ghossoub, R., Blisnick, T., Meunier, A., Serres, C., Silbermann, F., Emmerson, C., Romeo, K., Bourdoncle, P., Schmitt, A., et al. (2010). The ciliary pocket: an endocytic membrane domain at the base of primary and motile cilia. *Journal of Cell Science* 123, 1785–1795.

Nachtergaele, S., Mydock, L.K., Krishnan, K., Rammohan, J., Schlesinger, P.H., Covey, D.F., and Rohatgi, R. (2012). Oxysterols are allosteric activators of the oncoprotein Smoothed. *Nat Chem Biol* 8, 211–220.

Nachury, M.V., Loktev, A.V., Zhang, Q., Westlake, C.J., Peränen, J., Merdes, A., Slusarski, D.C., Scheller, R.H., Bazan, J.F., Sheffield, V.C., et al. (2007). A core complex of BBS proteins cooperates with the GTPase Rab8 to promote ciliary membrane biogenesis. *Cell* 129, 1201–1213.

Nachury, M.V., Seeley, E.S., and Jin, H. (2010). Trafficking to the ciliary membrane: how to get across the periciliary diffusion barrier? *Annu. Rev. Cell Dev. Biol.* 26, 59–87.

Nigg, E.A., and Raff, J.W. (2009). Centrioles, centrosomes, and cilia in health and disease. *Cell* 139, 663–678.

Nonaka, S., Tanaka, Y., Okada, Y., Takeda, S., Harada, A., Kanai, Y., Kido, M., and Hirokawa, N. (1998). Randomization of left-right asymmetry due to loss of nodal cilia generating leftward flow of extraembryonic fluid in mice lacking KIF3B motor protein. *Cell* 95, 829–837.

Novarino, G., Akizu, N., and Gleeson, J.G. (2011). Modeling Human Disease in Humans: The Ciliopathies. *Cell* 147, 70–79.

Nüsslein-Volhard, C., and Wieschaus, E. (1980). Mutations affecting segment number and polarity in *Drosophila*. *Nature* 287, 795–801.

Obado, S.O., and Rout, M.P. (2012). Ciliary and nuclear transport: different places, similar routes? *Developmental Cell* 22, 693–694.

Ocbina, P.J.R., and Anderson, K.V. (2008). Intraflagellar transport, cilia, and

mammalian Hedgehog signaling: analysis in mouse embryonic fibroblasts. *Dev. Dyn.* 237, 2030–2038.

Ocbina, P.J.R., Eggenschwiler, J.T., Moskowitz, I., and Anderson, K.V. (2011). Complex interactions between genes controlling trafficking in primary cilia. *Nat. Genet.* 43, 547–553.

Ochman, H., Gerber, A.S., and Hartl, D.L. (1988). Genetic applications of an inverse polymerase chain reaction. *Genetics* 120, 621–623.

Ong, S.-E., Blagoev, B., Kratchmarova, I., Kristensen, D.B., Steen, H., Pandey, A., and Mann, M. (2002). Stable isotope labeling by amino acids in cell culture, SILAC, as a simple and accurate approach to expression proteomics. *Mol. Cell Proteomics* 1, 376–386.

Orozco, J.T., Wedaman, K.P., Signor, D., Brown, H., Rose, L., and Scholey, J.M. (1999). Movement of motor and cargo along cilia. *Nature* 398, 674.

Osawa, H., Ohnishi, H., Takano, K., Noguti, T., Mashima, H., Hoshino, H., Kita, H., Sato, K., Matsui, H., and Sugano, K. (2006). Sonic hedgehog stimulates the proliferation of rat gastric mucosal cells through ERK activation by elevating intracellular calcium concentration. *Biochem. Biophys. Res. Commun.* 344, 680–687.

Otto, E.A., Schermer, B., Obara, T., O'Toole, J.F., Hiller, K.S., Mueller, A.M., Ruf, R.G., Hoefele, J., Beekmann, F., Landau, D., et al. (2003). Mutations in *INVS* encoding inversin cause nephronophthisis type 2, linking renal cystic disease to the function of primary cilia and left-right axis determination. *Nat. Genet.* 34, 413–420.

Pan, Y., Bai, C.B., Joyner, A.L., and Wang, B. (2006). Sonic hedgehog signaling regulates *Gli2* transcriptional activity by suppressing its processing and degradation. *Mol. Cell. Biol.* 26, 3365–3377.

Park, H.L., Bai, C., Platt, K.A., Matise, M.P., Beeghly, A., Hui, C.C., Nakashima, M., and Joyner, A.L. (2000). Mouse *Gli1* mutants are viable but have defects in SHH signaling in combination with a *Gli2* mutation. *Development* 127, 1593–1605.

Parmantier, E., Lynn, B., Lawson, D., Turmaine, M., Namini, S.S., Chakrabarti, L., McMahon, A.P., Jessen, K.R., and Mirsky, R. (1999). Schwann cell-derived Desert hedgehog controls the development of peripheral nerve sheaths. *Neuron* 23, 713–724.

Pazour, G.J., Dickert, B.L., Vucica, Y., Seeley, E.S., Rosenbaum, J.L., Witman, G.B., and Cole, D.G. (2000). *Chlamydomonas* IFT88 and its mouse homologue, polycystic kidney disease gene *tg737*, are required for assembly of cilia and flagella. *The Journal of Cell Biology* 151, 709–718.

Pazour, G.J., Wilkerson, C.G., and Witman, G.B. (1998). A dynein light chain is essential for the retrograde particle movement of intraflagellar transport (IFT). *The Journal of Cell Biology* 141, 979–992.

- Pear, W.S., Nolan, G.P., Scott, M.L., and Baltimore, D. (1993). Production of high-titer helper-free retroviruses by transient transfection. *Proc. Natl. Acad. Sci. U.S.a.* *90*, 8392–8396.
- Pedersen, L.B., and Rosenbaum, J.L. (2008). Intraflagellar transport (IFT) role in ciliary assembly, resorption and signalling. *Curr. Top. Dev. Biol.* *85*, 23–61.
- Pedersen, L.B., Veland, I.R., Schröder, J.M., and Christensen, S.T. (2008). Assembly of primary cilia. *Dev. Dyn.* *237*, 1993–2006.
- Piperno, G., and Mead, K. (1997). Transport of a novel complex in the cytoplasmic matrix of *Chlamydomonas* flagella. *Proc. Natl. Acad. Sci. U.S.a.* *94*, 4457–4462.
- Piperno, G., LeDizet, M., and Chang, X.J. (1987). Microtubules containing acetylated alpha-tubulin in mammalian cells in culture. *The Journal of Cell Biology* *104*, 289–302.
- Pires-daSilva, A., and Sommer, R.J. (2003). The evolution of signalling pathways in animal development. *Nat. Rev. Genet.* *4*, 39–49.
- Polizio, A.H., Chinchilla, P., Chen, X., Kim, S., Manning, D.R., and Riobo, N.A. (2011). Heterotrimeric Gi proteins link Hedgehog signaling to activation of Rho small GTPases to promote fibroblast migration. *J. Biol. Chem.* *286*, 19589–19596.
- Qin, J., Lin, Y., Norman, R.X., Ko, H.W., and Eggenschwiler, J.T. (2011). Intraflagellar transport protein 122 antagonizes Sonic Hedgehog signaling and controls ciliary localization of pathway components. *Proc. Natl. Acad. Sci. U.S.a.* *108*, 1456–1461.
- Quinlan, R.J., Tobin, J.L., and Beales, P.L. (2008). Modeling ciliopathies: Primary cilia in development and disease. *Curr. Top. Dev. Biol.* *84*, 249–310.
- Ribes, V., and Briscoe, J. (2009). Establishing and interpreting graded Sonic Hedgehog signaling during vertebrate neural tube patterning: the role of negative feedback. *Cold Spring Harb Perspect Biol* *1*, a002014.
- Riddle, R.D., Johnson, R.L., Laufer, E., and Tabin, C. (1993). Sonic hedgehog mediates the polarizing activity of the ZPA. *Cell* *75*, 1401–1416.
- Rigaut, G., Shevchenko, A., Rutz, B., Wilm, M., Mann, M., and Séraphin, B. (1999). A generic protein purification method for protein complex characterization and proteome exploration. *Nat. Biotechnol.* *17*, 1030–1032.
- Riobo, N.A., Saucy, B., Dilizio, C., and Manning, D.R. (2006). Activation of heterotrimeric G proteins by Smoothed. *Proc. Natl. Acad. Sci. U.S.a.* *103*, 12607–12612.
- Robarge, K.D., Brunton, S.A., Castanedo, G.M., Cui, Y., Dina, M.S., Goldsmith, R., Gould, S.E., Guichert, O., Gunzner, J.L., Halladay, J., et al. (2009). GDC-0449-a potent inhibitor of the hedgehog pathway. *Bioorg. Med. Chem. Lett.* *19*, 5576–5581.

- Rohatgi, R., and Snell, W.J. (2010). The ciliary membrane. *Curr. Opin. Cell Biol.* 22, 541–546.
- Rohatgi, R., Milenkovic, L., and Scott, M.P. (2007). Patched1 Regulates Hedgehog Signaling at the Primary Cilium. *Science* 317, 372–376.
- Rohatgi, R., Milenkovic, L., Corcoran, R.B., and Scott, M.P. (2009). Hedgehog signal transduction by Smoothed: pharmacologic evidence for a 2-step activation process. *Proc. Natl. Acad. Sci. U.S.A.* 106, 3196–3201.
- Rothbauer, U., Zolghadr, K., Muyldermans, S., Schepers, A., Cardoso, M.C., and Leonhardt, H. (2008). A versatile nanotrap for biochemical and functional studies with fluorescent fusion proteins. *Mol. Cell Proteomics* 7, 282–289.
- Roy, S. (2009). The motile cilium in development and disease: emerging new insights. *Bioessays* 31, 694–699.
- Rubin, L.L., and de Sauvage, F.J. (2006). Targeting the Hedgehog pathway in cancer. *Nat Rev Drug Discov* 5, 1026–1033.
- Ruiz-Perez, V.L., and Goodship, J.A. (2009). Ellis-van Creveld syndrome and Weyers acrodistal dysostosis are caused by cilia-mediated diminished response to hedgehog ligands. *Am. J. Med. Genet.* 151C, 341–351.
- Ruiz-Perez, V.L., Blair, H.J., Rodriguez-Andres, M.E., Blanco, M.J., Wilson, A., Liu, Y.-N., Miles, C., Peters, H., and Goodship, J.A. (2007). Evc is a positive mediator of Ihh-regulated bone growth that localises at the base of chondrocyte cilia. *Development* 134, 2903–2912.
- Ruiz-Perez, V.L., Ide, S.E., Strom, T.M., Lorenz, B., Wilson, D., Woods, K., King, L., Francomano, C., Freisinger, P., Spranger, S., et al. (2000). Mutations in a new gene in Ellis-van Creveld syndrome and Weyers acrodistal dysostosis. *Nat. Genet.* 24, 283–286.
- Ruiz-Perez, V.L., Tompson, S.W.J., Blair, H.J., Espinoza-Valdez, C., Lapunzina, P., Silva, E.O., Hamel, B., Gibbs, J.L., Young, I.D., Wright, M.J., et al. (2003). Mutations in two nonhomologous genes in a head-to-head configuration cause Ellis-van Creveld syndrome. *Am. J. Hum. Genet.* 72, 728–732.
- Ruppert, J.M., Kinzler, K.W., Wong, A.J., Bigner, S.H., Kao, F.T., Law, M.L., Seuanez, H.N., O'Brien, S.J., and Vogelstein, B. (1988). The GLI-Kruppel family of human genes. *Mol. Cell. Biol.* 8, 3104–3113.
- Ryan, K.E., and Chiang, C. (2012). Hedgehog secretion and signal transduction in vertebrates. *J. Biol. Chem.* 287, 17905–17913.
- Sasaki, H., Hui, C., Nakafuku, M., and Kondoh, H. (1997). A binding site for Gli proteins is essential for HNF-3beta floor plate enhancer activity in transgenics and

can respond to Shh in vitro. *Development* 124, 1313–1322.

Satir, P., Pedersen, L.B., and Christensen, S.T. (2010). The primary cilium at a glance. *Journal of Cell Science* 123, 499–503.

Scholey, J.M. (2008). Intraflagellar transport motors in cilia: moving along the cell's antenna. *The Journal of Cell Biology* 180, 23–29.

Shakir, M.A., Fukushige, T., Yasuda, H., Miwa, J., and Siddiqui, S.S. (1993). *C. elegans* *osm-3* gene mediating osmotic avoidance behaviour encodes a kinesin-like protein. *Neuroreport* 4, 891–894.

Shiba, D., Manning, D.K., Koga, H., Beier, D.R., and Yokoyama, T. (2010). *Inv* acts as a molecular anchor for *Nphp3* and *Nek8* in the proximal segment of primary cilia. *Cytoskeleton (Hoboken)* 67, 112–119.

Shiba, D., Yamaoka, Y., Hagiwara, H., Takamatsu, T., Hamada, H., and Yokoyama, T. (2008). Localization of *Inv* in a distinctive intraciliary compartment requires the C-terminal ninein-homolog-containing region. *Journal of Cell Science* 122, 44–54.

Signor, D., Wedaman, K.P., Rose, L.S., and Scholey, J.M. (1999). Two heteromeric kinesin complexes in chemosensory neurons and sensory cilia of *Caenorhabditis elegans*. *Mol. Biol. Cell* 10, 345–360.

Singh, S., Wang, Z., Liang Fei, D., Black, K.E., Goetz, J.A., Tokhunts, R., Giambelli, C., Rodriguez-Blanco, J., Long, J., Lee, E., et al. (2011). Hedgehog-producing cancer cells respond to and require autocrine Hedgehog activity. *Cancer Res.* 71, 4454–4463.

Singla, V., and Reiter, J.F. (2006). The primary cilium as the cell's antenna: signaling at a sensory organelle. *Science* 313, 629–633.

Sorokin, S. (1962). Centrioles and the formation of rudimentary cilia by fibroblasts and smooth muscle cells. *The Journal of Cell Biology* 15, 363–377.

Spektor, A., Tsang, W.Y., Khoo, D., and Dynlacht, B.D. (2007). *Cep97* and *CP110* suppress a cilia assembly program. *Cell* 130, 678–690.

Stanley, P. (2011). Golgi glycosylation. *Cold Spring Harb Perspect Biol* 3.

Stannard, W., and O'Callaghan, C. (2006). Ciliary function and the role of cilia in clearance. *J Aerosol Med* 19, 110–115.

Sulik, K., Dehart, D.B., Ilangaki, T., Carson, J.L., Vrablic, T., Gesteland, K., and Schoenwolf, G.C. (1994). Morphogenesis of the murine node and notochordal plate. *Dev. Dyn.* 201, 260–278.

Svärd, J., Henricson, K.H., Persson-Lek, M., Rozell, B., Lauth, M., Bergström, Å.,

- Ericson, J., Toftgård, R., and Teglund, S. (2006). Genetic Elimination of Suppressor of Fused Reveals an Essential Repressor Function in the Mammalian Hedgehog Signaling Pathway. *Developmental Cell* 10, 187–197.
- Taipale, J., Chen, J.K., Cooper, M.K., Wang, B., Mann, R.K., Milenkovic, L., Scott, M.P., and Beachy, P.A. (2000). Effects of oncogenic mutations in Smoothed and Patched can be reversed by cyclopamine. *Nature* 406, 1005–1009.
- Taipale, J., Cooper, M.K., Maiti, T., and Beachy, P.A. (2002). Patched acts catalytically to suppress the activity of Smoothed. *Nature* 418, 892–897.
- Takeda, H., Takami, M., Oguni, T., Tsuji, T., Yoneda, K., Sato, H., Ihara, N., Itoh, T., Kata, S.R., Mishina, Y., et al. (2002). Positional cloning of the gene LIMBIN responsible for bovine chondrodysplastic dwarfism. *Proc. Natl. Acad. Sci. U.S.a.* 99, 10549–10554.
- Tempé, D., Casas, M., Karaz, S., Blanchet-Tournier, M.-F., and Concordet, J.-P. (2006). Multisite protein kinase A and glycogen synthase kinase 3beta phosphorylation leads to Gli3 ubiquitination by SCFbetaTrCP. *Mol. Cell. Biol.* 26, 4316–4326.
- Temtamy, S.A., Aglan, M.S., Valencia, M., Cocchi, G., Pacheco, M., Ashour, A.M., Amr, K.S., Helmy, S.M.H., El-Gammal, M.A., Wright, M., et al. (2008). Long interspersed nuclear element-1 (LINE1)-mediated deletion of EVC, EVC2, C4orf6, and STK32B in Ellis-van Creveld syndrome with borderline intelligence. *Hum. Mutat.* 29, 931–938.
- Tran, P.V., Haycraft, C.J., Besschetnova, T.Y., Turbe-Doan, A., Stottmann, R.W., Herron, B.J., Chesebro, A.L., Qiu, H., Scherz, P.J., Shah, J.V., et al. (2008). THM1 negatively modulates mouse sonic hedgehog signal transduction and affects retrograde intraflagellar transport in cilia. *Nat. Genet.* 40, 403–410.
- Tucker, R.W., Pardee, A.B., and Fujiwara, K. (1979). Centriole ciliation is related to quiescence and DNA synthesis in 3T3 cells. *Cell* 17, 527–535.
- Tukachinsky, H., Kuzmickas, R.P., Jao, C.Y., Liu, J., and Salic, A. (2012). Dispatched and Scube Mediate the Efficient Secretion of the Cholesterol-Modified Hedgehog Ligand. *Cell Rep.*
- Tukachinsky, H., Lopez, L.V., and Salic, A. (2010). A mechanism for vertebrate Hedgehog signaling: recruitment to cilia and dissociation of SuFu-Gli protein complexes. *The Journal of Cell Biology* 191, 415–428.
- Tuson, M., He, M., and Anderson, K.V. (2011). Protein kinase A acts at the basal body of the primary cilium to prevent Gli2 activation and ventralization of the mouse neural tube. *Development* 138, 4921–4930.
- Tzelepi, V., Karlou, M., Wen, S., Hoang, A., Logothetis, C., Troncoso, P., and

- Efstathiou, E. (2011). Expression of hedgehog pathway components in prostate carcinoma microenvironment: shifting the balance towards autocrine signalling. *Histopathology* 58, 1037–1047.
- Unden, A.B., Zaphiropoulos, P.G., Bruce, K., Toftgard, R., and Ståhle-Bäckdahl, M. (1997). Human patched (PTCH) mRNA is overexpressed consistently in tumor cells of both familial and sporadic basal cell carcinoma. *Cancer Res.* 57, 2336–2340.
- Valencia, M., Lapunzina, P., Lim, D., Zannolli, R., Bartholdi, D., Wollnik, B., Al-Ajlouni, O., Eid, S.S., Cox, H., Buoni, S., et al. (2009). Widening the mutation spectrum of EVC and EVC2: ectopic expression of Weyer variants in NIH 3T3 fibroblasts disrupts hedgehog signaling. *Hum. Mutat.* 30, 1667–1675.
- van den Heuvel, M., and Ingham, P.W. (1996). *smoothed* encodes a receptor-like serpentine protein required for hedgehog signalling. *Nature* 382, 547–551.
- Verhey, K.J., Dishinger, J., and Kee, H.L. (2011). Kinesin motors and primary cilia. *Biochem. Soc. Trans.* 39, 1120–1125.
- Vortkamp, A., Lee, K., Lanske, B., Segre, G.V., Kronenberg, H.M., and Tabin, C.J. (1996). Regulation of rate of cartilage differentiation by Indian hedgehog and PTH-related protein. *Science* 273, 613–622.
- Walczak-Sztulpa, J., Eggenschwiler, J., Osborn, D., Brown, D.A., Emma, F., Klingenberg, C., Hennekam, R.C., Torre, G., Garshasbi, M., Tzschach, A., et al. (2010). Cranioectodermal Dysplasia, Sensenbrenner syndrome, is a ciliopathy caused by mutations in the IFT122 gene. *Am. J. Hum. Genet.* 86, 949–956.
- Wang, B., and Li, Y. (2006). Evidence for the direct involvement of  $\beta$ TrCP in Gli3 protein processing. *Proc. Natl. Acad. Sci. U.S.A.* 103, 33–38.
- Wang, B., Fallon, J.F., and Beachy, P.A. (2000). Hedgehog-Regulated Processing of Gli3 Produces an Anterior/Posterior Repressor Gradient in the Developing Vertebrate Limb. *Cell* 100, 423–434.
- Watanabe, D., Saijoh, Y., Nonaka, S., Sasaki, G., Ikawa, Y., Yokoyama, T., and Hamada, H. (2003). The left-right determinant *Inversin* is a component of node monocilia and other 9+0 cilia. *Development* 130, 1725–1734.
- Waters, A.M., and Beales, P.L. (2011). Ciliopathies: an expanding disease spectrum. *Pediatr Nephrol* 26, 1039–1056.
- Watkins, D.N., Berman, D.M., Burkholder, S.G., Wang, B., Beachy, P.A., and Baylin, S.B. (2003). Hedgehog signalling within airway epithelial progenitors and in small-cell lung cancer. *Nature* 422, 313–317.
- Weatherbee, S.D., Niswander, L.A., and Anderson, K.V. (2009). A mouse model for Meckel syndrome reveals *Mks1* is required for ciliogenesis and Hedgehog signaling.

Hum. Mol. Genet. *18*, 4565–4575.

Wong, S.Y., and Reiter, J.F. (2008). The primary cilium at the crossroads of mammalian hedgehog signaling. *Curr. Top. Dev. Biol.* *85*, 225–260.

Wu, V.M., Chen, S.C., Arkin, M.R., and Reiter, J.F. (2012). Small molecule inhibitors of Smoothed ciliary localization and ciliogenesis. *Proc. Natl. Acad. Sci. U.S.a.* *109*, 13644–13649.

Xie, J., Murone, M., Luoh, S.M., Ryan, A., Gu, Q., Zhang, C., Bonifas, J.M., Lam, C.W., Hynes, M., Goddard, A., et al. (1998). Activating Smoothed mutations in sporadic basal-cell carcinoma. *Nature* *391*, 90–92.

Zhang, Q., Zhang, L., Wang, B., Ou, C.-Y., Chien, C.-T., and Jiang, J. (2006). A hedgehog-induced BTB protein modulates hedgehog signaling by degrading Ci/Gli transcription factor. *Developmental Cell* *10*, 719–729.

Zhang, X.M., Ramalho-Santos, M., and McMahon, A.P. (2001). Smoothed mutants reveal redundant roles for Shh and Ihh signaling including regulation of L/R asymmetry by the mouse node. *Cell* *105*, 781–792.

## 9. APPENDIX

### 9.1 The output of Hedgehog signaling is controlled by the dynamic association between Suppressor of Fused and the Gli proteins

This work has been published in:

Humke, E.W., **Dorn, K.V.**, Milenkovic, L., Scott, M.P., and Rohatgi, R. (2010). The output of Hedgehog signaling is controlled by the dynamic association between Suppressor of Fused and the Gli proteins. *Genes Dev.* 24, 670–682.

#### 9.1.1 Summary

Gli3, and to some extent Gli2, exist in a transcriptional repressor (GliR) form and an activator form (GliA). In this publication, we shed light on the regulation of GliA and GliR formation and showed that this critical step in Hh signaling is regulated by the interaction of the Gli proteins with Suppressor of Fused (SuFu). In the off-state of the pathway, SuFu restrains Gli3 in the cytoplasm promoting its processing to the repressor form, an event eventually leading to the inhibition of Hh target gene expression. In the presence of Hh signaling, SuFu dissociates from Gli3, which allows for the movement of Gli3 into the nucleus, where it becomes a labile, differentially phosphorylated Gli3 transcriptional activator. The model that emerges from this study is that the SuFu-Gli3 interaction is an important control point in Hh signaling as it controls the balance between Gli3R versus Gli3A formation.

#### 9.1.2 Contribution

My contribution to this publication was the development of a subcellular fractionation protocol with the goal to follow the distribution of the Gli proteins and other Hh components in the cell upon pathway activation. This assay is based on differential centrifugation allowing for the clean separation of nuclear, cytoplasmic and membrane fractions of cultured mammalian cells. This assay revealed that in untreated, serum-starved NIH/3T3 cells (Hh pathway is off) full-length Gli3 (Gli3FL)

and SuFu were mainly localized in the cytoplasm, while Gli3R was located in the nucleus (Figure A1). Upon pathway activation, Gli3FL shifted from the cytoplasm to the nucleus, whereas SuFu and Gli3R remained in the cytoplasm. In addition, the subcellular fractionation assay allowed for the visualization of a mobility-shift of nuclear Gli3FL due to phosphorylation upon pathway activation. Based on this assay it was also possible to evaluate the effects of Protein kinase A (PKA) on Gli3 activator formation as treatment with forskolin (FSK), which activates PKA, inhibited the SAG-induced movement of Gli3FL in the nucleus. The same result, a block in Gli3FL nuclear translocation, was observed with nocodazole, a microtubule-disrupting agent, suggesting that the movement of Gli3FL in the nucleus depends on cytoplasmic microtubules.

In summary, the subcellular fractionation assay set the foundation for various figures in this manuscript and allowed for the characterization of the events required for GliA formation. It is a viable and robust assay, which is transferable to other cell lines than NIH/3T3 cells. It will most likely serve as an important tool to study the mechanisms of GliA activator formation in greater detail. For example, it will allow for the isolation and characterization of the phosphorylated nuclear Gli3 fraction upon pathway activation, which could give insights not only on the phosphorylation sites on Gli3, but also could lead to the identification of the kinase involved in this process.

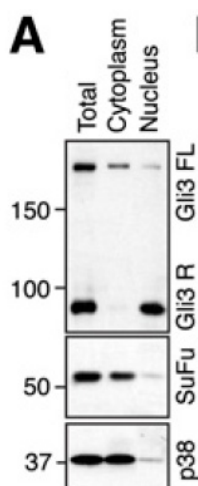


**Figure A1: The localization of Gli3 in the absence of Hh-signal.** Immunoblot of a subcellular fractionation assay in NIH/3T3 showing that under baseline full-length Gli3 (Gli3FL) and SuFu localized predominantly to the cytoplasm. The repressor form of Gli3 (Gli3R) is located in the nucleus. P38 was used as a cytoplasmic marker protein. This is Figure 5A in Humke et al. (2012).

## 9.2 Sequences of Oligonucleotides used in this study

Name	Sequence 5'-3'	Purpose
mEvc1381Fsef	GGATAAGGCCGGCCAGAGCTCACACAGACCCAAGAAGAAG	Evc antigen
mEvc3016Ascr	GATGGCGCGCCTCATGCAGCAGATTGCTTCCTTTC	Evc antigen
EvcScalHindf	TACAGTACTCCAAGCTTACCTGCACTAAAGATGCC	Evc cloning
EvcSalf	GATAGTCGACACCATGACCTGCACTAAAGATGCC	Evc cloning
EvcMlur	CTGTACGCGTCAGATTGCTTCCTTTCTGC	Evc cloning
Evc2231Fsef	GGATAAGGCCGGCCAAGGGGTCGATGTCTGCAG	Evc2 antigen
Evc2Ecof	GAAGAATTCCACCATGGGGGCGACGGGCC	Evc2 cloning
Evc2Mlur	GTAACGCGTGTCCAAGCCAAGGCC	Evc2 cloning
EVC2ala1-f	GCTGCAGGAGAAAAGATCTTTGTATTGATTCAGAAGCCCAAG	Evc2 mutagenesis
EVC2ala1-r	GGCTGCGTCCATAGCGTCTGCCCCAGTG	Evc2 mutagenesis
EVC2ala10-f	GCAGCTGTTCCCTCCAGGAGGAAAAAGAATTTCC	Evc2 mutagenesis
EVC2ala10-r	AGCTGCCTCGGGCTCCCTTGGGCTTC	Evc2 mutagenesis
EVC2ala2-f	GCAGCCAAGATCTTTGTATTGATTCAGAAGCCCAAGGGAG	Evc2 mutagenesis
EVC2ala2-r	AGCGGCTAATATGTCCATAGCGTCTGCCCCAG	Evc2 mutagenesis
EVC2ala3-f	GCTGCCTTTGTATTGATTCAGAAGCCCAAGGGAGCC	Evc2 mutagenesis
EVC2ala3-r	AGCTGCCGTGTTTAATATGTCCATAGCGTCTGCC	Evc2 mutagenesis
EVC2ala4-f	GCTGCATTGATTCAGAAGCCCAAGGGAGCCCGAG	Evc2 mutagenesis
EVC2ala4-r	GGCAGCTTCTCCCGTGTTTAATATGTCCATAGCGTC	Evc2 mutagenesis
EVC2ala5-f	GCTGCCAGCCCAAGGGAGCCCGAGATC	Evc2 mutagenesis
EVC2ala5-r	TGCAGCGATCTTTTCTCCCGTGTTTAATATGTCCATAGC	Evc2 mutagenesis
EVC2ala6-f	GCTGCAAGGGAGCCCGAGATCTCTTTGCGTG	Evc2 mutagenesis
EVC2ala6-r	TGCAGCTACAAAGATCTTTTCTCCCGTGTTTAATATGTCC	Evc2 mutagenesis
EVC2ala7-f	GCTGCACCCGAGATCTCTTTGCGTGTTCTCTC	Evc2 mutagenesis
EVC2ala7-r	TGCAGCTCTGAATACAAAGATCTTTTCTCCCGTGTTTAATATG	Evc2 mutagenesis
EVC2ala8-f	GCTGCAATCTCTTTGCGTGTTCTCTCCAGGAG	Evc2 mutagenesis
EVC2ala8-r	GGCAGCTGGGCTTCTGAATACAAAGATCTTTTCTCCC	Evc2 mutagenesis
EVC2ala9-f	GCTGCATTGCGTGTTCTCTCCAGGAGAAAAAG	Evc2 mutagenesis
EVC2ala9-r	GGCTGCCTCCCTTGGGCTTCTGAATACAAAGATC	Evc2 mutagenesis
DelN184Evc2For	ACT CAG CTA AAA GCC CCC TTT ACC	Evc2 mutagenesis
DelN61Evc2Rev	CTG CGA GCT TGC CCA GGG TCC TG	Evc2 mutagenesis
EVC2_del10_IV_r	GGC ATT CAG GAA ATT CTT TTT CCT CCT GGG AGG AAC ACG CAA AGA G	Evc2 mutagenesis
EVC2_IV_f	ACG CGT GGC GGA ACA CCA GGA TCT GGC GGA GAT TAC AAG GAC G	Evc2 mutagenesis
EVC2del10inv-f	AAGAAGGCCAACAGGGCCTTGGGCTTGGACACGCGTGCGG	Evc2 mutagenesis
EVC2del22_IV_r	ACG CAA AGA GAT CTC GGG CTC CCT TGG GCT TCT GAA TAC AAA G	Evc2 mutagenesis

EVC2del22inv-f	GTTCTCCCAGGAGGAAAAAGAATTCCTGAATGCCAAGAAGGCCAACAGGGC C	Evc2 mutagenesis
EVC2del31_IV_r	GCT TCT GAA TAC AAA GAT CTT TTC TCC CGT GTT TAA TAT GTC CAT AGC GTC	Evc2 mutagenesis
EVC2del31inv-f	CCAAGGGAGCCCGAGATCTCTTTGCGTGTTCCTCCCAGGAGG	Evc2 mutagenesis
EVC2del87_IV_r	GCG CTC CTT CTT CTG GCG GGC CCA GAG CAT CCT C	Evc2 mutagenesis
EVCdel43_IV_r	GTC CAT AGC GTC TGC CCC AGT GAT GGG GAT GGG AGC CAG TTC	Evc2 mutagenesis
mEvc2del64r	CAGGTGTGGCCAGCTTCCTTTCCCAGG	Evc2 mutagenesis
mEvcdel1157- 1176f	ATATTAACACGGGAGAAAAGATCTTTGTATTGATCAG	Evc2 mutagenesis
Evc2del43Mlur	GTAACGCGTGTCCATAGCGTCTGCCCC	Evc2ΔW cloning
Evcbp1Ecorlf	GAAGAATTCAAGGATGGCCAGCAACCCTGGAAG	Evcbp1 coning
Evcbp1EcorVr	GATGATATCTTAAGCTACAAGAGAATACACACAACAATATATCC	Evcbp1 coning
Evcbp2Ecorlf	GAAGAATTCAAGGATGAGCCTGGGCACCACAG	Evcbp2 cloning
Evcbp2EcorrVr	GATGATATCTTAGAACGGGGAGGGGCTTTTCTTC	Evcbp2 cloning
mSMO574delC-f	GAGCAAGATGATCGCCTAGGCCTTCTCTAAGCGG	Smo mutagenesis
mSMO574delC-r	CCGCTTAGAGAAGGCCTAGGCGATCATCTTGCTC	Smo mutagenesis
Smod570_581f	GAGCTGCTGCAGAACCCGGGCCAG	Smo mutagenesis
Smod570_581r	CTTCTTGATTCTCTTGGGCTCATCATCACTGTGC	Smo mutagenesis
Smod68_183f	AACGAGGTACAAAACATCAAGTTCAACAGCTCAGG	Smo mutagenesis
Smod68_183r	GTGGCTCAGCAGCGGCGGCGGAG	Smo mutagenesis
Evc21178Fsef	GGATAAGGCCGGCCAAACACGGGAGAAAAGATC	W-peptide cloning
Evc21221Ascr	GATGGCGCGCCTCAGTCCAAGCCCAAGGC	W-peptide cloning

## 10. ACKNOWLEDGEMENTS

I wish to convey my thanks to **Prof. Dr. Ulrich Rüter** for giving me the possibility of pursuing this dissertation at the “Institut für Entwicklungs- und Molekularbiologie der Tiere”, Heinrich-Heine University Düsseldorf, for his support, valuable discussions, and comments.

My very special thanks go to **Dr. Rajat Rohatgi** for giving me the opportunity to perform my doctoral research at Stanford University, USA. I thank him for the supervision of the research project and I am grateful for his support and motivation, great ideas, innumerable discussions, and for simply being a great teacher of science to me.

I thank **Prof. Dr. Thomas Klein** for his review of the thesis.

Thanks are due to **all the members of the Rüter Lab**, especially the “*Ftm*-team” for many conversations and scientific discussions and for the many Senseo coffees.

I am indebted to **all my Rohatgi Lab (ex-)colleagues** Eric Humke, Siggy Nachtergaele, Pawel Niewiadomski, Yan Ma, Andres Lebenssohn, Giovanni Luchetti, and Sara Peyrot for many fruitful discussion, their support in the lab, happy “Happy Hours”, supporting my coffee addiction, and for giving me a good time in the Rohatgi Lab.

Special thanks go to **Casey Hughes** who helped me A LOT by cloning many, many constructs.

I thank **Annika, Eva, Yence, and Oli** for wonderfully crazy weekends and for sharing their Postdoc-wisdom with me.

Many thanks to **Jessica** for being a wonderful friend!

I thank **my parents and family** for supporting me in all possible ways and for coming over to California to visit me.

**Mein lieber Felix**, dir danke ich von ganzem Herzen für deine ununterbrochene Geduld und liebevolle Unterstützung, deine Motivation – vor allem wenn es der “Science-God” mal nicht so gut mit mir meinte – und dafür, dass du immer für mich da bist. Danke!

## 1 1 . CURRICULUM VITAE

### Personal Information

Karolin Viktoria Dorn

Born July 23<sup>rd</sup> 1983 in Rottweil, Germany

Diploma in Biology, Albert-Ludwigs-Universität,  
Freiburg, Germany

### Education

- 09/2008                      Diploma in Biology at the Albert-Ludwigs University in Freiburg, Germany.  
Diploma thesis: "Molecular and Biochemical characterization of plastidic J-domain proteins in *Chlamydomonas reinhardtii*"
- 10/2003-09/2008        Studies in Biology at the University of Freiburg, Germany.  
Major: Biochemistry  
Minor: Microbiology, Cell Biology, Virology  
Grade: 1.0 (excellent)
- 08/2006-12/2006        ERASMUS scholarship for international research and studies at the University of Iceland (Hàskoli Íslands) in Reykjavík.
- 06/2002                      Abitur at the Albertus-Magnus-Gymnasium in Rottweil, Germany  
Grade: 1.4 (very good), awarded for excellent grades.
- 1989-1993                      Joseph-von-Eichendorff Grundschule in Rottweil, Germany

## Working Experience

- Since 01/2009 PhD candidate at the “Institut für Entwicklungs- und Molekularbiologie der Tiere der Heinrich-Heine-Universität Düsseldorf“ under supervision of Prof. Dr. U. Rütter.  
Research performed in the laboratory of Prof. Dr. R. Rohatgi, School of Medicine, Stanford University, USA
- Identification and functional characterization of novel Hedgehog components using a combination of proteomics and cell biological approaches
  - Analysis of the molecular pathophysiology of cilia diseases (ciliopathies).
- 11/2008-12/2008 Internship with Prof. Dr. J. Frydman, Department of Biology, Stanford University, CA, USA.
- Affinity purification of the eukaryotic chaperonin complex from *Saccharomyces cerevisiae*
- 01/2008-09/2008 Diploma thesis with Jun. Prof. Dr. M. Schroda, Department of Biochemistry, University of Freiburg, Germany.
- Biochemical analysis of the interplay between plastidic HSP70/90 and their J-domain containing co-chaperones.
- 02/2007-12/2007 Research assistant in the laboratory of Jun. Prof. Dr. M. Schroda, Department of Biochemistry, University of Freiburg, Germany.
- Molecular subcloning, protein affinity purification, immunoprecipitation experiments
- 08/2006-12/2006 Visiting researcher (ERASMUS scholarship) in the laboratory of G.H. Gudmundsson, Department of Cell Biology, Háskóli Ísland in Reykjavík, Iceland.

- Project: “Searching for cathelicidin in Fish - a family of antimicrobial peptides”

08/2005-09/2005 Internship in the laboratory of Dr. S. Eschenburg at the Max-Planck Institute for Molecular Physiology, Department of Structural Biology in Dortmund, Germany.

**Scientific Publications:**

**Dorn KV**, Hughes CE, Rohatgi R (2012) A Smoothened-Evc2 complex transduces the Hedgehog Signal at the primary cilium. *Developmental Cell*, doi:10.1016/j.devcel.2012.07.004.

Humke EW, **Dorn KV**, Milenkovic L, Scott MP, Rohatgi R (2010) The output of Hedgehog signaling is controlled by the dynamic association between Suppressor of Fused and the Gli proteins. *Genes Dev.* Apr 1;24(7):670-82.

**Dorn KV**, Willmund F, Henselmann C, Heß B, Pohl T, Friedrich T, Nickelsen J, Drepper F, Haehnel W and Schroda M (2010) Chloroplast DnaJ-like proteins 3 and 4 (CDJ3/4) from *Chlamydomonas reinhardtii* contain redox-active Fe-S clusters and interact with stromal HSP70B. *Biochem J.* Mar 29;427(2):205-15.

Willmund F, **Dorn KV**, Schulz-Raffelt M, and Schroda M (2008) The chloroplast DnaJ homolog CDJ1 of *Chlamydomonas reinhardtii* is part of a multi-chaperone complex containing HSP70B, CGE1, and HSP90C. *Plant Phys.* 148(4):2070-82.

Maier VH, **Dorn KV**, Gudmundsdottir BK, Gudmundsson GH (2008) Characterisation of cathelicidin gene family members in divergent fish species. *Mol Immunol.* 45(14):3723-30.

## 12. DECLARATION

I declare that I prepared the present dissertation independently and without any impermissible help. The thesis has not been submitted in the present form to any other institution. Hitherto, I have not performed unsuccessful efforts to get a doctoral degree.

Karolin V. Dorn